2007

Vadose zone processes affecting water table fluctuations: Conceptualization and modeling considerations

Nirjhar Shah
University of South Florida

Vadose Zone Processes Affecting Water Fluctuations: Conceptualization and Modeling Considerations

by

Nirjhar Shah

A dissertation submitted in partial fulfillment
of the requirements for the degree of
Doctor of Philosophy
Department of Civil and Environmental Engineering
College of Engineering
University of South Florida

Co-Major Professor: Mark A. Ross, Ph.D.
Co-Major Professor: Mahmood H. Nachabe, Ph.D.
David M. Sumner, Ph.D.
Mark Rains, Ph.D.
Rafael Perez, Ph.D.

Date of Approval:
October 18, 2007

Keywords: shallow water table, evapotranspiration, extinction depth, variable specific yield, root water uptake

Dedication

To my grandfather, the late Mr. L.D. Shah, a great teacher, who from very childhood instilled in me a sense of appreciation of science and a never ending pursuit of understanding it. *Dadaji* this is for you.

Acknowledgements

First and foremost I would like to thank my family, especially my parents, who worked very hard to ensure that I received an excellent education. Their constant love, support, patience, and encouragement guided me and helped me to successfully reach my goals. I am grateful to all of my friends and relatives for being there whenever I needed them.

I would also like to express the deepest appreciation to Dr. Mark Ross, Dr. Mahmood Nachabe, and all my committee members for their constant support and guidance throughout my tenure at the university. I am thankful that Dr. Ken Trout was always there to listen to my grievances and for offering constructive ideas. I also want to thank all of my CMHAS colleagues, especially Jeff Vomacka, Lisa Foster, Dr. Jing Zhang, Ken Nilsson, and Makhan Virdi, for all of their useful input, problem solving expertise, and overall assistance.

Finally, I want to thank my lovely fiancé, and soon to be wife, Swarna. I cannot express how grateful I am for all the encouragement, love, and friendship she has provided me with throughout this journey.

Table of Contents

List of Tables

List of Figures

Vadose Zone Processes Affecting Water Table Fluctuations: Conceptualization and Modeling Considerations

Nirjhar Shah

ABSTRACT

This dissertation focuses on a variety of vadose zone processes that impact water table fluctuations. The development of vadose zone process conceptualization has been limited due to both the lack of recognition of the importance of the vadose zone and the absence of suitable field data. Recent studies have, however, shown that vadose zone soil moisture dynamics, especially in shallow water table environments, can have a significant effect on processes such as infiltration, recharge to the water table, and evapotranspiration. This dissertation, hence, attempts to elucidate approaches for modeling vadose zone soil moisture dynamics. The ultimate objective is to predict different vertical and horizontal hydrological fluxes.

The first part of the dissertation demonstrates a new methodology using soil moisture and water table data collected along a flow transect. The methodology was found to be successful in the estimation of hydrological fluxes such as evapotranspiration, infiltration, runoff, etc. The observed dataset was also used to verify an exponential model developed to quantify the ground water component of total evapotranspiration. This analysis was followed by a study which analyzed the impact of soil moisture variability in the vadose zone on water table fluctuations. It was found that

antecedent soil moisture conditions in the vadose zone greatly affected the specific yield values, causing a broad range of water table fluctuations for similar boundary fluxes. Hence, use of a constant specific yield value can produce inaccurate results. Having gained insight into the process of evapotranspiration and specific yield, a threshold based model to determine evapotranspiration and subsequent water table fluctuation was conceptualized and validated.

A discussion of plant root water uptake and its impact on vadose zone soil moisture dynamics is presented in the latter half of this dissertation. A methodology utilizing soil moisture and water table data to determine the root water uptake from different sections of roots is also described. It was found that, unlike traditional empirical root water uptake models, the uptake was not only proportional to the root fraction, but was also dependent on the ambient soil moisture conditions. A modeling framework based on root hydraulic characteristics is provided as well.

Lastly, a preliminary analysis of observed data indicated that, under certain field conditions, air entrapment and air pressurization can significantly affect the observed water table values. A modeling technique must be developed to correct such observations.

Chapter 1: Overview

Vadose zone processes are recognized for controlling both short term dynamics in watershed hydrology and long term water balances of hydrologic basins. The soil moisture variability in the vadose zone also determines the functional type of vegetation that grows in a particular area (Rodriguez-Iturbe and Porporato 2004). In shallow water table environments (depth to the water table < 2 m) the vadose zone not only impacts the surface hydrological processes but also affects the ground water system by influencing processes such as (a) the time scale of recharge to the water table, (b) actual recharge to the water table, (c) evapotranspiration from the soil, and (d) water table fluctuations.

Despite its significance, vadose zone process conceptualization and modeling capabilities are not as developed as those of ground water and/or surface water modeling is (Harter and Hopman 2004). Traditionally the vadose zone has been treated as a lower boundary for the surface water models like HSPF (Bicknell et al. 2001), acting primarily as a sink term to simulate evapotranspiration and recharge or treated as an upper boundary for ground water models like MODFLOW (Harbaugh et al. 2005) where it is conceptualized as a source term thorough which an empirically generate recharge is applied.

The treatment of the vadose zone as a lumped source or sink term, instead of a separate hydrologic system with its own dynamics, can be attributed primarily to two reasons. The first and foremost reason is the absence of suitable data to develop and test

conceptualizations for modeling vadose zone processes, while the second reason lies in the desired output from any modeling exercise. Be it surface water or ground water modeling, the objectives are to either simulate runoff or stream flow, or potentiometric surface, and in the process empirical relationships are used to simulate the expected vadose zone behavior. For instance, the value of recharge is arbitrarily assumed to be some fraction of rainfall and the whole time scale and actual amount of recharge that is influenced by the antecedent vadose zone condition is ignored.

Over last decade or so, however, with an increase in computation power and the need for more accurate modeling, the focus of hydrological modeling has shifted from separate surface and ground water models to an integrated modeling approach wherein both surface and ground water models are run simultaneously and the output of one is used as the input to the other. The critical component of integrated modeling philosophy is the vadose zone which forms the vital link between the surface and ground water models. Hence, it is of real importance to advance the modeling and predictive capabilities for all the vadose zone process.

This dissertation focuses on data collection and conceptualizations to enhance the understanding and modeling of vadose zone processes which ultimately impact the fluctuation of the water table. This document is divided into eight chapters, including this overview chapter. The majority of the text for each chapter is adapted from a corresponding journal article written on the topic. The following chapter describes a data collection effort in which continuous soil moisture data along with water table elevation data is recorded along a flow transect. The chapter, which is adapted in large part from Nachabe, Shah et al. (2005) and Rahgozar, Shah et al. (2007), talks about how the

collected data can be analyzed at a point scale or a along transect to determine evapotranspiration and other water budget components. The approach helps in developing a comprehensive dataset involving time series, spanning approximately two and half years, of all the water budget components. This dataset can prove ideal for constructing and testing modeling considerations as demonstrated in Chapters 3, 4, 6, and 7.

The third chapter, which derives its content from Shah et al. (2007a), talks about a very important problem about extinction depth and partitioning of evapotranspiration between vadose zone and ground water. In many landscapes, vegetation extracts water from both the unsaturated and saturated zones. The partitioning of evapotranspiration (*ET*) into vadose zone *ET* and ground water *ET* is complex because it depends on land cover and subsurface characteristics. Traditionally, the ground water *ET* fraction is assumed to decay with increasing depth to the water table, attaining a value of zero at what is termed the extinction depth. A simple assumption of linear decay with depth is often utilized, but has never been rigorously examined using unsaturated-saturated flow simulations. Furthermore, it is not well understood how to relate extinction depths to characteristics of land cover and soil texture.

Variable saturation flow theory is utilized to simulate ground water *ET* for three land covers and a range of soil properties under drying soil conditions. For a water table within a half a meter of the land surface, nearly all *ET* is extracted from ground water due to the close hydraulic connection between the unsaturated and saturated zones. For deep-rooted vegetation, the decoupling of ground water and vadose zone was found to begin at water table depths between 30 and 100 cm, depending on the soil texture. The decline of

ET with depth to the water table is better simulated by an exponential decay function than the commonly used linear decay. A comparison with field data is consistent with the findings of this study. Tables are also provided to vary the extinction depth for heterogeneous landscapes with different vegetation cover and soil properties.

In Chapter 4, which is based on Shah and Ross (2007), an investigation is provided concerning the variable behavior of specific yield (S_Y) under shallow water table conditions. Traditionally, specific yield has been defined as the volume of water released per unit area from pumping of a phreatic aquifer down by a unit head. It is often used as a fixed value in ground water flow models. The chapter seeks to elucidate S_Y variability due to natural processes of evapotranspiration and recharge. S_Y variability is of fundamental importance for modeling hydrologic response from stresses and for determination of the water budget of a catchment. HYDRUS 1D – a numerical model solving Richard's equation for saturated – unsaturated flow in one dimension was used to simulate the behavior of specific yield for a soil type representative of west-central Florida. It was found, that for various cases examined (e.g., *ET* and infiltration), the magnitude of specific yield varied with depth to the water table. For infiltration response, the variation in the specific yield exhibited strong dependence on the inter-event time. For *ET* stress, the specific yield first increased rapidly to attain a maximum value and then declined steadily to ultimately become less than specific yield at equilibrium moisture conditions. The results indicated that assumptions of constant specific yield for different stresses can yield erroneous results especially in shallow water table environments. For deeper water tables, it was found that specific yield variation was not that pronounced and a constant

value of specific yield can be used as an approximate value for simulating water table fluctuations.

Chapter 5, adapted from Shah et al. (2007b), talks about use of HYDRUS-1D, to analyze evapotranspiration (*ET*) contributions from different regions of the vadose zone. This analysis was based on solving Richard's equation for a soil column subject to *ET* stress and analyzing the changes in the soil water content along the column. The results of the analysis can be used in developing and validating integrated surface and ground water models. Fundamental to integrated modeling is the concept to allocate *ET* demand within the saturated and unsaturated zones. A comparison of the approach of the Integrated Hydrologic Model (IHM) with the solution derived by the one dimensional analysis is presented. The simulation results matched those derived from the IHM three-layer concept. The results validated three of the four thresholds that control *ET* distribution demand along a soil column, as defined in IHM. The fourth threshold matched, but to lesser degree, due to the difference of capillary fringe definitions between the two models.

Chapter 6, adapted from Shah et al. (2007c), describes a dynamic model of water uptake from plants growing in naturally vegetated areas subjected to a rainfall and evaporation time series. The model results are compared and contrasted with popular pre-existing models. Also, the effects of the uptake pattern on the movement of water across multiple soil layers are also analyzed. The results showed that contrary to common modeling approaches, root water uptake is both a function of root distribution and variability in water content.

Following the comparison of derived root water uptake with the traditionally used models, a modeling framework based on physical root distribution and hydraulic characteristics of xylems is presented. The framework using empirical data is found to provide results that closely match the observed root water uptake values. The results greatly increased the confidence in the framework and warrant a more detailed future investigation.

Chapter 7, adapted from Shah et al. (2007d), talks about air entrapment which plays a significant role in controlling infiltration and depth to water table in shallow water table environments. The chapter describes use of field data and numerical modeling, using HYDRUS-1D to quantify the variation of air pressurization values. It was found that lateral flow of air and evapotranspiration between precipitation events have significant effects on soil air pressures. The observations of water table in the field data depart significantly on occasions from the theoretical values using a calibrated Richard's equation solution. Antecedent conditions were also found to be very important in controlling air pressurization. A simple analysis based on the Ideal Gas Law was also done to help understand air pressurization effects. Results indicate that there is a high sensitivity of pressure changes with small air volume changes. Also, an assumption of uniform air pressure over the vadose zone over predicts the pressure decline. The significant contribution of the current analysis is the adaptation of an approach which incorporates multi-event field measurements with varying antecedent conditions. Also, observed and model predicted *ET* volume recovery is explored providing strong evidence of long duration excess air pressures in shallow water table environments.

Chapter 8 concludes the dissertation with summarizing all the important results, their implications on the current state of vadose zone modeling, and talks about the future work needed.

Chapter 2: Estimation of Evapotranspiration and Water Budget Components Using Concurrent Soil Moisture and Water Table Monitoring

2.1 Introduction

It is often useful in modeling or other hydrological studies to quantify components of a water budget. For upland and wetland settings, water budgets are driven principally by precipitation (*P*) and evapotranspiration (*ET).* Given the magnitude of *ET* relative to other processes e.g., infiltration and runoff, quantification of *ET* for different land cover types is critical to transient hydrologic analysis (Sumner 2006). Understanding of the contribution of *ET* from different sources (e.g., interception, shallow, and deep soil) is very valuable for simulation modeling (Ross et al. 2005). Accurate measurement of *ET* components is, however, difficult and unreliable (Nachabe et al. 2005). In humid regions such as west-central Florida, *ET* is estimated to be 70% of precipitation on an average annual basis (Bidlake et al. 1993; Knowles 1996; Sumner 2001). Despite its significance, *ET* is traditionally inferred from values of potential *ET* (*PET*) or reference *ET* (Doorenbos and Pruitt 1977). *PET* data are more readily available and can be computed from either pan evaporation or from energy budget methods (e.g., Penman 1948; Thornthwaite 1948; Monteith 1965; Priestly and Taylor 1972). The above methodologies, though simple, suffer from the fact that meteorological data collected in the field for *PET* are mostly under non-potential conditions, rendering *ET* estimates as erroneous (Brutsaert 1982; Sumner 2006).

Lysimeters can be used to determine *ET* from mass balance, however, for shallow water table environments, they are found to give erroneous readings due to air entrapment (Fayer and Hillel 1986), as well as fluctuating water table (Yang et al. 2000). Remote sensing techniques used in studies such as Kite and Droogers (2000) and Mo et al. (2004) are especially useful for large scale studies. However, in case of highly heterogeneous landscapes, the resolution of *ET* may become problematic owing to the coarse resolution of the data (Nachabe et al. 2005). The energy budget or eddy correlation methodologies are also limited to computing net *ET* and cannot resolve *ET* contribution from different sources.

Recently, Sumner (2006) provided a detailed review of the approximations used in the calculation of *ET*, and based on eddy correlation measurements recommended values of vegetation coefficients to be used to reduce *PET* to *ET*. The coefficients though simple to use in hydrologic models are more a function of ambient water content and particular seasonal rainfall pattern at the time of measurement rather than actual plant tendencies. Hence, during periods of excessive rainfall they may under predict the actual *ET*. Therefore, the use of these coefficients is primarily restricted to areas with similar climatic pattern and water table conditions.

For shallow water table environments, continuous soil moisture measurements have been found to accurately determine *ET* (Nachabe et al. 2005; Fares and Alva 2000). Past studies, e.g., Robock et al. (2000), Mahmood and Hubbard (2003), and Nachabe et al. (2005), have clearly shown that soil moisture monitoring can be successfully used to determine *ET* from a hydrologic balance. The objective of this chapter is to describe two methodologies, one based on estimation of lateral flow, from water table fluctuations, to

determine daily evapotranspiration on non rainy days at a point scale and the second methodology which involves a one dimensional transect model and its use in calculating evapotranspiration along with other components of water budget such as lateral flow, infiltration, interception capture, surface runoff and other fluxes. Specifically, the objectives of this chapter are to: (a) introduce a methodology to estimate the spatiotemporal distribution of *ET* as a function of fluctuating water table measurements, (b) develop a hydrologic model to quantify constituents of the water budget, and (c) study variation of hydrologic fluxes with changes in land use.

The approach herein involves use of soil moisture and water table data collected at different locations along a flow path. For the first model, soil moisture and water table observations from individual wells were used to determine *ET* values on non rainy days while the second model is based on a set of wells along a flow transect and attempts to comprehensively resolve other components of the water budget at the study site. The two approaches show that point scale soil moisture and water table observation may be sufficient to resolve evapotranspiration; however, to get a handle at other components of water budget, transect modeling is needed.

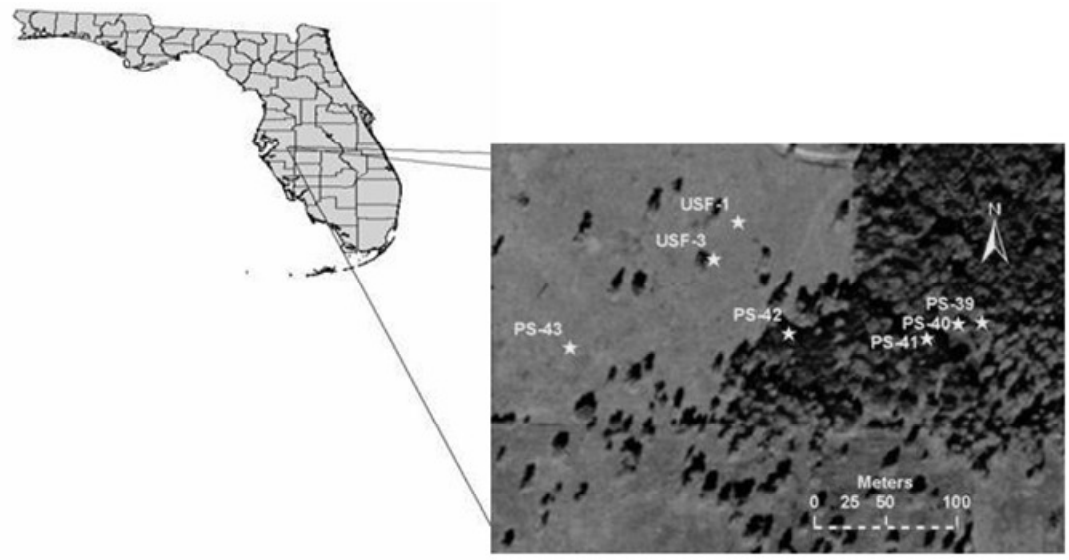

Figure 2.1 Location of the Study Site in Hillsborough County, Florida.

2.2 Materials and Methods

2.2.1 Study Site

The site for this particular study was located in the sub basin of Long Flat Creek, a tributary of the Alafia River, adjacent to the Tampa Bay regional reservoir in Lithia, Florida. Figure 2.1 shows the regional and aerial view of the site location. Two sets of monitoring well transects were installed on the west side of Long Flat Creek. One set of wells designated as PS-39, PS-40, PS-41, PS-42, and PS-43 ran from east to west while the other set consisting of two wells was roughly parallel to the stream (Long Flat Creek), running in the North-South direction. The wells were designated as USF-1 and USF-3.

The topography of the area slopes towards the stream with PS-43 being located at roughly the highest point for both transects. The vegetation varied from ungrazed Bahia grass in the upland areas (in proximity of PS-43, USF-1, and USF-3), to alluvial wetland forest composed of slash pine/ hardwood trees near the stream. The area close to PS-42 is

characterized as a mixed zone. Horizontal distance between the wells is approximately 16, 22, 96, 153 m from PS-39 to PS-43, with PS-39 being approximately 6 m from the creek. Horizontal distance between USF-1 and USF-3 was 33 m. All wells were surveyed and land surface elevations were determined with respect to National Geodetic Vertical Datum 1927 (NGVD).

Extensive soil investigations were performed on the soil cores taken from the study site. The soil in the study area is primarily Myakka fine sand (of marine origins) with high permeability (10^{-1} to 10 m/d) in the surface and subsurface layers (Carlisle et al. 1989). Figure 2.2(a and b) shows sample soil stratiagraphy obtained from two cores taken from the study site close to wells PS-39 and PS-43. The results of soil sampling at a number of locations along the East-West as well as North-South transect showed that the soil was primarily sand with the presence of a clay layer at a depth, that varied from 4m below land surface in the upland regions to about 2.5 m below land surface near the stream region. Detailed information on soil and site characteristics can be found in Thompson (2003) and Trout and Ross (2005). Apart from the study specific tests, information about extent of the confining clay layer, hydraulic conductivity values of the confinement, head differences between surficial and intermediate aquifer, were obtained from the geotechnical and site characterization report (HDR and Tampa Bay Water 1999) prepared as a part of the construction of Tampa Bay regional reservoir. The report indicates (Refer to volume 1 section 3) that thickness of the clay layer averages around 3-5 m with average head differences between the surficial and intermediate aquifer being

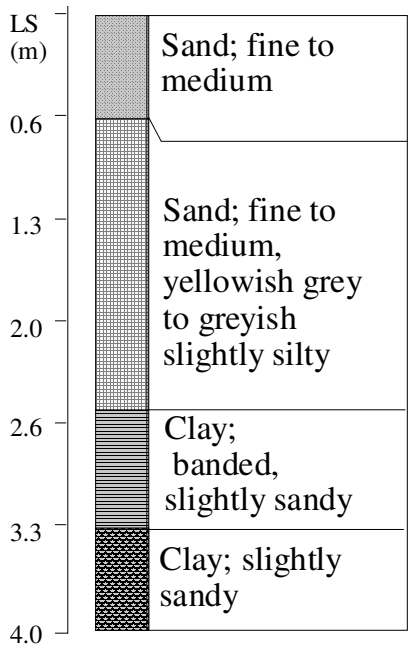

(a)

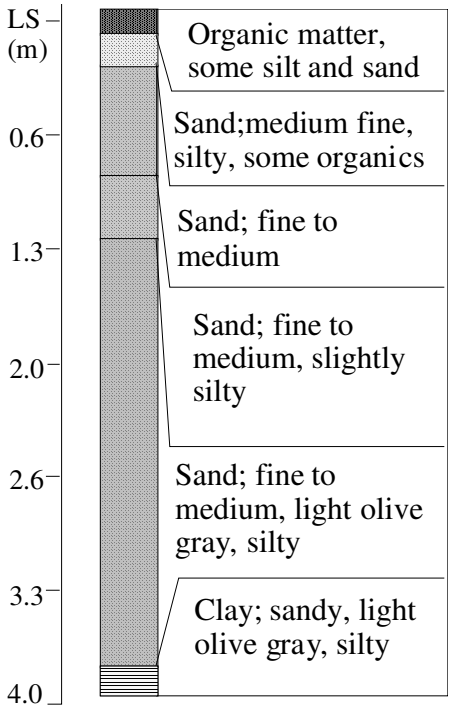

(b)

Figure 2.2 Soil Stratiagraphy of Cores Taken from Locations Adjacent to (a) PS-39 and (b) PS-43. Notice that Soil at Both Locations is Primarily Sandy Bounded by a Clay Layer.

approximately 6 m. The hydraulic conductivity values – as determined by slug test and deep aquifer performance test – for the confining clay layer varied from 10^{-4} m/day to 10^{-5} m/day. The lower confining layer can hence be assumed as an impermeable layer. Data collection for the study was done from January 2002 through June 2004.

2.2.2 Instrumentation

All transect wells housed Instrumentation Northwest (Kirkland, WA) 0-34 kPa (0-5 psi) submersible pressure transducers, accurate to 0.034 kPa (0.005 psi). Adjacent to each well, an EnviroSMART® soil moisture probe (Sentek Pty. Ltd., Adelaide, Australia) carrying eight sensors was installed (see Figure 2.3). The soil moisture sensors allowed measurement of moisture content along a vertical profile at different depths from land surface. The sensors were deployed at 10, 20, 30, 50, 70, 90, 110, and 150 cm from the land surface. The sensors work on the principle of frequency domain reflectometery (FDR) to convert electrical capacitance shift to volumetric water content ranging from oven dryness to saturation with a resolution of 0.1% (Buss 1993). Default factory calibration equations were used for calibrating these sensors. Fares and Alva (2000) and Morgan et al. (1999) found no significant difference in the values of observed recorded water content from the sensors when compared with the manually measured values.
In addition to pressure transducers and soil moisture probes, stream gages were placed at three locations in the adjacent perennial creek (Long Flat Creek). Two tipping bucket and two manual rain gages were also installed to record the amount of precipitation.

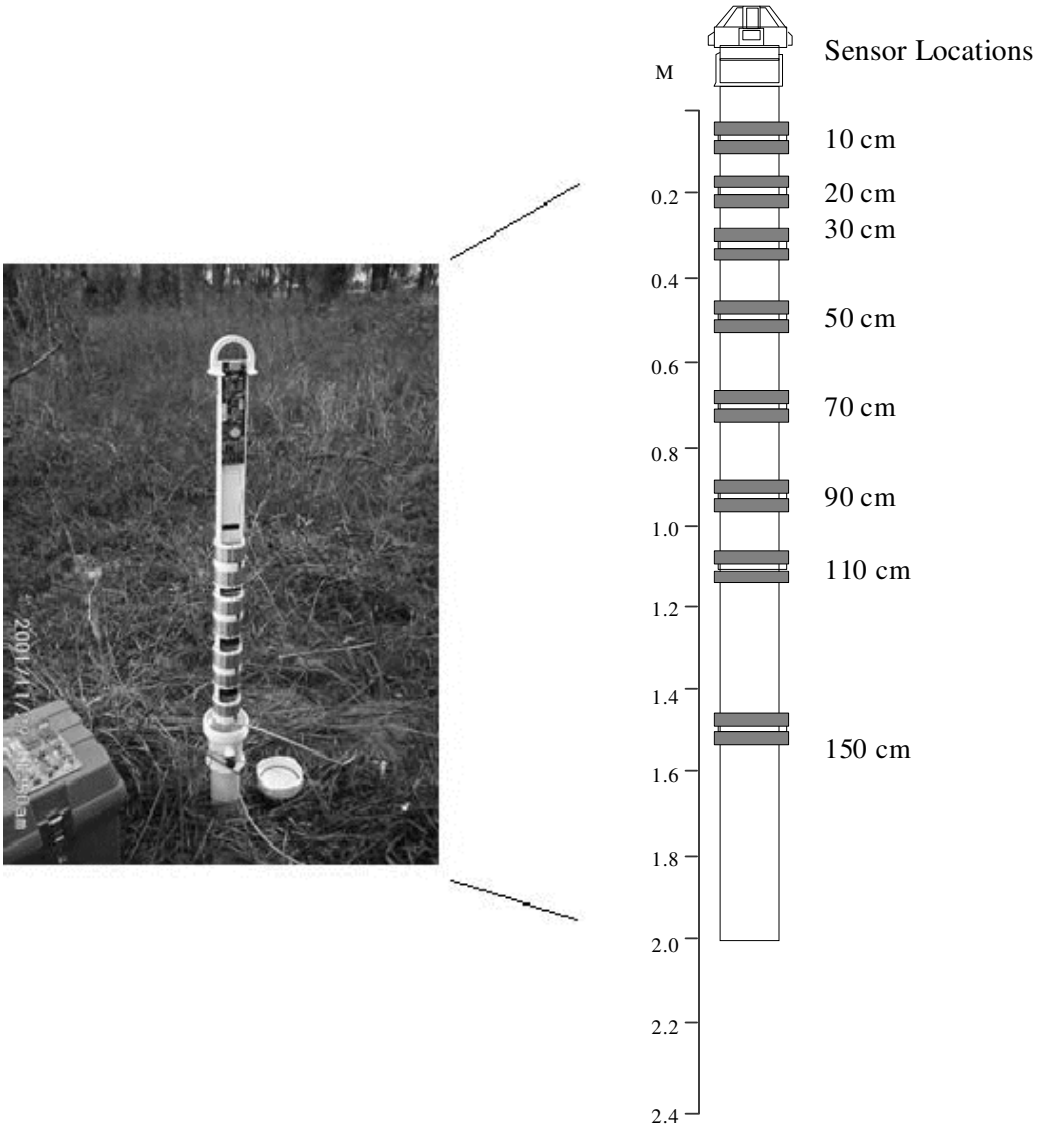

Figure 2.3 Soil Moisture Probe on the Left Showing the Mounted Sensors Along with Schematics on the Right.

All equipments were installed according to National Weather Service or USGS standards where applicable. The data were collected on a 5 minute interval (instantaneous) and were averaged to hourly values.

In case of missing water table elevation data from a particular location, interpolation of water table heads from the adjacent station was used to complete the record. For soil moisture data, however, no attempt was made to simulate the missing data. Instead, a different methodology, relying on water table observations and a variable specific yield calculation, calibrated for the site based on the results of Said et al. (2005), was used to derive storage changes. Data gaps were, however, infrequent and comprised less than 5% of the data record. During the entire study period the water table was found to fluctuate between land surface and a maximum depth of about 140 cm for all of the well locations.

2.2.3 Point Scale Modeling of Evapotranspiration

At any given well location, variation in total soil moisture on non-rainy days can be due to (a) subsurface flow from or to the one dimensional soil column (0–155 cm below land surface) over which soil moisture is measured and (b) evapotranspiration from this soil column. Mathematically it can be expressed as

$$\frac{\partial TSM}{\partial t} = Q - ET \tag{2.1}$$

where t is time (h), Q is subsurface flow rate (m/h), and ET is evapotranspiration rate (m/h). TSM is total soil moisture, determined as below

$$TSM = \int_{\varsigma} \theta \, dz \tag{2.2}$$

where θ [L^3L^{-3}] is the measured water content, z [L] is the depth below land surface ζ [L] is the depth of monitored soil column (155 cm).

The negative sign in front of *ET* in Equation 2.1 indicates that *ET* depletes the *TSM* in the column. The subsurface flow rate can be either positive or negative. In a ground water discharge area, the subsurface flow rate, *Q*, is positive because it acts to replenish the *TSM* in the soil column (Freeze and Cherry 1979). Obviously, this flow rate is negative in a ground water recharge area. Figure 2.4 illustrates the role of subsurface flow in replenishing or depleting total soil moisture in the column. To estimate both *ET* and Q in Equation 2.1, it was important to decouple these fluxes. In this model the subsurface flow rate was estimated from the diurnal fluctuation in *TSM*. Assuming *ET* is effectively zero between midnight and 0400h, *Q* can be easily calculated from Equation 2.3 using:

$$Q = \frac{TSM_{0400\ h} - TSM_{midnight}}{4} \tag{2.3}$$

where TSM_{0400h} and $TSM_{midnight}$ are total soil moisture measured at 0400 h and midnight, respectively. The denominator in Equation 2.3 is 4h, corresponding to the time difference between the two TSM measurements. The assumption of negligible *ET* between midnight and 0400h is not new, but was adopted in the early works of White (1932) and Meyboom (1967) in analyzing diurnal water table fluctuations. It is a reasonable assumption to make at night when sunlight is absent.

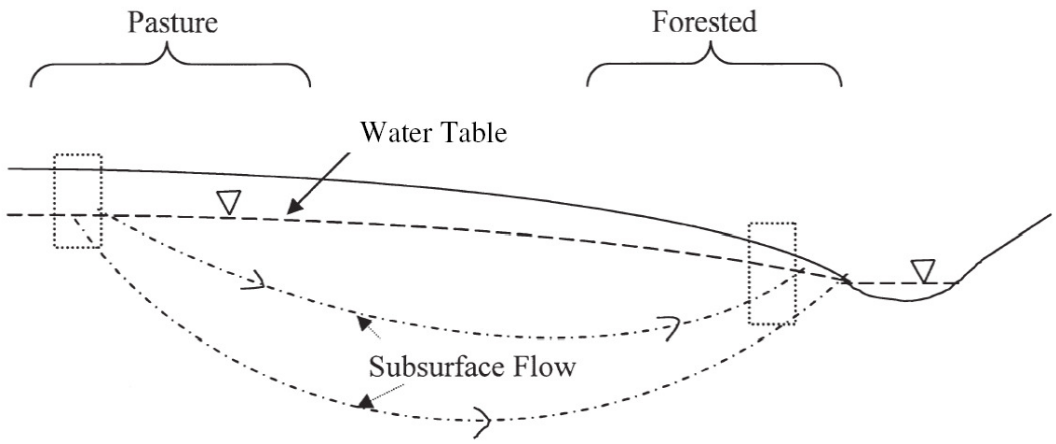

Figure 2.4 Total Soil Moisture is Estimated in Two Soil Columns. The First is in a Ground Water Recharge Area (Pasture), and the Second is in a Ground Water Discharge Area (Forested). In the Ground Water Discharge Area, Subsurface Flow Acts to Replenish the Total Soil Moisture.

Taking Q as constant for a 24h period (White 1932; Meyboom 1967), the ET consumption in any single day was calculated from the following equation

$$ET = TSM_{j} - TSM_{j+1} + 24 \times Q \qquad (2.4)$$

where TSM_j is the total soil moisture at midnight on day j, and TSM_{j+1} is the total soil moisture 24h later (midnight the following day). Q is multiplied by 24 as the Equation 2.4 provides daily ET values. Figure 2.5(a and b) show a sample observations for 5 day period showing the evolution of TSM in a ground water discharge and recharge area respectively. Also marked on the graphs are different quantities calculated to determine ET from the observations.

Equation 2.1 applies for dry periods only, because it does not account for the contribution of interception storage to ET on rainy days. Also, the changes in soil moisture on rainy days can occur due to other processes like infiltration, upstream runoff

infiltration (as will be discussed later), etc. The results obtained from the above model were averaged based on the land cover of each well and are presented as *ET* values for grass or forested land cover. The values for the grassed land cover were also compared against *ET* values derived from pan evaporation measurements. The model results, as well as comparison graphs are discussed in the results section.

2.2.4 One Dimensional Transect Model

In an attempt to comprehensively determine other components of water budget for both rainy or non rainy days two separate transect models were developed, one for wells PS-39 to PS-43 and one for wells USF-1 to USF-3. The first model was setup with five grid cells, with the location of the observation wells being the center of each of the grid cells and the observed values representative of the whole grid. Transect's upland flow divide comprised one boundary (no flow) and the stream with variable stage comprised the other (stage boundary). The second model, however, had just two cells with USF-1 and USF-3 representing the two internal storage measurements. Flows at each internal cell boundary were derived from nodal (cell centered) observed records and a simple Darcian flow calculation. Figure 2.6 shows the transect model for wells PS-39 to PS-43 with details about land surface elevation, distances between the wells, etc.

For both the models, the upper boundary was the land surface and the lower boundary was conceptualized as a no-flow boundary condition, quite appropriate for the surficial aquifer at the site (Trout and Ross 2005; HDR and Tampa Bay Water 1999). The

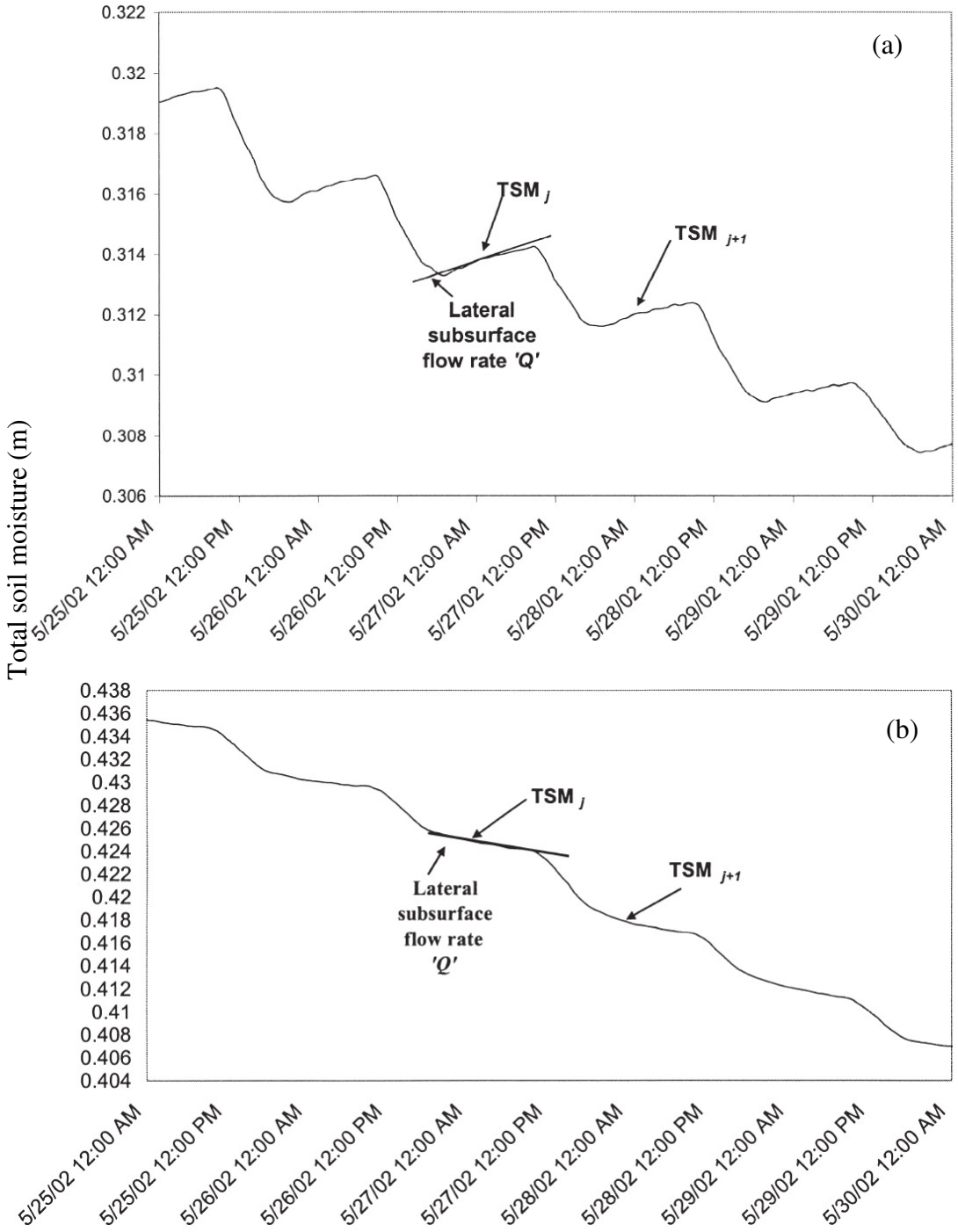

Figure 2.5 Total Soil Moisture versus Time in the (a) Ground Water Discharge Area and (b) Ground Water Recharge Area. The Subsurface Flux is the Positive Slope of the Line between Midnight and 4 AM.

flow thickness was determined by the depth to the water table and the local depth to the underlying clay confinement. The flow occurring along the transect was assumed to be uniform (non-convergent) across the width of the model.

For each grid cell the equivalent hydraulic conductivity obtained from the laboratory measurements (refer to section 2.2.4.1) was used in the application of the mass balance equations. The following paragraphs summarize the basis of the one dimensional transect model used to derive *ET*. Table 2.1 lists the notation with description and dimensions of each of the symbols used.

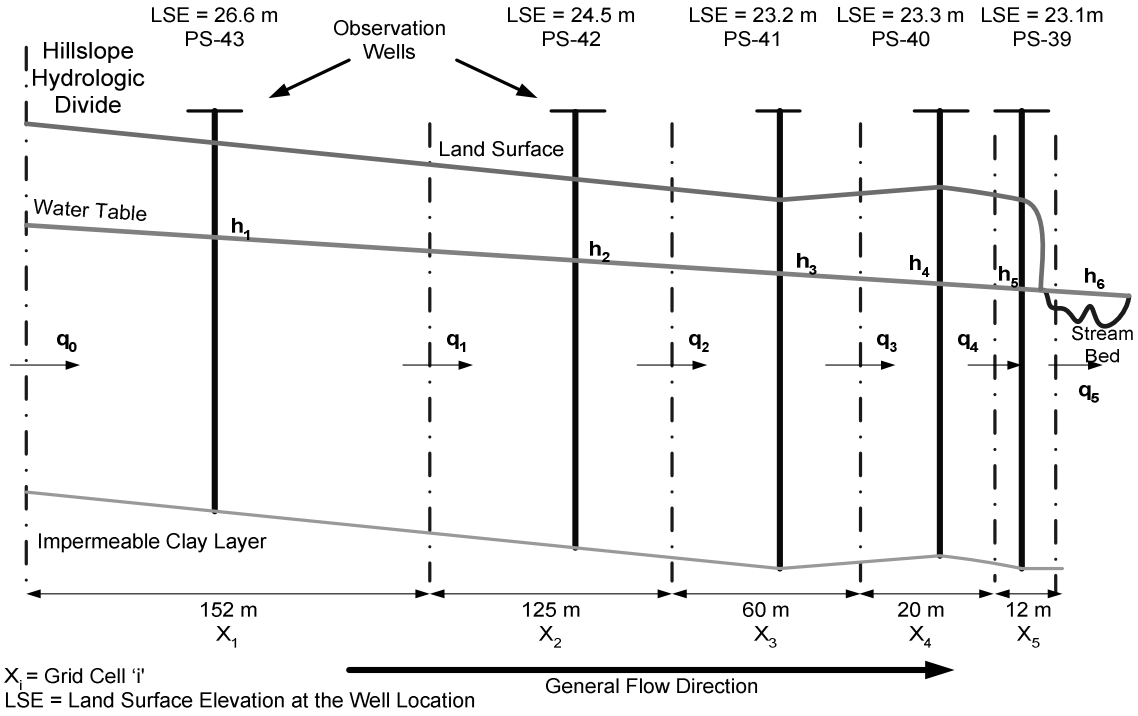

Figure 2.6 One Dimensional Transect Model for Well Transect PS-39 to PS-43 (Not to Scale).

Table 2.1 Notations Used in the 1D Transect Model Along with Description and Units of Each Symbol.

Notation	Description	Units
P	Precipitation	$[LT^{-1}]$
d_{wt}	Depth to the water table	[L]
ET	Evapotranspiration	$[LT^{-1}]$
I	Infiltration	$[LT^{-1}]$
I_S	Daily soil infiltration	$[L^3L^{-2}]$*
$SMET$	Evapotranspiration from soil moisture	$[LT^{-1}]$
q	Specific lateral discharge	$[L^3L^{-1}T^{-1}]$
S	Water storage in the soil column per unit width	$[L^3L^{-1}]$
θ	Water content	$[L^3L^{-3}]$
ΔX_i	Lateral dimension of i^{th} grid cell	[L]
K	Hydraulic conductivity	$[LT^{-1}]$
τ_i	Effective flow thickness in the i^{th} grid cell	[L]
P_E	Effective rainfall	$[L^3L^{-2}]$*
I_C	Interception capture	$[L^3L^{-2}]$*
URI	Upstream runoff infiltration	$[L^3L^{-2}]$*
$DS\ ET$	Evapotranspiration from depression storage	$[L^3L^{-2}]$*
TET	Total evapotranspiration	$[L^3L^{-2}]$*
TRE	Total rainfall excess	$[L^3L^{-2}]$*
NR	Net runoff	$[L^3L^{-2}]$*
HR	Hortonian runoff	$[L^3L^{-2}]$*
SER	Saturation excess runoff	$[L^3L^{-2}]$*
SI	Soil infiltration	$[LT^{-1}]$

*Accumulated on daily time step

The water budget equation for the model can be written as:

$$[SI - SMET]\Delta X = \Delta S/\Delta t + \Delta q \tag{2.5}$$

where SI [$L^3L^{-2}T^{-1}$] represents soil infiltration, $SMET$ [$L^3L^{-2}T^{-1}$] is soil moisture evapotranspiration from the soil column, ΔX is the lateral dimension of a grid cell (see Figure 2.6) , Δq [$L^3L^{-2}T^{-1}$] is net lateral flow from the adjoining cell(s), ΔS is change in total storage of water in the grid cell [L^3L^{-1}] per unit width, and Δt [T] represents the time step (one hour).

As the maximum depth to the water table (d_{WT}) was 140 cm, changes in the water storage in any grid cell can be effectively inferred by integrating the observed soil moisture through the soil profile (0-155 cm), and subtracting the consecutive storage values in time. The trapezoidal rule of numerical integration was used to calculate the total soil moisture from the observed values from the sensors. Mathematically, the changes in storage per unit width at any time'$t + \Delta t$' from time't' for a given grid cell 'i' of lateral dimension ΔX_i [L] can be computed as

$$\Delta S(t+\Delta t)_i = \left(\int_0^{\lambda} \theta(z, t+\Delta t)\,dz - \int_0^{\lambda} \theta(z, t)\,dz \right) \Delta X_i \tag{2.6}$$

where λ [L] is a fixed depth of soil which for all the wells was 155 cm.

From recorded values of d_{WT} and known land surface elevations, water table head, h_i (at any cell *'i'*), with respect to NGVD can be computed. Hence, using Darcy's Law with computed values of equivalent hydraulic conductivity, $\overline{K}_i$ [LT^{-1}], for a given grid cell *'i'*, flow from cell *'i-1'* to cell *'i'* , q_{i-1} at any time 't', can be computed as :

$$q_{i-1} = -\overline{K}_i \overline{\tau}_i \left[\frac{h_i^t - h_{i-1}^t}{\Delta X_i} \right] \tag{2.7}$$

where $\bar{\tau}_i$ [L]is the effective flow thickness for the cell, which is the difference between the water table elevation and the elevation of the confining clay layer at each time step. Other symbols are as previously defined. By simply changing the parameters, flow from cell *i* to cell *i+1,* q_i can be similarly computed. For the fifth cell (PS-39), however, the stream stage was used as the head value to compute the lateral flow going into or coming from the stream.Net lateral flow into cell *'i'* can thus be calculated as in Equation 2.8.

$$\Delta q_i^t = q_{i-1}^t - q_i^t \tag{2.8}$$

In a given time step (hourly), depending on the algebraic sum of terms on the right hand side of Equation 2.5, either soil infiltration or soil evapotranspiration is assumed to be occurring. An inherent assumption made here is that, during the small time interval (hourly) of the analysis, either soil surface evaporation or infiltration can take place. *SMET* is representative of direct soil evaporation and/or plant transpiration from the soil column. *SMET* values from soil moisture change, for each cell, are summed up over a 24 hour period (midnight to midnight) to get an estimate of daily soil moisture *ET (SMET)* from that grid cell. To determine total *ET* (*TET*), depression storage *ET* (*DS ET,*) and interception *ET* (I_C *ET*) (explained in sections 2.2.5.5 and 2.2.5.1 respectively) are also added to daily *SMET*. On the other hand, the soil infiltration values were associated directly with precipitation and/or upstream runoff infiltration (refer to section 2.2.5.3). Like the *SMET,* values soil infiltration, were further aggregated over 24 hours to determine net Infiltration (I_S), which is used to find other water budget components such as total rainfall excess, runoff, etc. (refer to section 2.2.5)

2.2.4.1 Estimation of Hydraulic Conductivity

To get a good idea about the soil conditions at the study site several undisturbed soil samples, using a hydraulic coring machine (GeoProbe®), were obtained. The samples were then analyzed to determine the stratiagraphy. The section of soil cores corresponding to each stratum were then cut and wetted for two days to saturate them completely. Falling head permeameter analysis was done to determine the saturated hydraulic conductivity (K) of the samples. For specific details about permeameter tests and other soil analyses please refer to Thompson (2003). Table 2.2 shows the depths and corresponding values of hydraulic conductivity values obtained for samples close to different well locations. Each soil strata was assumed to be isotropic and hence within a given strata of soil, vertical hydraulic conductivity will be same as the horizontal hydraulic conductivity. Using this assumption equivalent horizontal saturated hydraulic conductivity can be determined using the thickness weighted average of individual hydraulic conductivity values (Equation 2.9)

$$\overline{K} = \frac{\sum K_i dz}{\sum dz} \tag{2.9}$$

where dz is the depth of each strata, K_i is the corresponding values of saturated hydraulic conductivity and $\overline{K}$ as defined above, is the equivalent hydraulic conductivity. At any time step depending on the depth to the water table, the zone of saturation is determined and, based on the saturated soil layers, the equivalent value of hydraulic conductivity is calculated for each time step.

Apart from the permeameter test, in situ slug tests were done to estimate the general hydraulic conductivity of the surficial aquifer. The results of the slug tests were

analyzed using the Bower-Rice as well as the Hvorslev methods. The results indicated the horizontal hydraulic conductivity of the aquifer varied between around 0.5 m/day to 0.1 m/day which is within 10-15% of the laboratory obtained values. For further details about the results please refer to Thompson (2003).

Table 2.2 Values of Hydraulic Conductivity Obtained from Permeameter Analysis Done on Soil Core Samples Taken at Different Depths Below Land Surface [Adapted from Thompson (2003)].

Location (Closest Well)	Mean Depth Below LS (m)	Hydraulic Conductivity (m/day)
USF-1	0.76	1.33
	1.11	0.084
	1.675	2.72E-04
USF-3	0.61	0.44
	1.11	0.08
	1.98	2.20E-04
	2.27	1.67E-04
PS-43	0.45	5.60E-02
	1.675	3.30E-01
	2.89	4.10E-01
	3.5	3.79E-04
PS-42	0.45	1.23E+00
	0.99	3.50E-01
	1.145	4.20E-02
	2.34	3.30E-02
PS-41	0.54	2.00E-01
	1.15	1.27E-03
	2.36	1.05E-04
PS-39/PS-40	0.125	1.03
	0.3	0.64
	2.89	4.74E-04
	3.12	1.40E-04

2.2.5 Estimation of Lateral and Vertical Fluxes

The one dimensional transect model was run on hourly time steps to calculate the lateral flow, soil infiltration and soil moisture *ET*. Soil moisture evapotranspiration and infiltration were then aggregated over 24 hours to determine the values of daily *SMET* and daily soil infiltration (I_S). Using these aggregated daily values and the procedure described in the following subsections, other water budget components were calculated on a daily time step.

2.2.5.1 Interception Capture (I_C)

Interception capture is the initial extraction from a rainfall event. If there is no runoff accompanied with of a given rainfall event, than, theoretically, it can be estimated by subtracting the observed rainfall from the observed infiltration.

In absence of any direct measurement of runoff, interception capture can be estimated by selecting isolated events with intensity less than the hydraulic conductivity of the surface soil layers, occurring after dry antecedent conditions (deep water table conditions); for such events, runoff can be assumed to be negligible. For this particular study, for a particular land cover, individual rainfall events, which satisfied the above mentioned criteria, were manually selected and were plotted against the observed soil infiltration during the time the event lasted. Assuming that the interception capture is same for all the events for a given land cover the intercept of the best fit line on the precipitation versus infiltration curve will give the value of the interception capture (I_C). To avoid any bias arising out of small precipitation events (smaller than interception

capture), all the precipitation events for which no soil infiltration was observed were ignored during the linear regression to get equation of the best fit line.

2.2.5.2 Effective Precipitation (P_E)

On a daily time step effective precipitation *(P_E)* is defined as the difference between the cumulative precipitation (from midnight to midnight) and the interception capture

$$P_E = \sum_{24\,hrs} P - I_C \tag{2.10}$$

where, P [LT^{-1}] is the recorded precipitation, and I_C [L] is the interception capture.

2.2.5.3 Upstream Runoff Infiltration (*URI*)

For any well location if daily soil infiltration (I_S) is greater than the effective precipitation (P_E), the difference between the two is assumed to correspond to upstream runoff infiltration (*URI*). Mathematically, it can be written as

$$URI = \begin{cases} I_S - P_E & if \;\; I_S > P_E \\ 0 & Otherwise \end{cases} \tag{2.11}$$

2.2.5.4 Infiltration (*I*)

Daily infiltration (*I*) is defined as the difference between daily soil infiltration and upstream runoff infiltration. The value indicates how much of the water from the rainfall actually went in to the ground and is useful when quantifying runoff.

$$I = I_S - URI \tag{2.12}$$

2.2.5.5 Depression Storage *ET* (*DS ET*)

It is known that when the water table is close to the land surface, such that the capillary fringe (zone of tension saturation) starts intersecting the land surface (i.e. d_{WT} < capillary fringe), the evapotranspiration occurs at potential (Shah et al. 2007). Hence, to calculate the depression storage *ET* under these conditions, potential *ET* values needs to be estimated. Subtracting interception capture and daily *SMET* from the potential *ET* will hence result in *DS ET*.

To estimate the potential *ET* several methods can be used. For this particular study, the Jensen and Haise (1963) method was used to estimate *PET*. The equation (Equation 2.13) used is

$$ETP_{J\&H} = \left[\frac{R_S}{2450} \times ((0.025 \times T_{ave}) + 0.08) \right] \tag{2.13}$$

The input parameters to get hourly values of $ETP_{J\&H}$ are solar radiation (R_S) (kJ/m^2/hr) and average temperature (T_{ave}) (°C). The hourly values were accumulated over one day to get daily $ETP_{J\&H}$. At the site, USGS standard class A pan and a weather station measuring solar radiation, temperature and relative humidity were installed and monitored. The site measured data was further supplemented with National Weather Service (NWS) Ona station [NWS station # 086539-4] record. A constant pan factor of 0.7 was used to reduce the $ETP_{J\&H}$ values to potential *ET* values appropriate for the study site (Ross et al. 2005). During these brief, shallow water table periods, the sum of interception capture and soil moisture *ET* were than subtracted from the calculated potential *ET* to estimate the depression storage *ET*.

From a field study, Said et al. (2005) found that, on average, the capillary fringe value for the soils in the study area (for all land covers) was uniform and approximately 0.3 m. Therefore, the depth to the water table threshold for assumption of evapotranspiration being at potential was set for all times when daily average depth to the water table ≤ 0.3 m. Mathematically, for depth to the water table less than 0.3 m, *DS ET* can be calculated by

$$DS\ ET = PET - I_C - daily\ SMET \tag{2.14}$$

2.2.5.6 Total *ET* (*TET*)

Total *ET* (*TET*) was determined on a daily basis by summing up the value of daily SM*ET*, *DS ET* and the interception capture (*Ic*). The underlying assumption being that all the interception capture evaporates within one day, considered reasonable for the sub-tropical west-central Florida conditions at the study site (Nachabe et al. 2005).

2.2.5.7 Total Rainfall Excess (*TRE*)

Total rainfall excess (*TRE*) is defined as the amount of effective precipitation that is not reflected as infiltration. Mathematically, for any time step, TRE can be computed as

$$TRE = P_E - I \tag{2.15}$$

2.2.5.8 Saturation Excess Runoff (*SER*), Hortonian Runoff (*HR*), and Net Runoff (*NR*)

As mentioned previously in section 2.2.5.5, the capillary fringe depth for the study site was found to be 0.3 m. Therefore, if the d_{WT} is less than this value, then all of

the rainfall excess is assumed to be contributing to Saturation Excess Runoff (*SER*). *TRE* is otherwise assumed to be associated with Hortonian Runoff (*HR*). Mathematically,

$$TRE = \begin{cases} SER & if \quad d_{WT} \le 0.3m \\ HR & if \quad d_{WT} > 0.3m \end{cases} \tag{2.16}$$

On a daily basis, total rainfall excess goes into filling up surface depressions as well as part of it runs off downstream. Hence the amount of rainfall excess that runs off from a particular well (Net Runoff NR), and infiltrates downstream (as URI for a downstream well) and/or flows into the stream can be quantified using Equation 2.19. If total rainfall excess was found to be smaller than *DS ET*, than *NR* was assumed to be zero

$$NR = TRE - DS\ ET \tag{2.17}$$

The results presented in this paper were then averaged to obtain quarterly values, i.e., four values per year. In the results and discussion section, the winter quarter represents the months of January to March, spring represents April through June, the summer quarter goes from July through September and fall ranges from October to December. On a quarterly basis, to check the performance of the model, mass balance was done on quarterly values of all the water budget components.

Figure 2.7 shows a flow chart which shows the whole process of calculation of different components of the water budget.

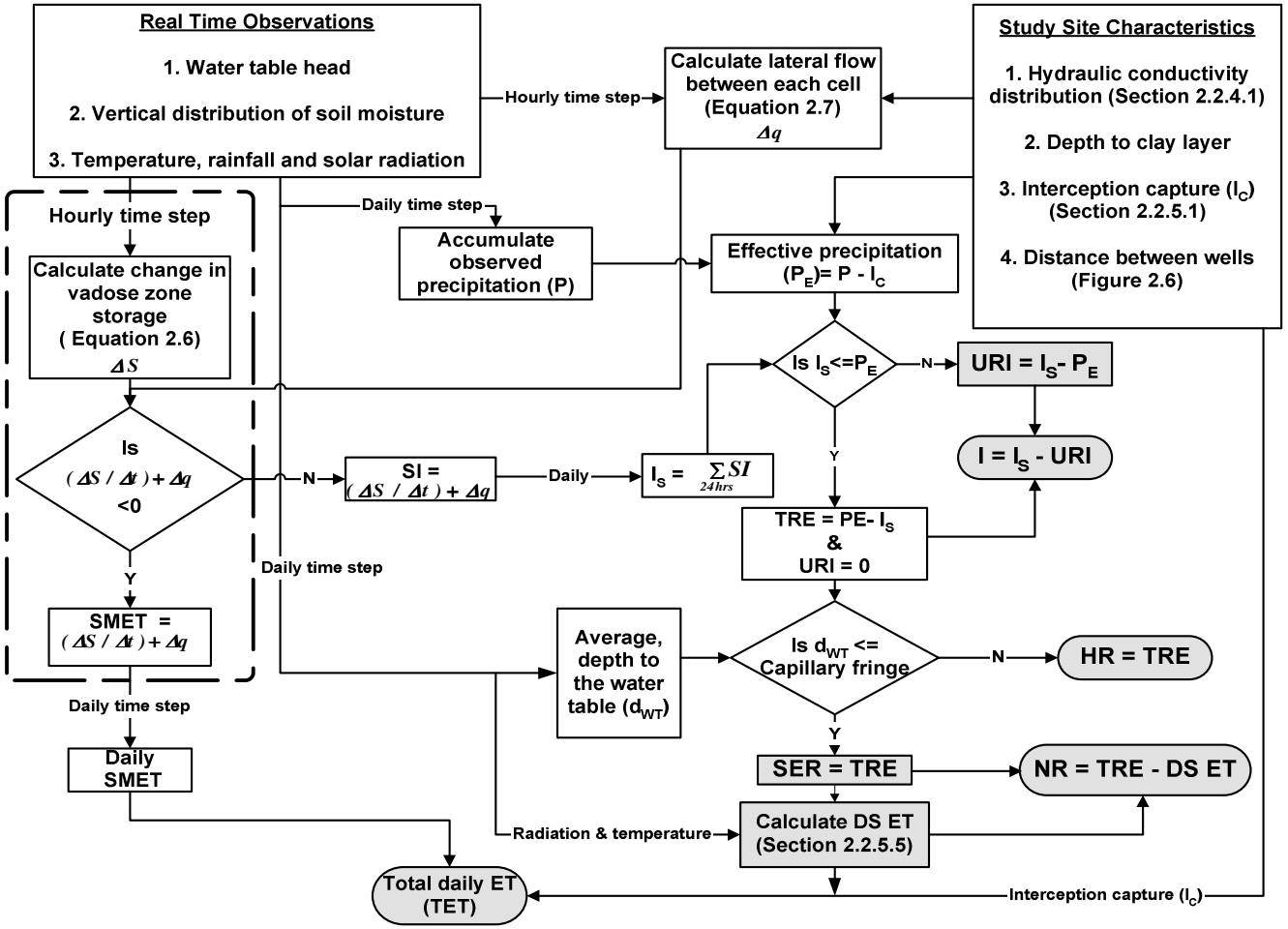

Figure 2.7 Process Flow Diagram Showing the Sequence of Calculation of the Water Budget Components. The Gray Boxes Show the Computed Components. The Area Marked Out by the Dashed Line Represent the One Dimensional Transect Model Running on Hourly Time Step.

2.2.6 Assumptions

Before discussing the results obtained from the analysis it is very important to categorically define the important assumptions in the methodology. This will help the reader in deciding which of the assumptions hold true as well as which assumptions have to be adapted for successful extension of the above methodology at a site different that the study area for this paper.

(a) For any given small time step (hourly), it was assumed that there was either net infiltration into or a net evapotranspiration out of soil grid cell.

(b) The interception capture values for the land cover adjacent to a given well were assumed to be constant for all the quarters.

(c) On a daily basis, interception capture is the initial extraction from total rainfall which is bounded by an upper limit controlled by the vegetation.

(d) On a daily basis interception capture is assumed to be totally evaporated before the start of the next day.

(e) Owing to the low value of permeability of the confining clay layer leakage to intermediate aquifer was neglected.

2.3 Results and Discussion

An important aspect to be considered for the success of this framework is the time scale of variation of the soil moisture storage with respect to external stresses. Figure 2.8(a) to (d) shows the response of the soil moisture storage to different external factors; water table fluctuations, rainfall, and solar radiation. The figures show that soil moisture changes are very responsive (time scale of minutes) to imposed stresses. Also, integrated

storage changes accumulated over time are very consistent with observed rainfall fluxes. Figure 2.8(b) shows that even at sub-hour time steps, changes in the solar radiation (due to passing clouds, etc.) caused variations in the soil moisture storage (root water uptake). Figures 2.8(c) and (d) show the contrasting diurnal fluctuations of the soil moisture changes along with the water table for two locations, one in a forested area (PS-41) and the other in a grassed area (PS-43). Finally, Figure 2.8(a) shows the intuitive, yet important process of soil moisture increase due to rainfall and decrease in its absence. It is noted that, repeatedly, the magnitude of integrated soil moisture change is consistent with the observed rainfall totals (minus interception capture). Overall, Figures 2.8(a) to 2.8(d) conclusively show that the soil moisture measurements can be used as an effective indicator (with high reliability) of soil moisture changes at the time scale of hours. Thus, a high degree of confidence in the use of soil moisture observations for deriving soil moisture fluxes can be expected.

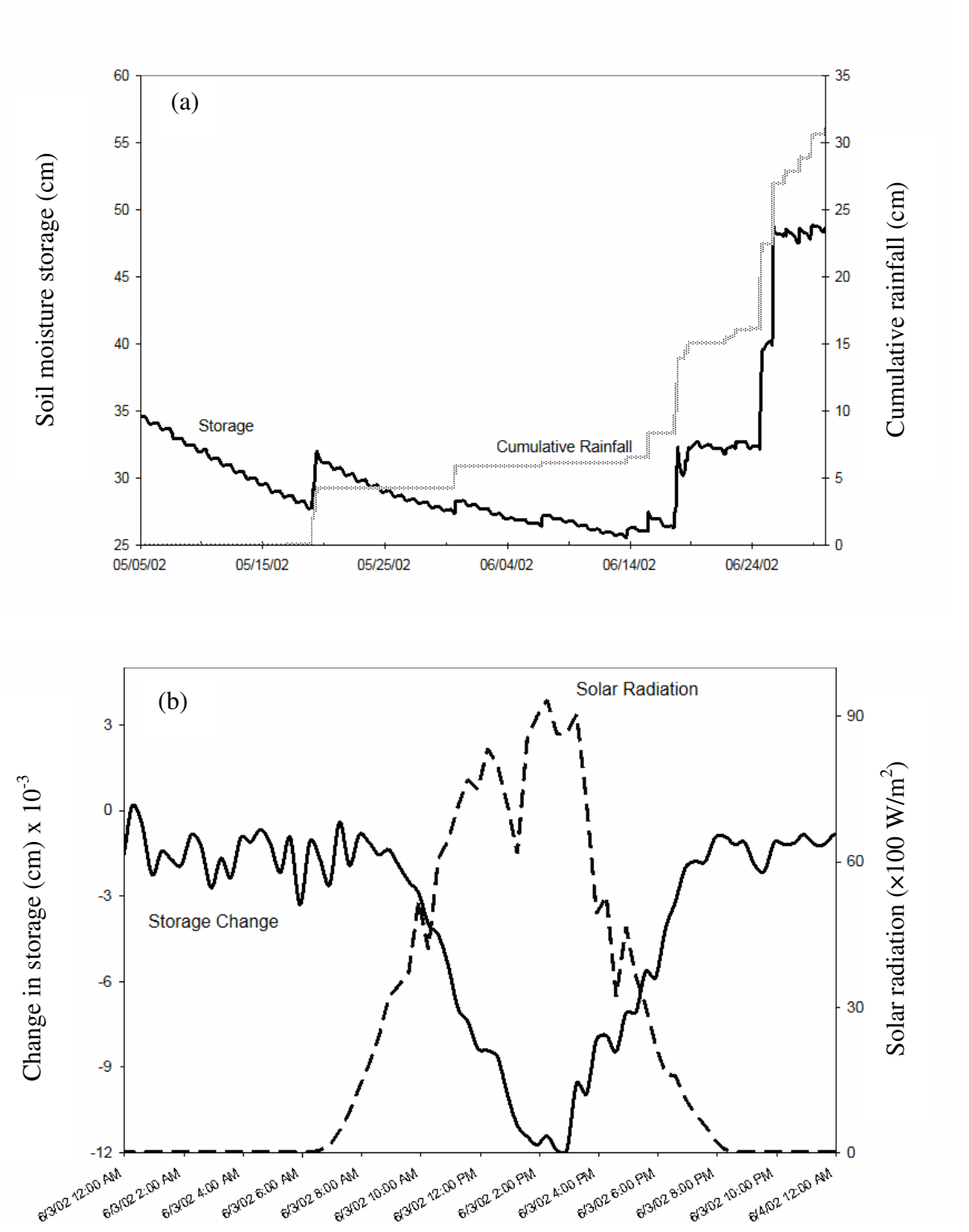

Figure 2.8 Variation of Soil Moisture Storage Due to Different Stresses. (a) Rainfall, (b) Solar Radiation, (c) Water Table for PS-41, and (d), Water Table for PS-43.

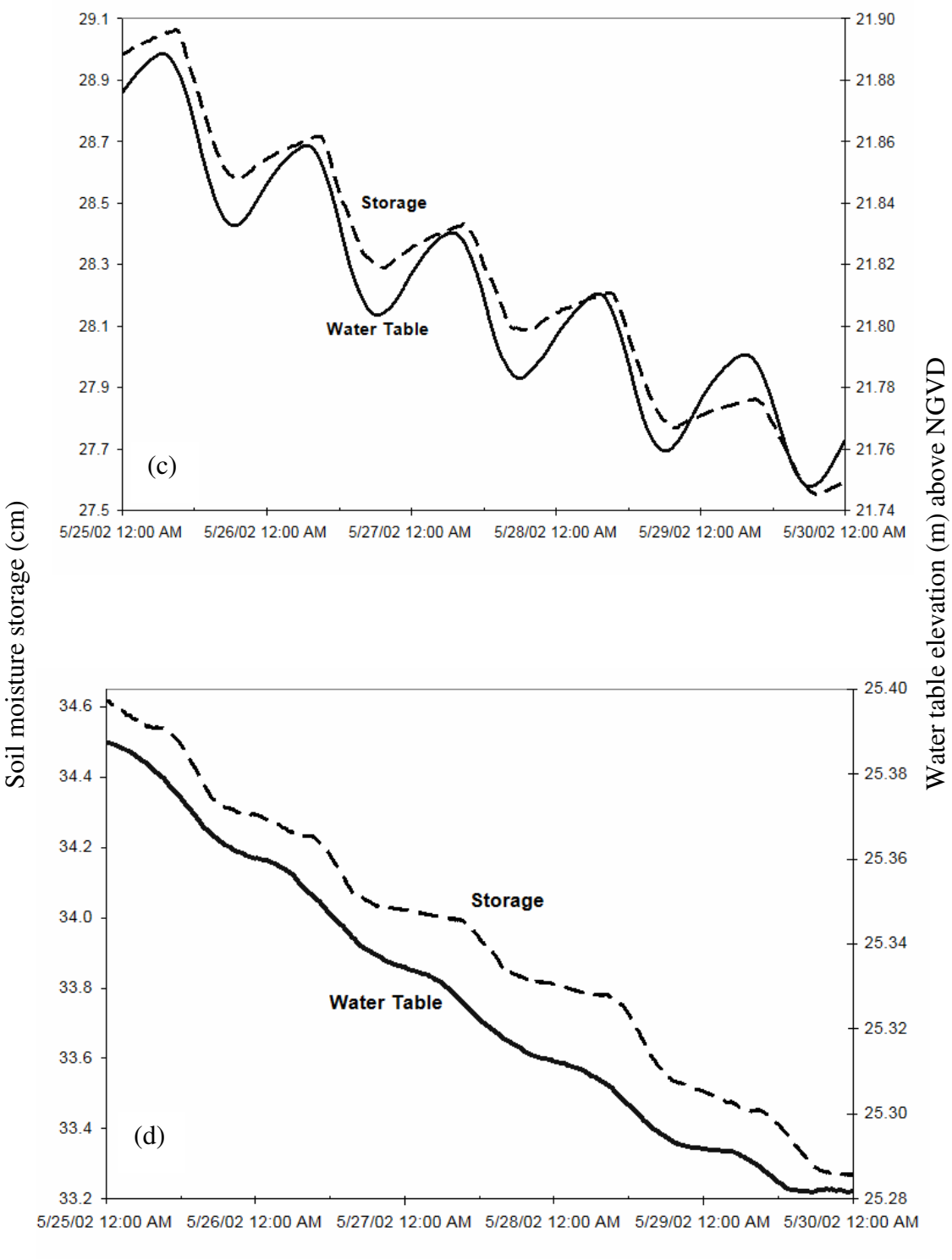

Figure 2.8 (Continued)

2.3.1 Point Scale Model

The results of the point scale model are shown in Figure 2.9 with graph showing the monthly variability in the values of *ET* for a period of about a year and half. It can be seen from Figure 2.9 that the method was successful in capturing spatial variability in the *ET* rates based on the changes in the land cover, as the *ET* rate of forested land cover was found to be always higher than that of the grassland. In addition to spatial variability, the method seemed to capture well the temporal variability in *ET*. The temporal variability for this particular analysis existed at two time scales, a short-scale daily variation associated with daily changes in atmospheric conditions (e.g., local cloud cover, wind speed, etc.) and a long term, seasonal, climatic variation. The short-scale variation tends to be less systematic and is demonstrated in Figure 2.9 by the range marks. The seasonal variation is more systematic and pronounced and is clearly captured by the method.

Table 2.3 Pan Coefficients Used to Obtain Pasture Evapotranspiration for Different Months.

Month	Coefficient
January	0.4
February	0.45
March	0.55
April	0.64
May	0.7
June	0.7
July	0.7
August	0.7
September	0.7
October	0.6
November	0.5
December	0.5

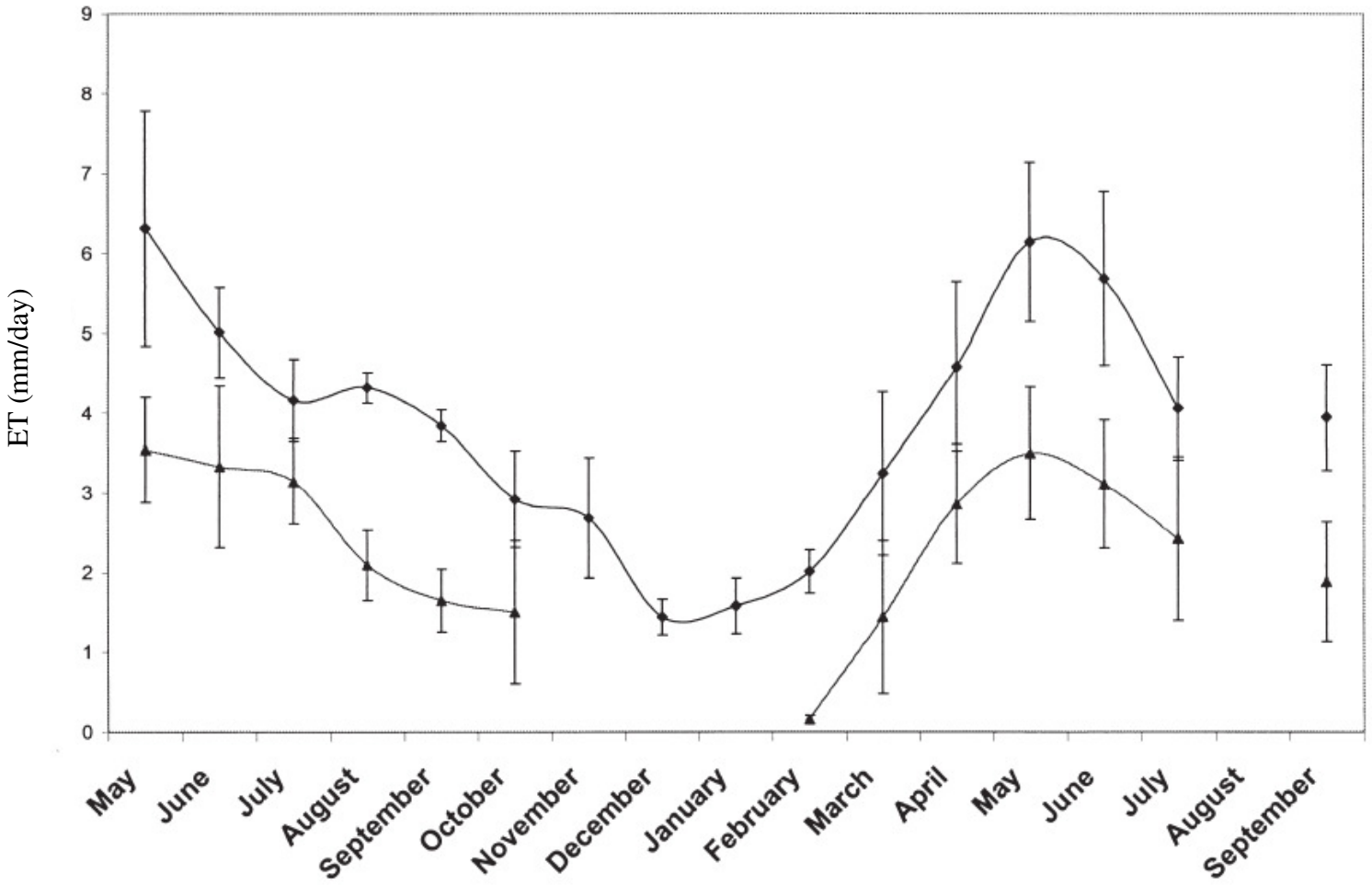

Figure 2.9 Monthly Average of Evapotranspiration (*ET*) Daily Values in Forested (Diamonds) and Pasture (Triangles) Areas. The Gap in the Graph Represents a Period of Missing Data. Standard Deviations of Daily Values are also Shown in the Range Limits.

2.3.1.1 Comparison with Pan Evaporation

To assess the robustness of the model, the estimated *ET* values for pasture were compared with *ET* estimated from the evaporation pan. The measured pan evaporation was multiplied by a pan coefficient for pasture to estimate *ET* for this vegetation cover. A monthly variable crop coefficient was adopted (Doorenbos and Pruitt, 1977) to account for changes associated with seasonal plant phenology (see Table 2.3). The consumptive water use or the crop evapotranspiration is calculated as:

$$ET_C = E_P \times K_C \tag{2.18}$$

where E_P is the measured pan evaporation, K_C is a pan coefficient for pastureland, and ET_C is the estimated evapotranspiration (mm/d) by the pan evaporation method. Figure 2.10 compares the *ET* estimated by both the evaporation pan and moisture sensors for pasture. Although the two methods are fundamentally different, on average, estimated *ET* agreed well with an r^2 coefficient of 0.78. This supported the validity of the soil moisture methodology, which further captured the daily variability of *ET* ranging from a low of 0.3 mm/d to a maximum of 4.9 mm/d. The differences between the two methods can be attributed to fundamental discrepancies that should be obvious. The pan results are based on atmospheric potential with crude average monthly coefficients while the TSM approach inherently incorporates plant physiology and actual moisture limitations. Indeed, both methods suffer from limitations. The pan coefficient is generic and does not account for regional variation in vegetation phenology or other local influences such as soil texture and fertility. Similarly, the accuracy of the soil moisture method proposed in this study depends on the number of sensors used in monitoring total moisture in the soil column.

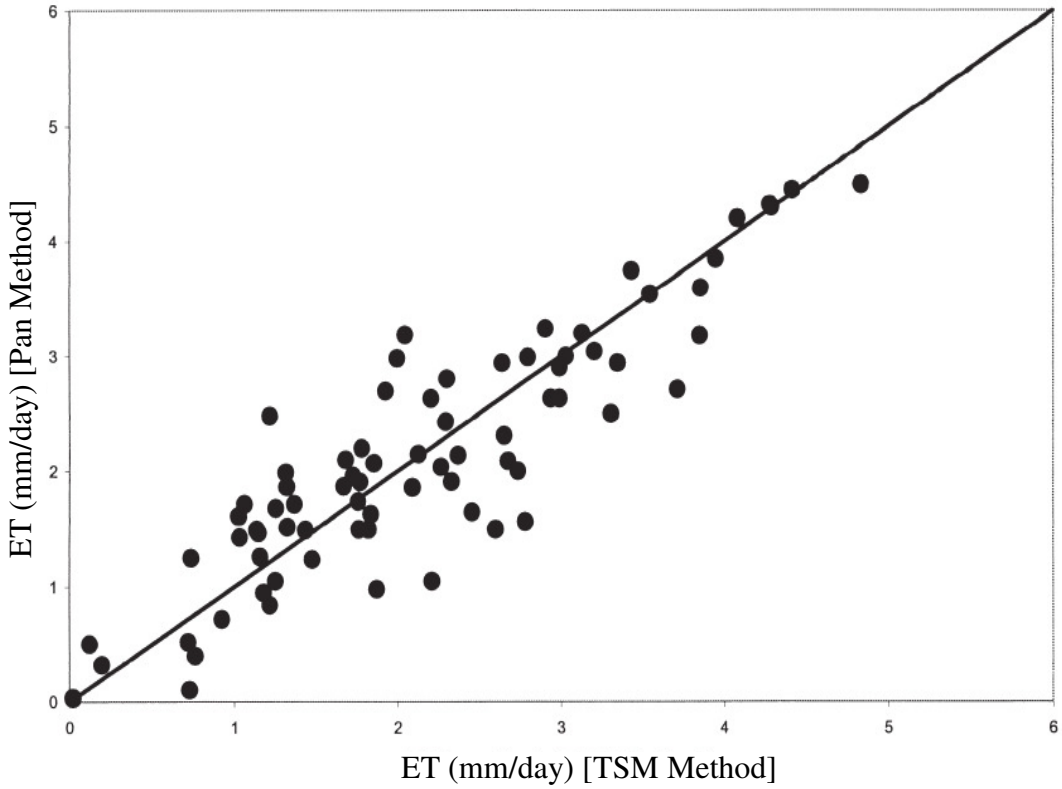

Figure 2.10 Evapotranspiration Estimates for Pasture by the Pan and Point Scale Model. Data Points Represent the Daily Values of *ET* from both Techniques.

2.3.2 One Dimensional Transect Model

Water budget components, calculated from the one dimensional transect model using soil moisture and water table observations in 2002 – 2004 revealed that almost all components display a consistent seasonal behavior. Quarterly averaged observed fluctuations in *SMET* (soil moisture *ET*), *DS ET* (depression storage *ET*), *TET* (Total *ET*), *I* (infiltration), *TRE* (Total rainfall excess), *SER* (Saturation excess runoff), and the d_{WT} (depth to the water table) are shown in Figures 2.11 to 2.18.

Figure 2.19(a) and (b) shows sample plots of precipitation versus infiltration for two of the wells (PS-43 and PS-41 respectively) along with the equation of the best fit

line. The intercept obtained from the best fit line was used for the determination of interception capture. The average value of daily maximum interception capture from the y-intercept was found to be 1.3 mm for grassland and 2.5 mm for the flat-woods forested land cover. The values of interception capture found using the described methodology is consistent with literature values (e.g., Viesman and Lewis 2002, pg. 132). From the annual water budget tables (Table 2.4-2.7) the annual value of interception capture varied from 106 to 221 mm.

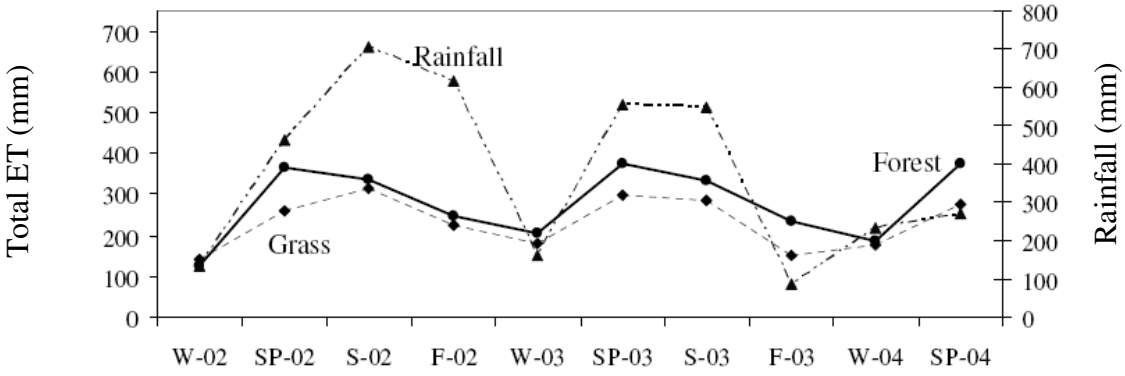

Figure 2.11 Variation in Total *ET* for Grass and Forest Land Covers.

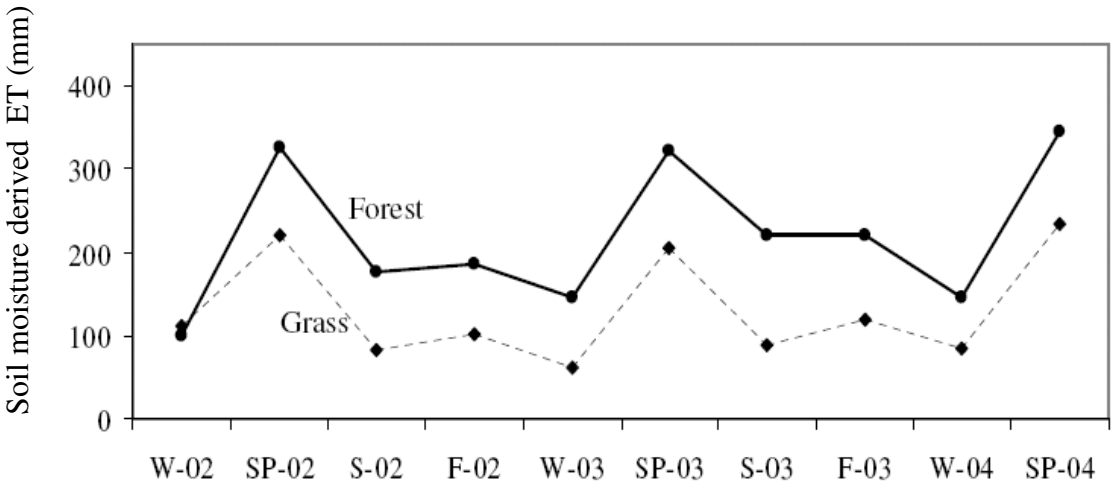

Figure 2.12 Variation in *ET* Derived from Soil Moisture Changes for Grass and Forest Land Covers.

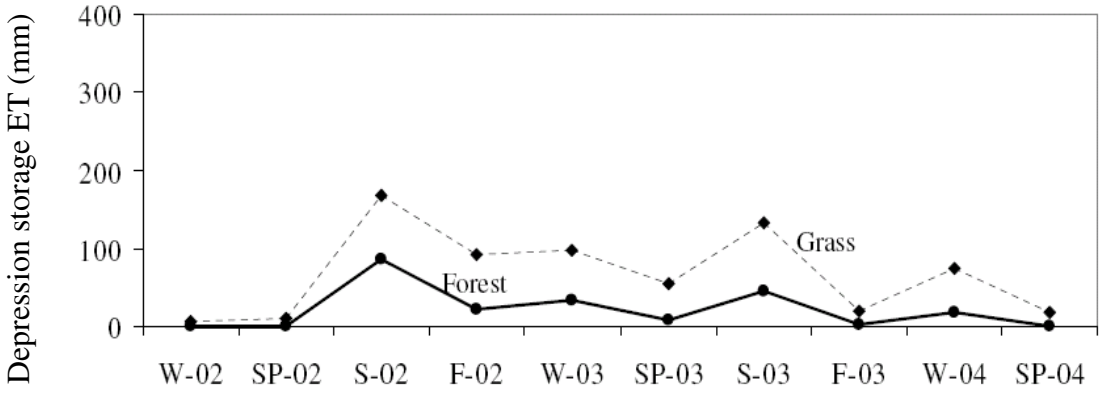

Figure 2.13 Variation of Depression Storage *ET* for Grass and Forest Land Covers.

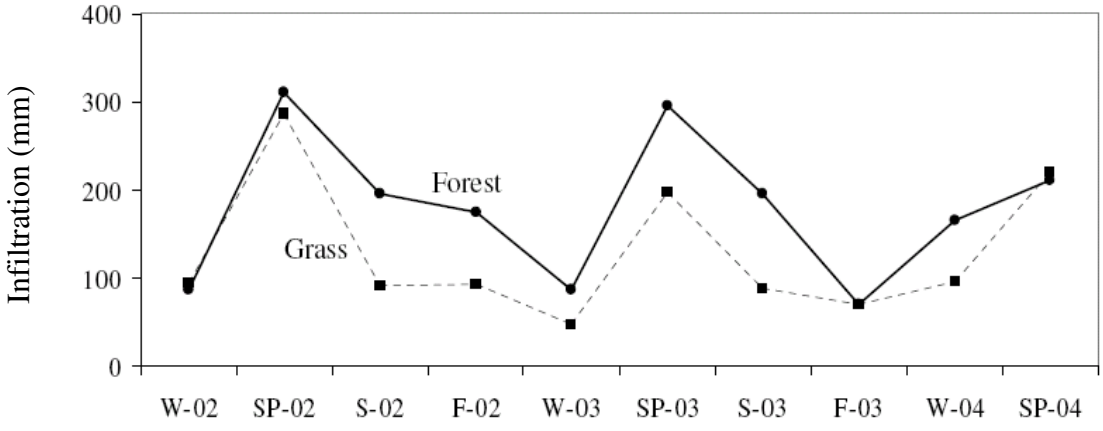

Figure 2.14 Variation of Infiltration for Grass and Forest Land Covers.

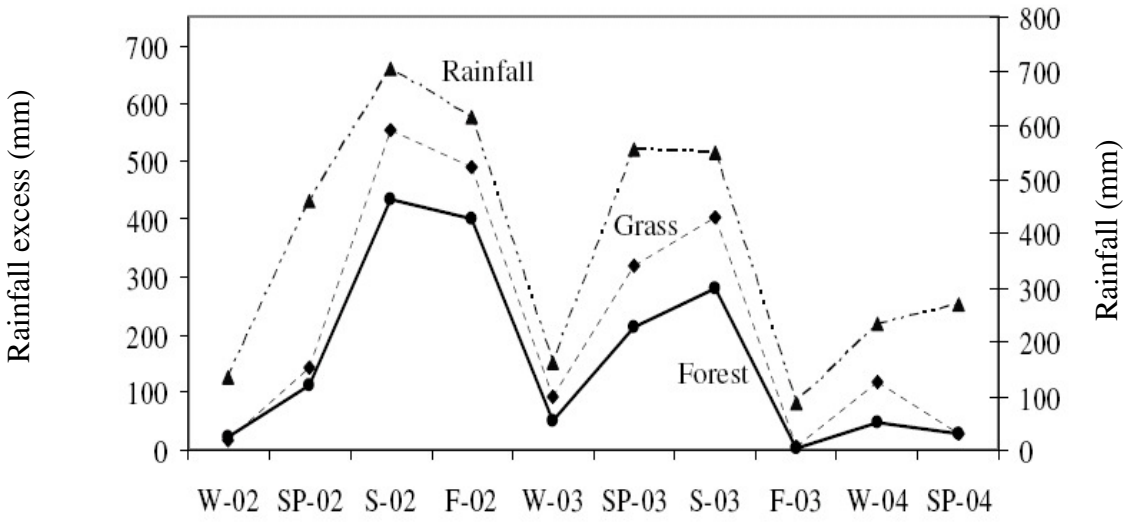

Figure 2.15 Rainfall Excess for Grass and Forest Land Covers.

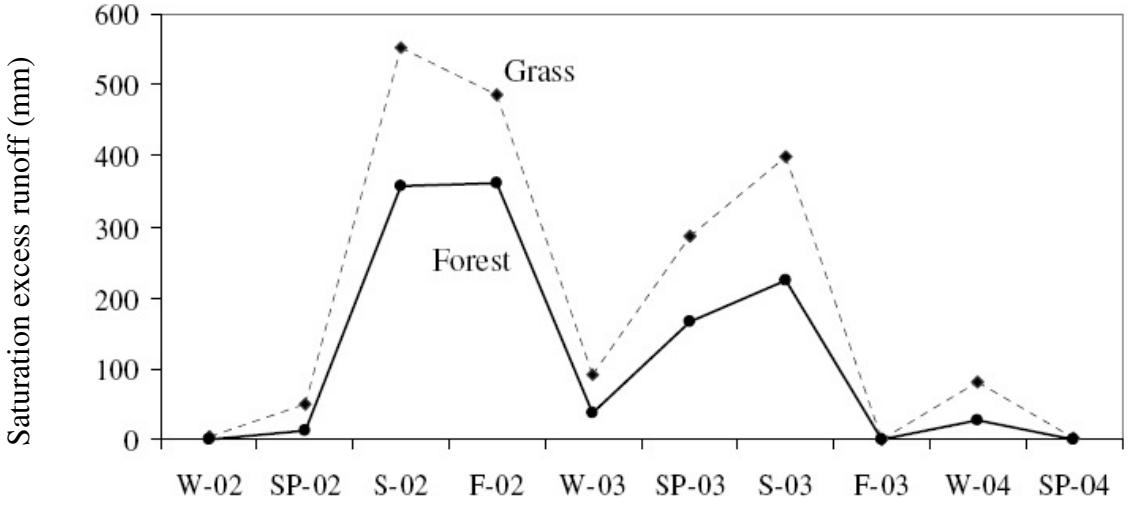

Figure 2.16 Saturation Excess Runoff Variation for Grass and Forest Land Covers.

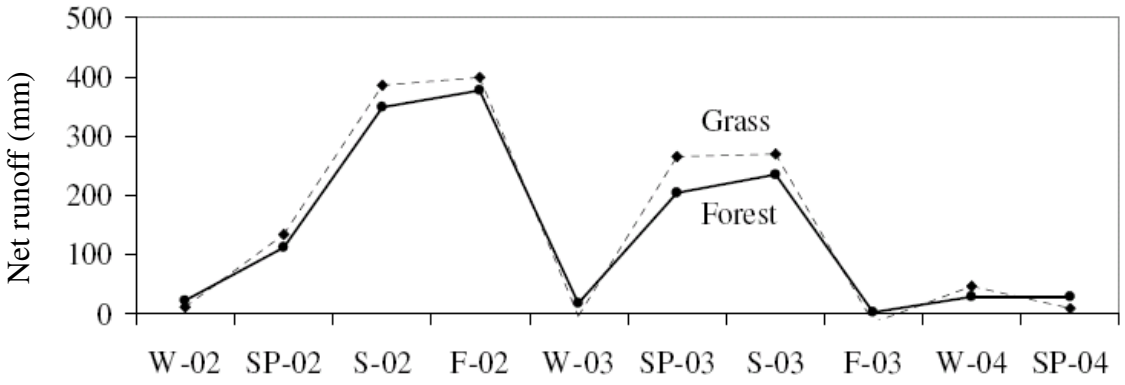

Figure 2.17 Net Runoff for Grass and Forest Land Covers.

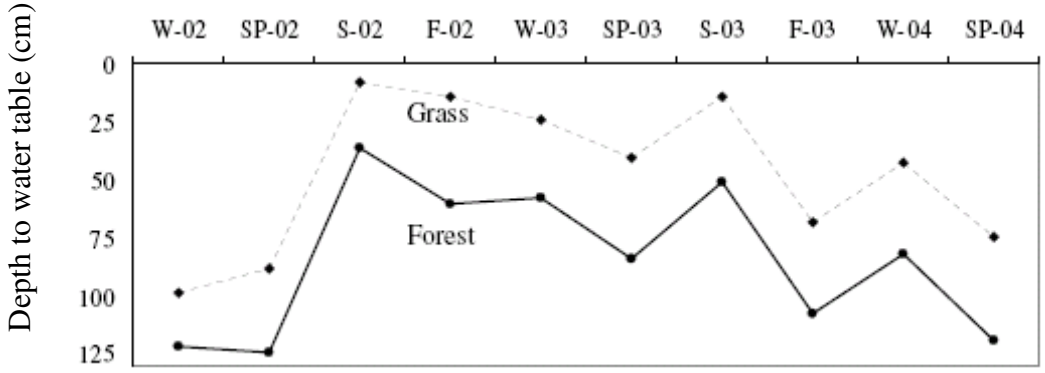

Figure 2.18 Variation in Depth to the Water Table for Grass and Forest Land Covers.

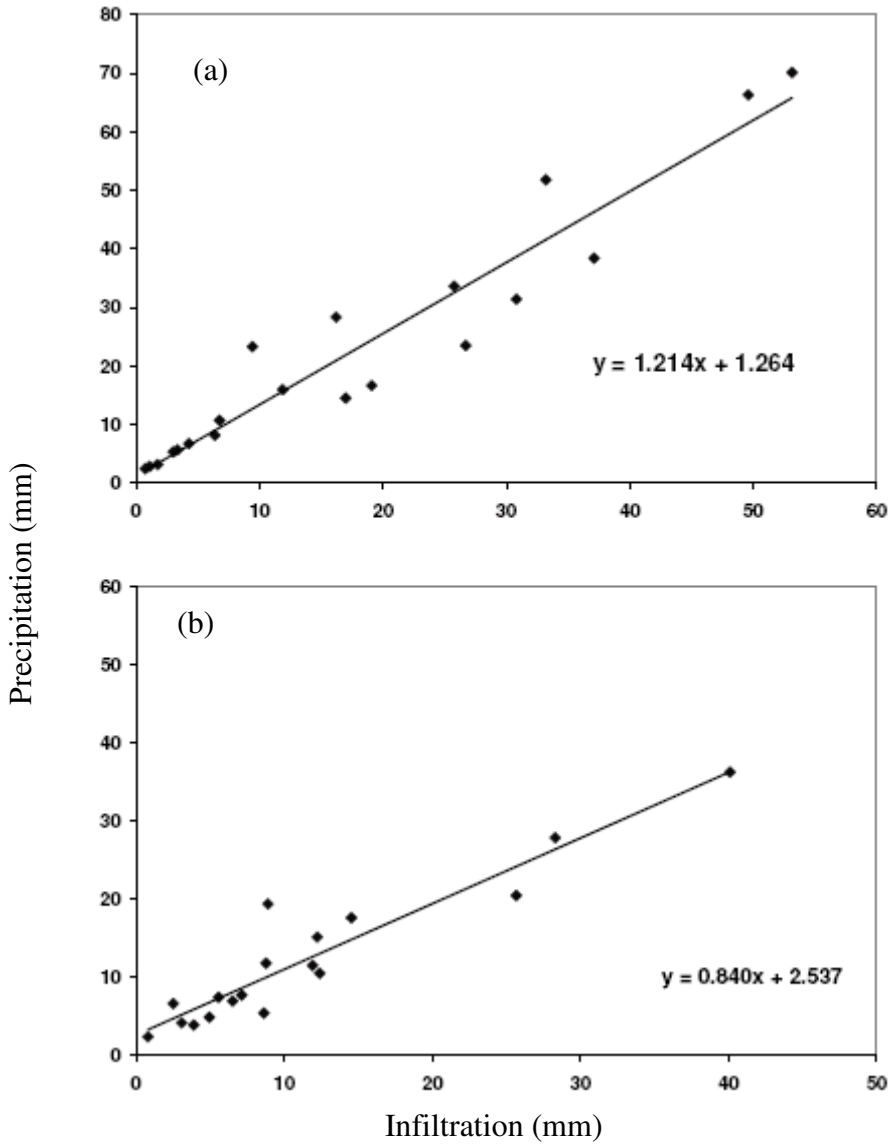

Figure 2.19 Precipitation versus Infiltration for (a) Grassed Land Cover and (b) Forested Land Cover. The Equation Shown is the Equation of the Best Fit Line.

Comparison of quarterly values of water budget components for different years shows some interesting behavior. Derived *ET* components vary in a similar manner in corresponding quarters. Infiltration and runoff components, on the other hand, varied significantly depending on available precipitation and quarterly *ET*. For instance, rainfall

magnitude in summer 2002 was about 200 mm more than that observed during summer 2003 (see Figure 2.11). However, the corresponding *ET* magnitudes for both grassland and forest cover stayed pretty much the same. This shows that under normal or wet conditions *ET* is strictly a function of ambient atmospheric conditions, while runoff is directly proportional to both the amount of precipitation occurring during a particular quarter and the magnitude of the *ET* in that period. This conclusion holds significance for predictive modeling, wherein models of runoff behavior must be expected to reproduce strong seasonally varying *ET* behavior to insure predictive capability.

Annual observed water budget components in the two land cover environments in 2002, 2003 and 2004 are summarized in Tables 2.4, 2.5, and 2.6 respectively. A clear trend in seasonal and annual behavior of the water budget components is observed for the upland versus near stream region. The upland grassland, with corresponding lower *ET*, exhibits higher runoff annually than the down-slope forested land cover. This result is supported by the shallower d_{WT} exhibited by the grassed upland (Figure 2.18).

Table 2.4 Total Annual Water Budget for 2002 (a) *ET*, Runoff, and (b) Other Water Budget Components.

(a)

Total Annual Water Budget 2002											
Land Use	Wells	Rain (mm)	ET (mm)				Runoff (mm)				
	ID	P	Ic	SMET	DS ET	TET	TRE	SER	HR	URI	NR
Grass	USF-3	1914	147	514	344	1005	1231	1113	118	282	888
Grass	USF-1	1914	147	516	287	950	1143	1111	32	235	856
Grass	PS-43	1914	147	521	195	863	1235	1050	185	220	1040
Mixed	PS-42	1914	121	746	145	1012	1034	908	126	303	889
Forest	PS-41	1914	221	690	171	1082	1055	904	151	300	884
Forest	PS-40	1914	197	877	8	1082	816	383	433	396	808
Forest	PS-39	1914	197	882	17	1096	819	404	415	399	802

(b)

Total Annual Water Budget 2002 (Contd.)						
Land Use	Wells	Lateral Flow	Infiltration	Depth to Water Table	Change in Storage	Mass Balance Error
		(mm)	(mm)	(cm)	(mm)	(mm)
	ID	q	I	d_{WT}	S	e
Grass	USF-3	0*	536	45	212	0
Grass	USF-1	0*	624	41	223	0
Grass	PS-43	23	532	71	247	45
Mixed	PS-42	13	759	77	307	-20
Forest	PS-41	14	638	70	237	2
Forest	PS-40	9	900	109	374	-9
Forest	PS-39	-2	898	93	374	-18

* Insignificant

Table 2.5 Total Annual Water Budget for 2003 (a) *ET*, Runoff, and (b) Other Water Budget Components.

(a)

Total Annual Water Budget 2003											
Land Use	Wells	Rain (mm)	ET (mm)				Runoff (mm)				
	ID	P	Ic	SMET	DS ET	TET	TRE	SER	HR	URI	NR
Grass	USF-3	1350	128	411	314	853	862	790	72	64	547
Grass	USF-1	1350	128	458	374	960	799	782	17	167	426
Grass	PS-43	1350	128	550	228	906	801	759	42	69	573
Mixed	PS-42	1350	106	896	91	1093	604	533	71	190	513
Forest	PS-41	1350	192	784	162	1138	592	531	61	104	430
Forest	PS-40	1350	171	1042	9	1222	437	219	218	153	428
Forest	PS-39	1350	171	1016	13	1200	436	250	186	159	423

(b)

Total Annual Water Budget 2003 (Contd.)						
Land Use	Wells	Lateral Flow	Infiltration	Depth to Water Table	Change in Storage	Mass Balance Error
		(mm)	(mm)	(cm)	(mm)	(mm)
	ID	q	I	d_{WT}	S	e
Grass	USF-3	0*	361	35	-6	1
Grass	USF-1	0*	423	26	65	0
Grass	PS-43	26	421	48	-75	55
Mixed	PS-42	14	640	62	-106	-16
Forest	PS-41	19	565	56	-141	14
Forest	PS-40	-11	741	107	-174	-59
Forest	PS-39	-5	742	85	-175	13

* Insignificant

Table 2.6 Semi-Annual Water Budget for 2004 (a) *ET*, Runoff, and (b) Other Water Budget Components.

(a)

Semi- Annual Water Budget 2004											
Land Use	Wells	Rain (mm)	ET (mm)				Runoff (mm)				
	ID	P	Ic	SMET	DS ET	TET	TRE	SER	HR	URI	NR
Grass	USF-3	502	42	382	127	551	182	129	53	86	55
Grass	USF-1	502	42	388	124	554	142	49	93	126	18
Grass	PS-43	502	42	384	25	451	112	71	41	134	87
Mixed	PS-42	502	34	499	27	560	98	51	47	162	71
Forest	PS-41	502	62	437	28	527	93	34	59	133	64
Forest	PS-40	502	56	538	0	594	35	0	35	176	35
Forest	PS-39	502	56	525	0	581	35	1	34	177	34

(b)

Semi- Annual Water Budget 2004 (Contd.)						
Land Use	Wells	Lateral Flow	Infiltration	Depth to Water Table	Change in Storage	Mass Balance Error
		(mm)	(mm)	(cm)	(mm)	(mm)
	ID	q	I	d_{WT}	S	e
Grass	USF-3	0*	278	46	195	0
Grass	USF-1	0*	319	45	58	0
Grass	PS-43	10	348	84	135	20
Mixed	PS-42	7	370	82	20	-7
Forest	PS-41	7	347	87	42	0
Forest	PS-40	-4	412	132	5	-21
Forest	PS-39	-3	412	111	6	3

*Insignificant

Various components of *ET* also revealed variability corresponding to land use regime. During dry periods, a relatively uniform magnitude of total *ET* (*TET*) is observed across the transect wells for each land cover. The highest magnitude of *TET* was observed in the spring, followed by summer periods regardless of the land use covers. *DS ET* magnitude was considerably higher for the upland area (exhibiting shallower d_{WT}) than near the stream region. This behavior was most pronounced in the summer (wet season) across transect wells and can be attributed to shallower d_{WT} in corresponding periods.

Concerning results obtained from the current analysis, it can be stated that evapotranspiration, to a significant degree, controls all the subsurface fluxes. Forest land cover has higher consumptive use of water resulting in lower elevation of the water table, as compared to the water table in the upland region. This condition, supported by the observed values, causes the initiation of lateral flux, whose magnitude is governed by the head difference between the upland and wetland (near stream) water table. At the same time, due to deep water table and dryer conditions in the vadose zone, the infiltration value is higher for forested land cover, thereby decreasing the total rainfall excess and runoff.

Also, interesting observations can be made concerning the diurnal behavior. In the night, as *ET* subsides, the lateral (and small vertical upward) flow is still observed and tends to partially replenish the water table as well as the vadose zone. Interestingly, from Figure 2.8(c) and (d) it can be seen that during the night time the water table elevation in the well in the forested area (PS-41) rises, while in PS-43 (grassed upland section) the water table, due to lateral flux out of the column, still shows decline. This observation is

typical of the observation between the recharge and discharge regions (as previously noted by Nachabe et al. 2005; Trout and Ross 2005; Freeze and Cherry 1979).

The values of *ET* obtained from the current study are consistent with the numbers found by other studies, also done in Florida, including Sumner (2006), Sumner (2001), Bidlake et al. (1993), and Knowles (1996), for land covers similar to the ones present at the study site. On an average, *ET* was found to vary between 60-70% of the long term average precipitation occurring in the area. However, as pointed out earlier, for higher than normal precipitation, the *ET* rates do not necessarily increase, hence, for years that are wetter than normal, the percentage of *ET* can be substantially lower. In the current study, 2002 was an abnormally wet year with annual recorded precipitation of about 2000 mm as compared to average annual values of 1300-1500 mm. This resulted in the percentage fraction of *ET* dropping from 70% to about 50%. However the absolute magnitude of *ET* was very consistent.

The consistency of the results across different years coupled with similarities to previous studies validates the current methodology. The small mass balance errors as can be seen from the water budget table (Table 2.4-2.6) can be attributed to error in the measurements as well as assumption of impermeable lower boundary conditions. However, the error is really small as compared to the values of other components of the water budget (see the following section for discussion on the error estimates).

The biggest advantage of this method lies in comprehensiveness with which one can estimate water budget components and determine seasonal or shorter time-scale variation. Another advantage is that very small land cover/soil type regions can be analyzed. Observations of *ET* components, derived plant coefficients and other variables

should prove extremely useful for predictive comprehensive surface and ground water models.

2.3.3 Error Estimates

Finally, it is very important to also comment about the error ranges of the equipment as well as error estimates of other hydrologic properties determined for the study site and their possible effects on the magnitude of the hydrologic components.

Section 2.2.2 mentions that the soil moisture observations as well as water table measurements are good to 0.1% water content and have been tested by manual measurements hence assuming the error to be random the net effect on the final results is expected to be negligible. This leaves the values of hydraulic conductivities and its effect on the lateral flow calculations. Section 2.2.4.1 discusses the determination of hydraulic conductivity. Both permeameter analysis and slug test gave values which were within 10-15%. As a matter of fact, apart from the wells in considerations, forty two other soil cores were taken and analyzed (Thompson 2003) and the results were very consistent, further increasing our confidence in the calculated numbers. Due to real small value of lateral flow, even if the hydraulic conductivity is assumed to be variable around 10-15% the final water budget (Table 2.4-2.6) will only change by less than 10 mm, which won't affect the annual or seasonal variation of the other water budget components.

Another factor that has the potential to introduce error is the choice of an equation for calculation of potential evapotranspiration. The selection of Jensen and Haise (1963) method was done primarily in lieu of the availability and quality of weather data. Use of standardized Penman Monteith equation requires a whole suite of weather parameters and

for this particular study the data were not consistently and continuously available. Apart from that problem, use of net radiation and wind speed from a supplemental dataset used from Ona weather station was thought to be fraught with error and hence only temperature and solar radiation data were used, limiting the choice of *ET* methods. Imrak et al. (2003) compared different methods of *ET* estimation versus the standardized Penman Monteith method and found that Jensen and Haise method fluctuated on either side with an error of 15%. Hence, the depression storage *ET* as well as net runoff is expected to be off by a maximum 15%. However the due fractional contribution towards total *ET* estimates, the values of *TET* can be easily expected to be put within a confidence bound of ±5%. As far as total rainfall excess, infiltration, etc. are concerned none of the other water budget component is expected to be effected.

Similarly, the fluctuation in the value of interception capture which is around 10% of total *ET* values is not expected to change the numbers that much. Hence, instead of quantifying on a seasonal basis, a constant average value for each vegetation cover was assumed.

Overall we can be pretty confident that the results obtained from the aforesaid analysis are with in acceptable errors (~5-10%) given that that methodology attempts to comprehensively determine all the water budget components. The consistency in the values of *ET* and other components calculated for other similar environments e.g., Sumner (2006), Sumner (2001), and Bidlake (1996) further increases our confidence in the results obtained.

2.4 Conclusions

A one dimensional point and transect models coupled with precise and highly resolved soil moisture profile and water table monitoring were developed to determine the magnitude and variation of different components of the water budget. Two and a half years of observed soil moisture and water table elevation data were used to derive all lateral and vertical fluxes comprising evapotranspiration components. The results successfully showed the variation of different fluxes with varying land cover and ambient weather conditions. Results also indicate a long term consistency in seasonality of different fluxes with short time scale differences occurring due to differences in antecedent conditions. *ET* was found to be a dominant factor controlling surface and sub surface fluxes including runoff and water table recharge, second only to precipitation. Lateral sub-surface flow was found to be less than 2% of the precipitation in the annual water budget. Thus, it remains to be seen how the methodology will function in higher lateral flow (and vertical leakage) settings. This aspect of the investigation is ongoing and results will be forthcoming.

The methodology used in the study, unlike other methods, such as eddy correlation or solar radiation based methods, gives a direct estimate of the soil moisture extracted by the roots and, hence, is expected to yield better plant based *ET* parameters, such as plant coefficients. The method excels at determining component fluxes such as *ET*, lateral flow, and rainfall excess (runoff). Even though the current study considered land cover variations, it did not take into account plant specifics like rooting depths, leaf area index, etc., which are known to affect the lateral and vertical fluxes for a given land cover and are key modeling parameters. Some attempt needs to be made to incorporate

these variables in the observations. The main drawback of the above methodology is that if the water table gets deeper than the deepest soil moisture sensors, errors in the calculation of storage changes can over or under predict fluxes. This could be a problem in deep water table environments. Another limitation occurs at the other end, when the water table is very shallow. While setting *ET* equal to potential *ET* is an acceptable assumption for water table at or near land surface (Shah et al. 2007), actual *PET* measurement is always problematic (Allen et al. 2005). Also, resolution of soil *ET* flux cannot be made during these times. Thus, reliability of the method is only achieved if sensors penetrate the deepest depths of soil moisture uptake and several methods are used to estimate *PET* during the wet conditions. Another important aspect that is relevant for the application of this methodology, especially in a different hydrogeological setting is the determination of vertical leakage. For the study site as the confining layer separating the surficial aquifer with the intermediate is thick and has very low permeability, assuming the boundary to be impermeable is appropriate; however, in high leakage environments, vertical leakage should be explicitly measured and accounted for in the mass balance equation.

Chapter 3: Extinction Depth and Evapotranspiration from Ground Water under Selected Land Covers

3.1 Introduction

Chapter 2 concluded that continuous soil moisture and water table observations can help estimate evapotranspiration and other components of the water budget. An important question, from the modeling perspective, which remains unanswered, is how much of the evapotranspiration comes from vadose zone and how much comes directly from ground water? Also, of importance to modeling, is the determination of the extinction depth, defined as the depth to the water table at which the contribution of ground water to the total evapotranspiration becomes negligible.

The current chapter is aimed at answering the above said questions about extinction depths, ground water, and vadose zone contribution to evapotranspiration as well as, developing some equations that can be used, depending on the land cover and soil type, to model the aforesaid processes.

3.2 Background

Evapotranspiration (*ET*) is a major component of the water budget in vegetated soils and shallow ground water systems. The impact of *ET* on ground water flow was recognized in the early works of White (1932) and Meyboom (1967) who attributed diurnal fluctuation in a shallow water table to ground water consumption by

phreatophytes. Phreatophytes, such as willow and cottonwood, flourish in riparian zones fringing streams, and their significant *ET* consumption influences the behavior of interconnected surface-ground water systems (Woessner 2000; Sophocleous 2002). In landscapes where the water table is within or slightly below the root zone, the vegetation can uptake water both from a thin unsaturated vadose zone and saturated ground water (water table). The partitioning of *ET* into Vadose Zone *ET* (*VZET*) and Ground Water *ET* (*GWET*) is challenging because it is controlled by many variables including soil hydraulic properties, depth to water table (d_{WT}), and root distribution. In particular, the management and modeling of shallow ground water systems requires an understanding of how the depth to water table impacts evapotranspiration, often a significant sink term in shallow ground water systems.

In ground water modeling, an early version of MODFLOW (McDonald and Harbaugh 1988) assumed that *GWET* decays linearly with increasing water table depth, with *GWET* reaching a value of zero at a depth designated as the extinction depth. The extinction depth can vary considerably as a function of the presence of phreatophytes, and seasonal and long term climatic conditions among other factors (Anderson and Woessner 1992). Surprisingly, few formal attempts (e.g., Blum et al. 2001) have challenged this linear decay approach. Banta (2000) revised the original evapotranspiration module in MODFLOW to allow a piece-wise linear decline of *ET* with increasing depth to the water table. This new approach is flexible and can better capture the exponential decay behavior that was proposed earlier by Gardner (1958). Recently, different MODFLOW modules have been released that have subroutines to simulate surface evaporation and root transpiration (Unsaturated-Zone Flow (UZF) package (Niswonger et al. 2006),

Variably Saturated Flow package (VSF) (Thoms et al. 2006), and Farm Process (FMP1) package (Schmid et al. 2006)). However, no common guidelines or functions are recommended for setting extinction depth for different soils or vegetative covers. Regardless of the parametric function adopted: linear, piece-wise linear, or exponential, the parameters of the *ET* module should vary over the spatial domain to reflect heterogeneities in soil and vegetative covers. Regional models for ground water management simulate large aquifer areas with varying vegetation covers on the land surface. Because ground water *ET* can be a significant component of the ground water budget, resolving the variability over the spatial domain is a necessity for managing interconnected surface-ground water systems.

In shallow ground water systems, the *ET* demand of plants is supported by two hydraulically connected domains: the shallow unsaturated soil (vadose zone) and the deeper saturated ground water system (Anderson and Woessner 1992; Thompson 2003). Previous studies by Nachabe (2002) and Nachabe et al. (2005) suggested that temporal fluctuations in a shallow water table control soil moisture conditions, associated root-water uptake, and *ET* across the ground water-vadose zone-atmosphere continuum. Figure 3.1 shows the variability of water table and soil moisture for a 5 day period in a ground water discharge zone. The water table, which declines rapidly during daylight due to *ET*, recovers partially at night. The partial recovery in the evening and night hours is attributed to lateral and vertical ground water flow to the discharge area as noted in earlier studies (e.g., Meyboom 1967; McWhorter and Sunada 1977). Interestingly, the soil moisture in the unsaturated zone above the water table displays similar diurnal fluctuation. The soil moisture partially recovers at night by upward flow from the

saturated zone. Although the soil moisture recovery lags by about two hours the recovery of the water table, the synchronization of soil moisture and water table indicates a close hydraulic connection between the two domains in shallow water table environments (Nachabe et al. 2005).

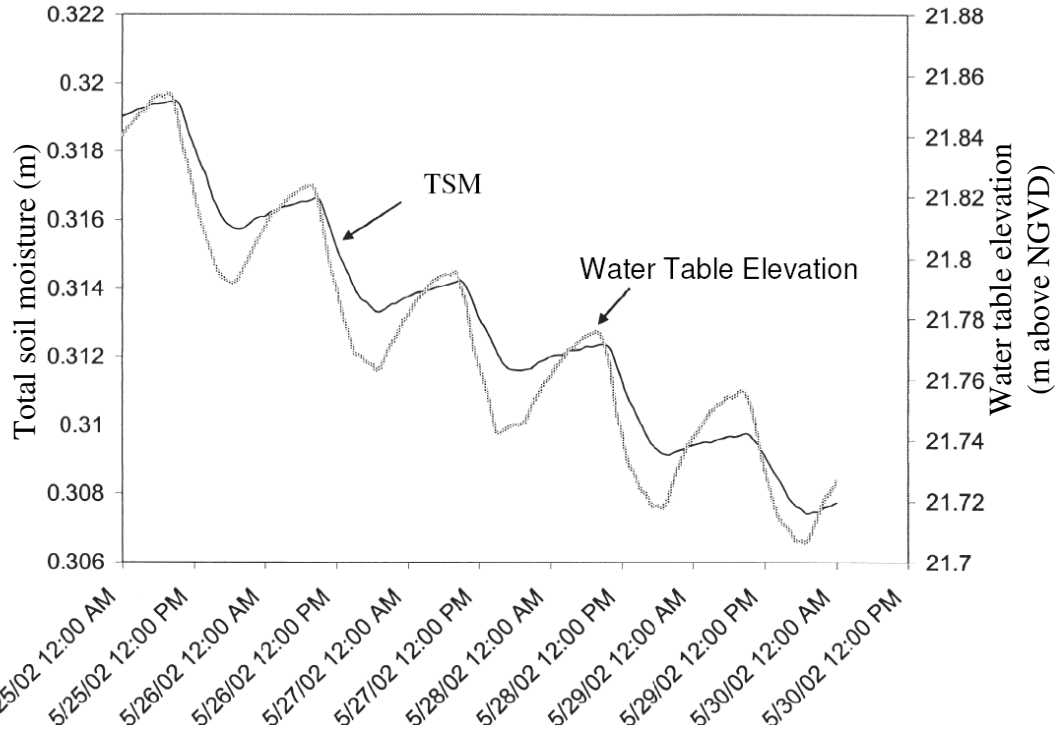

Figure 3.1 Water Table and Total Soil Moisture (TSM) Diurnal Variation with Time [Adapted from Nachabe et al. 2005]. The TSM was Calculated by Integrating the Observed Water Content in the Top 1.5 m of Soil [NGVD Refers to National Geodetic Vertical Datum].

3.2.1 Objectives and Scope

The objectives for this chapter are thus: (a) to study the relationships of total *ET* and *GWET* to d_{WT} using saturated/unsaturated flow simulations, (b) to introduce new analytic expressions to capture this relationship, (c) to assess if the proposed expressions are consistent with field data, and (d) to determine the impact of varying soil properties

and land cover on *GWET* and extinction depth. Three land covers will be considered: bare soil, shallow rooted vegetation (e.g., shrubs and grasses), and deep rooted vegetation (trees and forested landscapes). The primary finding is that an exponential decay function better describes the decline of *GWET* with water table depth. New equations are introduced to express the decline of *GWET* with variation in land cover and soil properties.

3.3 Methods

3.3.1 Numerical Simulations

Evapotranspiration extracts water from both the saturated and vadose zones. Water flow is driven by head gradients from the drying of the soil close to plant roots (root water uptake) and evaporation at the surface. In this study, HYDRUS, a variable saturation flow model (Simunek et al. 1998), is used to simulate the evapotranspiration process. Introduced by the U.S. Salinity Lab, this model has been previously used and verified in a number of studies (e.g., Hernandez et al. 2003; Simunek and van Genuchten 1999). Also, an independent team of hydrologists scrutinized HYDRUS and found the model to be reliable and highly capable (Diodato 2000).

The HYDRUS-1D model simulates variably saturated flow by solving Richard's equation written as:

$$\frac{\partial \theta}{\partial t} = \frac{\partial}{\partial x}[K\left(\frac{\partial h}{\partial x} + \cos\beta\right)] - S \qquad (3.1)$$

where h [L] is the water pressure head, θ [L^3L^{-3}] is the volumetric water content, t [T] is time, x [L] is the spatial coordinate, β [-] is the angle between the flow direction and the

vertical axis (for vertical columns $\beta = 0^o$), K [LT^{-1}] is the unsaturated hydraulic conductivity, and S [$L^3L^{-3}T^{-1}$] represents the sink term. Soil hydraulic properties characterizing volumetric water content $\theta(h)$ and hydraulic conductivity K(h) are assumed to be described by the van Genuchten (1980) model as:

$$\theta(h) = \begin{cases} \theta_r + \dfrac{\theta_s - \theta_r}{\left[1 + (\phi|h|)^n\right]^m} & h < 0 \\ \theta_s & h \geq 0 \end{cases} \tag{3.2}$$

$$K(h) = \begin{cases} K_S S_e^l [1 - (1 - S_e^{1/m})^m]^2 & h < 0 \\ K_S & h \geq 0 \end{cases} \tag{3.3.1}$$

$$S_e = \frac{\theta(h) - \theta_r}{\theta_s - \theta_r} \tag{3.3.2}$$

where $m = 1 - 1/n$ for $n > 1$, S_e [-] is the effective water content, K_S [LT^{-1}] is the saturated hydraulic conductivity of the soil column, θ_r [L^3L^{-3}] and θ_s [L^3L^{-3}] denote the residual and saturated water contents respectively, l [-] is the pore connectivity parameter assumed to be 0.5 as an average for most soils, and ϕ [L^{-1}], n [-] and m [-] are the van Genuchten empirical parameters. The soil column simulated in HYDRUS varied from 3 to 9 m in length depending on soil type and vegetative cover. The column was divided into 1000 elements to provide good spatial resolution. Increasing the number of elements did not change or improve the results of the numerical simulations presented here. Evapotranspiration is simulated as a sink term, S [$L^3L^{-3}T^{-1}$], on the right side of Equation 3.1. This sink term is distributed through the soil profile reflecting the plant root distribution in the domain as follows:

$$S(x) = \alpha(h)\, S_p(x) \tag{3.4}$$

where $\alpha(h)$ [-] is the root water uptake stress response function ($0 < \alpha(h) < 1$) as defined by Feddes et al. (1978), and $S_p(x)$ [$L^3L^{-3}T^{-1}$] is the spatial distribution of the potential transpiration rate over the soil profile as a function of depth x [L]. The potential rate represents the water uptake rate when the plant is not experiencing any water stress, that is $\alpha(h) = 1$. For vegetated covers, the upper surface was set as a no-flux boundary and the potential *ET* rate was distributed through the root system in the subsurface according to the function:

$$S_p(x) = b'(x)\, T_p \tag{3.5}$$

where T_p [LT^{-1}] is the potential rate and $b'(x)$ [L^{-1}] is the relative fraction of roots at any depth x. Jackson et al. (1996) analyzed the distribution of roots for a large number of vegetation and found that the model proposed by Gale and Grigal (1987) was successful in describing root distribution. This model of root distribution is adopted in this study and the root distribution is assumed as:

$$Y = 1 - \gamma^d \tag{3.6}$$

where Y is the cumulative fraction of roots from the surface to depth d, and γ is a numerical index of rooting distribution which depends on vegetation type. This relationship was used in the numerical simulations with γ equals 0.975 for forest and 0.952 for grass (Jackson et al. 1996). The root zone thickness (ξ_{RZ}) of 1 meter was assumed for grass (shallow rooted vegetation) and 2 meters for trees (Jackson et al. 1996). Throughout the study, the only differentiations that were considered concerning land cover were differences in rooting depths and distributions. Other physiological characteristics affecting *ET* such as the leaf area index were not considered.

For bare soil, the potential *ET* rate is applied as a surface evaporation boundary condition. In all simulations, the potential *ET* rate (*PET*) is assumed to follow a semi-sinusoidal function with a frequency of 12 hours to capture the diurnal variation in *PET*. The area under the rate curve is 0.5 cm, representing an average potential daily *ET* of 0.5 cm/day which is a reasonable average for many regions in the U.S (e.g., Nachabe et al. 2005; Linsley and Franzini 1972). These 12 hours of active *ET* are followed by 12 hours of zero potential *ET* to reflect night hours. Representing a day, this 24-hour cycle of upper boundary condition is repeated for the entire duration of the numerical simulation, which was also set as the model output time step. In all simulations, a no-flux boundary condition was defined at the column bottom. The initial depth to the water table (d_{WT}) was assumed zero, i.e., the water table coincided with the land surface. No further constraints were placed on the evolution of the water content profiles or location of the water table.

To assess the influence of soil texture, simulations for twelve texture classes were carried out for each land cover; van Genuchten parameters ϕ, n and m for the standard USDA twelve soil texture classes were adopted from the database of HYDRUS (Carsel and Parrish 1988).

3.3.2 Data Processing and Analysis

The numerical model solves for the pressure head and water content distributions in the domain subject to the *PET* conditions described above. The model results were used to track the evolution of the water table decline by tracking the location of the zero

pressure head with time. The partitioning of evapotranspiration (*ET*) into *VZ* and *GW* fractions was subsequently determined from mass balance relationships.

The first processing step included calculation of the model simulated total soil moisture (TSM) across the entire soil profile for all specified time steps. The TSM (in cm of water) is the total depth of water in the soil column and is calculated by integrating the water content along the soil column. The *ET* is a loss of water from the soil column and is determined by subtracting two sequential values of TSM. Mathematically the *ET* loss (expressed as a positive value) in a time step is calculated as:

$$ETL\Big|_{t_i} = \int_{\Delta S} \theta_{mod\ el}\, dz\Big|_{t_{i-1}} - \int_{\Delta S} \theta_{mod\ el}\, dz\Big|_{t_i} \tag{3.7}$$

where *ETL* is total *ET* loss in a time step, θ_{model} is the simulated water content at depth z from the land surface at time t_i , with i being a running index for time, and ΔS [L] is the length of soil column. The *ET* rate is then calculated as follows:

$$ET = \frac{ETL}{\Delta t} \tag{3.8}$$

where: $\Delta t = t_i - t_{i-1}$ is the time step. Mathematically, the *ETL* in Equation 3.7 was calculated using the trapezoidal rule of integration and the simulated water content.

$$ETL = \sum_{\Delta S}^{0} \frac{1}{2}\left(Z_{j+1} - Z_j\right)\left(\theta_{j+1} + \theta_j\right)\Big|_{t_{i-1}} - \sum_{\Delta S}^{0} \frac{1}{2}\left(Z_{j+1} - Z_j\right)\left(\theta_{j+1} + \theta_j\right)\Big|_{t_i} \tag{3.9}$$

At the end of a time step, the return of the pressure and water content distributions to hydrostatic equilibrium indicates that upward flow has replenished the unsaturated vadose zone and there is no further upward flow. In this case, *ET* is supported by ground water alone without a vadose zone contribution. With increasing depth to the water table,

however, the hydraulic connection between ground water and the vadose zone weakens, causing the vadose zone to lose water at a rate that exceeds the upward replenishment from the saturated zone. Hence, the vadose zone contribution (VZC) to *ET* in a time step $\Delta t = t_i - t_{i-1}$ was calculated from consecutive departure at time t_i and t_{i-1} of the water content profile from hydrostatic equilibrium. Mathematically,

$$VZC = (TSM_{eq} - TSM_{model})\Big|_{t_{i-1}} - (TSM_{eq} - TSM_{model})\Big|_{t_i} \tag{3.10}$$

where at any given instant in time, TSM_{eq} is the total soil moisture in the column for the corresponding depth to water table under hydrostatic equilibrium condition and TSM_{model} is the total soil moisture computed from the water content values simulated by HYDRUS for the corresponding time. The vadose zone *ET* rate can therefore be found as:

$$VZET = \frac{VZC}{\Delta t} \tag{3.11}$$

From mass balance, the ground water contribution (GWC) can be written as:

$$GWC = ETL - VZC \tag{3.12}$$

and ground water *ET* rate (*GWET*) is:

$$GWET = \frac{GWC}{\Delta t} \tag{3.13}$$

Theoretically, the water table extinction depth is reached when *GWET* becomes zero. It was observed, however, that *GWET* approaches zero only asymptotically. Thus, for practical consideration, the depth of water table is said to reach extinction when *GWET* is only 0.5% of the *PET* imposed at the boundary. The simulation time to reach extinction ranged from one month to a year depending on soil type and land cover.

3.3.3 Field Estimation of *GWET*

To assess the appropriateness of the proposed model, water table data from a ground water observation well in Hillsborough County, Florida were used. The depth to the water table in the well was measured at five-minute intervals with a submersible pressure transducer 0 to 5-psi (Instrumentation Northwest Inc., Kirkland, WA), accurate to 0.005 psi. This site is covered with shallow grass and the soil is predominantly sand with pockets of fines deposited as described in Trout and Ross (2004) and Said et al. (2005).

A methodology introduced by White (1932), and scrutinized recently by Loheide et al. (2005), was used to estimate the *GWET* from water table fluctuations. The equation to estimate *GWET* is (White 1932):

$$GWET = S_Y(\Delta s \pm 24R) \tag{3.14}$$

where *GWET* is ground water evapotranspiration (cm/day), S_Y is the specific yield [-], Δs is the daily change in the water table elevation (cm/day), and R is the net ground water inflow rate (cm/hour). The change in water level Δs is calculated as the difference between water levels over one day. Depending on the direction of hydraulic gradient, the ground water inflow rate, R, can be either a recharge or discharge term (Freeze and Cherry 1979). As recommended by White (1932), the ground water inflow rate, R, was determined from the slope of the water table hydrograph between midnight and 4 AM. Despite the simplicity of the methodology by White (1932), Equation 3.14 has serious limitations as noted recently by Loheide et al. (2005). This method assumes a constant ground water inflow rate for the entire day. Also, the specific yield, S_Y, is difficult to estimate because it varies non-linearly with d_{WT} due to the capillary fringe above the

water table (Duke 1972; Nachabe 2002). At this particular site, the equation introduced by Duke (1972) was calibrated by Said et al. (2005) to capture the specific yield variation with d_{WT}. This equation takes the form:

$$S_Y = (\Phi - S_r)\left[1 - \left(\frac{h_a}{d_{WT}}\right)^{\lambda}\right] \tag{3.15}$$

where λ [-] and h_a [L] are the pore size distribution index and soil air-entry (or bubbling) pressure head of the Brooks and Corey water retention model (Brooks and Corey 1966), d_{WT} [L] is depth to water table, S_r is the soil specific retention [L^3L^{-3}] and ϕ is the porosity [L^3L^{-3}]. For this site, values of (ϕ-S_r) = 0.12, λ = 0.7, ha = 33 cm were used in Equation 3.15 (Said et al. 2005; Nachabe 2002).

Equation 3.15 can be applied two or three days following rainfall, after infiltration and moisture redistribution have ceased in the unsaturated zone above the water table (Nachabe 2002; Said et al. 2005). Therefore, for each rainfall storm, three days were removed from the one year water table record. This step reduced considerably the data that can be used to estimate *GWET*, but it was necessary to have a reasonable estimate of specific yield values (Nachabe 2002; Said et al. 2005).

To determine values of potential evapotranspiration (*PET*), a USGS Class A pan housed in the weather station at the study site was used to measure pan evaporation (Nachabe et al. 2005). The difference in water level observed in the pan for a period of one day was multiplied by a pan coefficient of 0.7 (Doorenbos and Pruitt 1977) to get a reference value of evapotranspiration for pasture grass, representing the type of vegetation around the observation well.

3.4 Results and Discussion

The *ET* rates are plotted versus depth to water table in Figure 3.2 for the simulation with forest cover in a sandy clay soil. The simulated *ET* was normalized by the potential *ET* so *ET*/*PET* varied between 0 and 1. The figure shows that the *ET* is equal to its potential until the water table reaches a depth d' defined here as the 'transition depth'. At the transition depth, *ET* shifts from atmospheric controlled (*ET* is equal to *PET*) to soil moisture controlled. For water table conditions deeper than the transition depth d', *ET* is limited by the available moisture in the column. While Figure 3.2 shows total *ET* from both ground water and vadose zone, we are interested in estimating the ground water fraction (*GWET*) because of its influence on the ground water budget. Therefore it is important to partition the *ET* into *GWET* and *VZET* components.

Figure 3.3 demonstrates the partitioning of *ET* into the *GWET* and *VZET* fractions for a typical simulation. As shown in Figure 3.3, all evapotranspiration will be provided by the ground water if the water table is at a depth less than d'' referred here as the 'decoupling depth'. For water table less than the decoupling depth, all the evapotranspiration is borne by ground water, and the vadose zone acts as a conveyor being continuously replenished to hydrostatic equilibrium from the ground water below. Clearly, the vadose contribution to *ET* is zero for water table depth less than the decoupling depth. As the water table (d_{WT}) becomes deeper than the decoupling depth, the vadose zone loses moisture at a rate that exceeds the replenishment rate from ground water. This can be attributed to the weakening of the hydraulic coupling as d_{WT} increases beyond d''. After the water table reaches the decoupling depth, the *VZET* contribution increases with further increase in the depth to the water table, reaching a maximum

contribution at the transition depth d' (the depth at which *ET* is controlled by soil moisture availability). Obviously d' and d" are important parameters in describing the *ET* decline with d_{WT} both physically and mathematically.

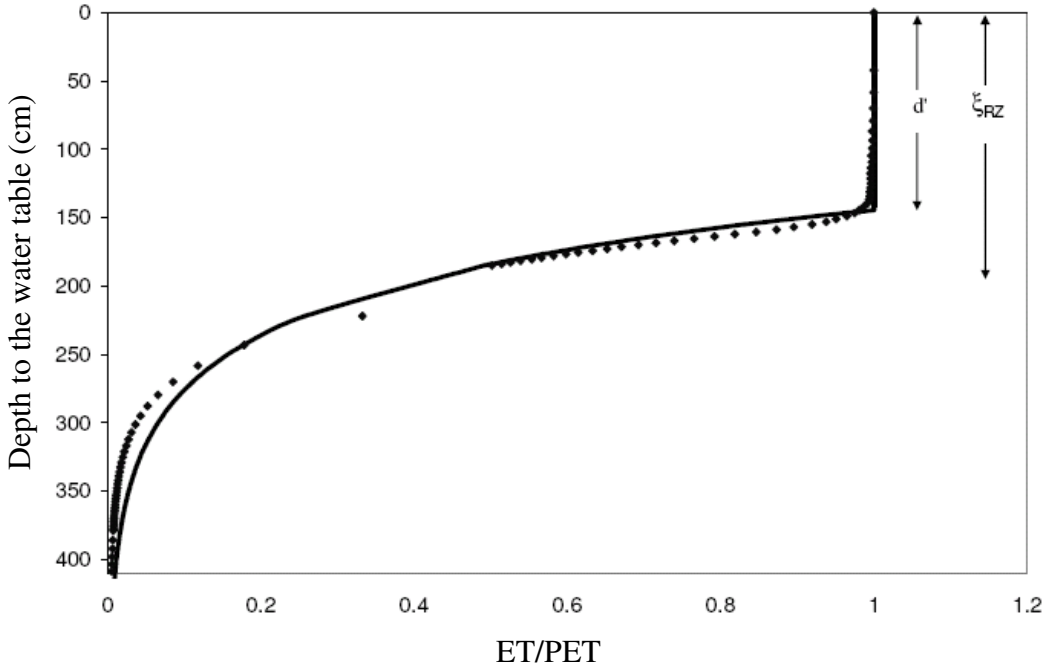

Figure 3.2 Simulated *ET* in Sandy Clay with Forest Land Cover. The Diamonds are the Simulated Values while the Solid Line is Curve Fitted using Equation 3.16. The Transition Depth, d', is the Depth at which *ET* becomes Limited by Available Water. ξ_{RZ} is the Maximum Root Depth (= 200 cm) for Forest Land Cover.

Clearly, the decline of *GWET* with increasing d_{WT} is not linear. This relationship is better fitted with an exponential decay function with parameters reflecting soil hydraulic properties and land cover. This observation concurs with the early work of Gardner (1958) and Gardner and Fireman (1958) who, based on laboratory experiment of evaporation from bare soils, proposed an exponential relationship for steady-state evaporation from a shallow water table.

This study, however, extends the early findings to, (a) transient conditions where the vadose zone, in addition to ground water, may contribute to *ET* and (b) vegetated landscapes where the sink is not limited to the land surface boundary but distributed through a root system in the unsaturated zone. Jury et al. (1991) and Hillel (1980) discuss the early work of Gardner (1958) and some of the inherent limitations, such as assumption of water evaporation as a steady-state process.

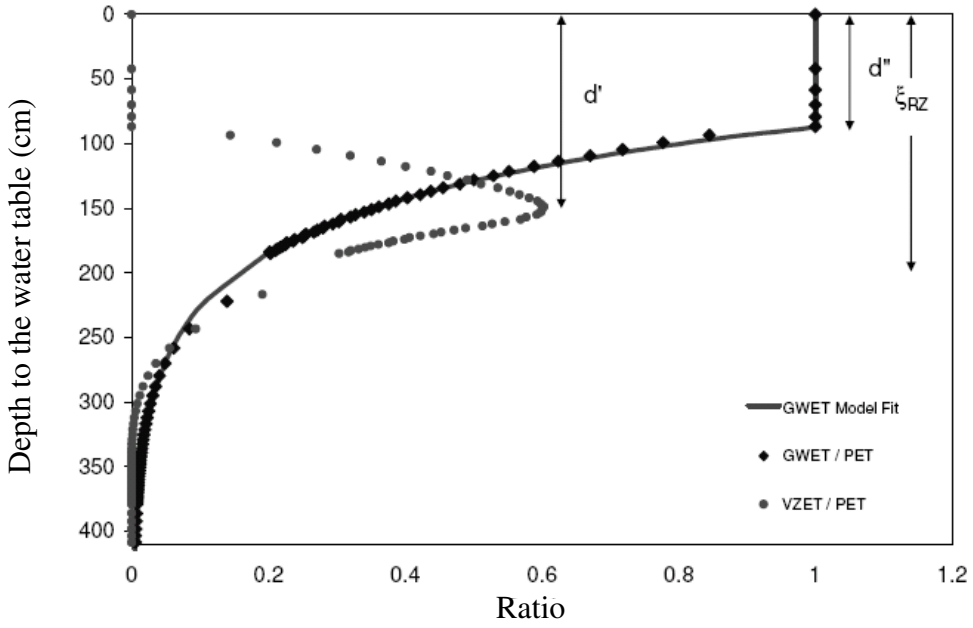

Figure 3.3 *GWET* and *VZET* in Sandy Clay Soil with Forested Land Cover. The Diamonds and Circles are the Simulated Values while the Solid Line is Curve Fitted with Equation 3.17. *d'* and *d"* Represent the Transition and Decoupling Depth Respectively. ξ_{RZ} is the Maximum Root Depth (= 200 cm) for Forest Land Cover.

3.4.1 Influence of Soil Properties and Land Cover

For a given distribution of roots the decoupling depth is not only a function of capillary fringe height (as defined by Carsel and Parrish 1988) but also the unsaturated hydraulic conductivity of the soil matrix. Under low suction pressure, sufficient upward

flow from the water table will occur to support *ET* on a daily time scale. However, as the time scale of water flow within the capillary fringe is lot less than the time scale across unsaturated media, capillary fringe height tends to be a dominating factor in deciding the decoupling depth. Thus, soils with thicker capillary fringe have greater decoupling depth as compared to coarser soils (refer to Figure 3.4).

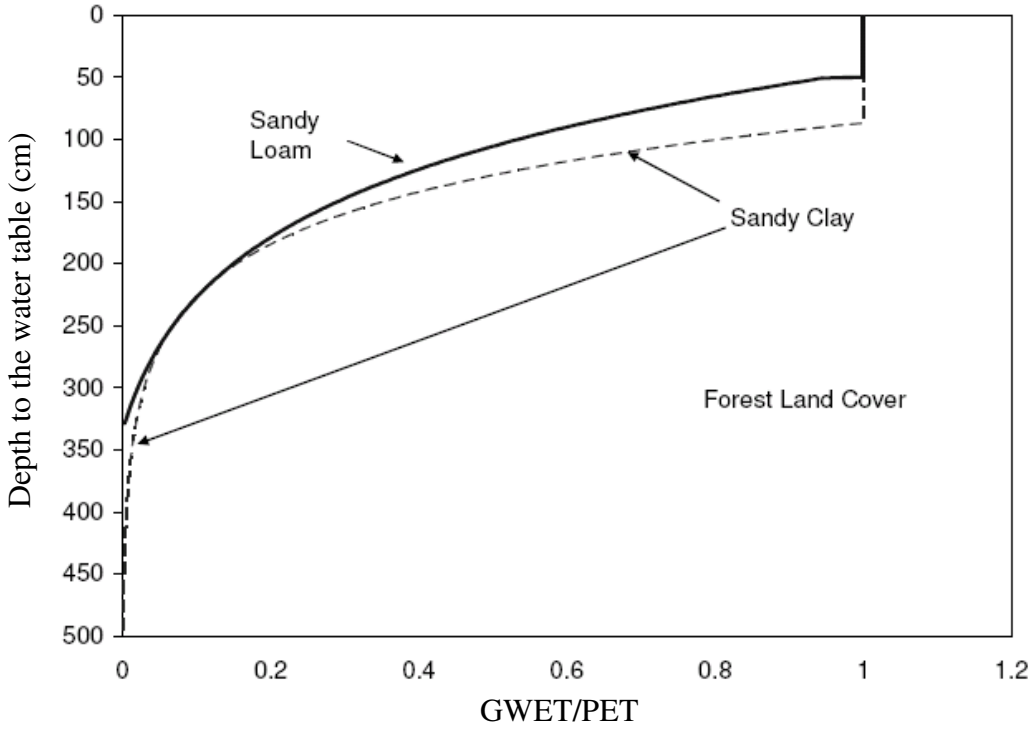

Figure 3.4 Variation of Ratio of GW*ET* with Water Table Depth for Two Soils. Height of Capillary Fringe for Sandy Clay and Sandy Loam is 30 cm and 15 cm, Respectively (Carsel and Parrish 1988).

Once the water table becomes deeper than the decoupling depth, the *GWET* starts declining rapidly in a fine textured soil. As shown in Figure 3.4, after the decoupling depth, the decline of *GWET* in sandy clay is faster than sandy loam. However, *GWET* in sandy clay is more persistent than *GWET* in sandy loam so the extinction depth is greater

in sandy clay than it is in sandy loam. This condition can be readily explained by the variation of hydraulic conductivity with increasing suction pressure has to be considered. When the water table is deeper than the root zone, water extracted by the roots from the unsaturated zone is replenished by upward flow from the water table. This flow depends on the unsaturated hydraulic conductivity of the media. It is well known (Jury et al. 1991, pg. 89; Hillel 1998, pg. 237) that the hydraulic conductivity of fine textured soil (sandy clay) is much less (e.g., two orders of magnitude) than that of coarse textured soils (sandy loam) for low suction pressures, which explain the rapid decrease in *GWET* after the decoupling depth for sandy clay. After some critical pressure, however, the unsaturated hydraulic conductivity of the fine textured soil becomes greater than that of the coarse textured soil. Therefore, in a relatively deep water table environment, a fine textured soil can sustain a greater upward flux than a coarse soil for the same head gradient, resulting in fine textured soils having a greater extinction depth. A similar observation was made by Gardner and Fireman (1958) for evaporation from bare soil.

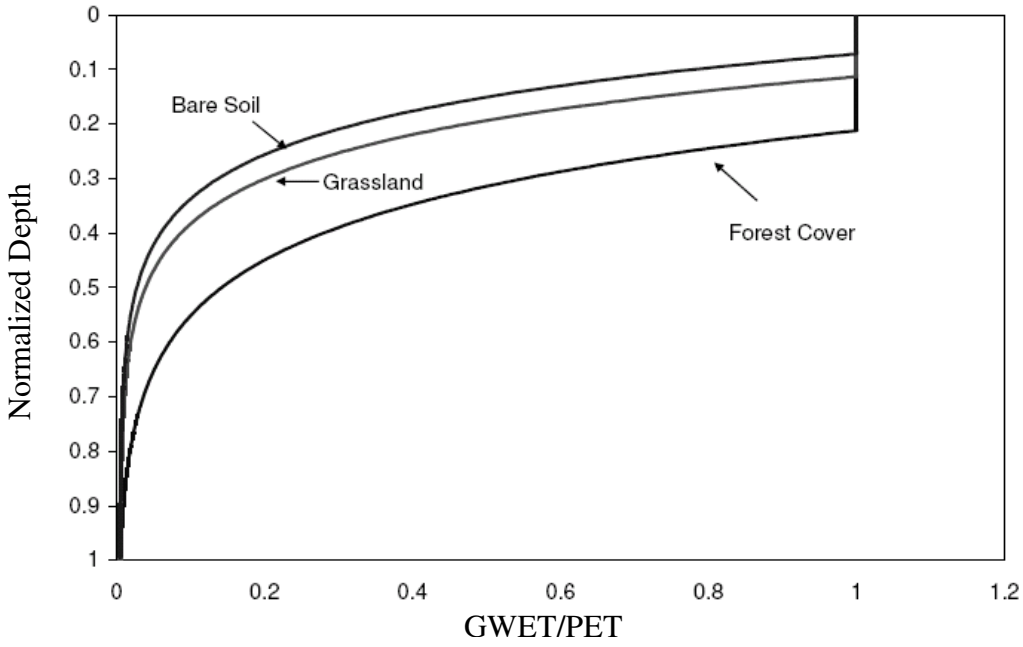

Figure 3.5 Variation in *GWET* for Different Land Covers in Sandy Clay. Normalized Depth (Depth to Water Table / Extinction Depth) is Used on the Vertical Axis to Facilitate Comparison.

To address the variability with land covers, Figure 3.5 shows *GWET* with d_{WT} for three land covers on the same soil. The d_{WT} on the ordinate is normalized by the extinction depth to capture the relative variation of the *GWET* for different land covers. As expected, the decoupling depth was the shallowest for bare soil, and deepest for the landscape with deep rooted vegetation. Obviously, deep roots support *GWET* from deeper water table depths. After the decoupling depth is reached, however, the behavior of the decline of *GWET* is similar for all land covers because the soils have the same conductivity.

Table 3.1 Extinction Depths for Different Soils and Land Covers. Depths are Rounded up to Nearest 5 cm. Maximum Rooting Depth (ξ_{RZ}) for Grassland and Forest was Assumed to be 100 and 200 cm, Respectively.

Soil Type	Land Cover ----------cm----------		
	Bare Soil	Grassland	Forest
Sand	50	145	250
Loamy Sand	70	170	270
Sandy Loam	130	230	330
Sandy Clay Loam	200	300	400
Sandy Clay	210	310	410
Loam	265	370	470
Silty Clay	335	430	530
Clay Loam	405	505	610
Silt Loam	420	515	615
Silt	430	530	630
Silty Clay loam	450	550	655
Clay	620	715	820

3.4.2 Variability in Extinction Depths

Extinction depths for different soils and land covers were rounded to the nearest 5 cm and presented in Table 3.1. Two trends are obvious from a close examination of this table. First, fine textured soils have larger extinction depth than coarse textured soils for a similar land cover. Secondly, extinction depth increased with increase in rooting depths. For shallow and deep rooted vegetation, the increase in extinction depth was almost the same as the increase in rooting depths.

The cause for this almost equal increase can be explained by the fundamentals of soil physics and the soil-root water interaction. Roots can extract water from the vadose zone only up to wilting point, which is normally assumed as the water content at 15 bar suction pressure (Hillel 1998, pg. 622). Hence, comparison of water content profiles when the water table is at extinction depth revealed that the presence of roots translates downward the bare soil drying profile by a depth approximately equal to the rooting depth.

The value of 0.5 cm/day used in the original simulations might be considered a reasonable *PET* rate for many regions in the U.S. (e.g., Nachabe et al. 2005; Linsley and Franzini 1972). To test the sensitivity of extinction depths to potential *ET* rates, additional simulations with *PET* values of 0.25 cm/day and 1.0 cm/day were performed. The behavior of *ET*, along with the transition and decoupling depths, changed slightly with changes in *PET* values. Lower *PET* rates caused less drying of the vadose zone, facilitating its replenishment by upward flow from the water table. Therefore, *ET* was closer to its potential for lower *PET*. Conversely, higher *PET* rates shortened the decoupling depth by permitting a higher contribution from the vadose zone (*VZET*). In addition, for a given *PET* rate, the maximum values of *VZET* for each combination of soil type and land cover were averaged. It was found that for a *PET* of 0.25 cm/day the average maximum *VZET* was around 28% of the *PET*, and for a *PET* of 1 cm/day this value rose to 45%. Extinction depths, however, did not seem to be sensitive to *PET*. An increase of *PET* rates by a factor of four resulted in less than a 15% reduction in extinction depths.

3.4.3 Fitting a Model for *ET* and *GWET* Variation with d_{WT}

As suggested by Figure 3.2, the decline of *ET* with depth to the water table seemed to follow an exponential decay function after the water table depth reached d', the transition depth . Therefore a simple model of the form

$$\frac{ET}{PET} = \begin{cases} 1 & for \quad d \le d' \\ e^{-b(d-d')} & for \quad d > d' \end{cases} \tag{3.16}$$

was fitted to the data, where *d'* is the transition depth, *d* is the depth to water table and *b* is a decay coefficient. Table 3.2 showed the values for the two parameters *d'* and *b* of this model for the different land covers and soils. The model fit the data well with r^2 values exceeding 95% for most cases, suggesting that the exponential model captured well the relationship between *ET* and depth to water table. The transition depth ranged between 18 cm for bare sand to a maximum of 186 cm for clay with forested land cover. As expected, the exponential decay coefficient *b* decreased with an increase in rooting depth. A smaller coefficient *b* indicates that higher vegetation evapotranspiration can be supported by accessing moisture from deeper soil layers.

Equation 3.16 was used again to simulate the decline of ground water evapotranspiration, *GWET*/*PET*, with decline in the water table. An analysis of the regression fit, however, revealed that the curve fitted well for shallow water tables but the fit was poor for deep water tables. For deep water tables, the regression fit was enhanced substantially by introducing a correction parameter y_o to the equation. Thus, the model that captured the decline of *GWET* with water table depth was:

$$\frac{GWET}{PET} = \begin{cases} 1 & for \quad d \le d'' \\ y_o + e^{-b(d-d'')} & for \quad d > d'' \end{cases} \tag{3.17}$$

where *d"* is the decoupling depth for the *GWET*, y_0 is a correction and *b* is the decay coefficient. Table 3.3 compiles values of the parameters for all the thirty-six cases. The small correction y_0 enhances the fit of the curve substantially at deep water table close to the extinction depth. Figure 3.3 shows an example fit of the regression equation to the generated data. The r^2 exceeded 95% for most cases considered here.

The new equations introduced in this study provide a mean to simulate *GWET* decline with water table in ground water models. The piece-wise-linear *ET* module in MODFLOW (Banta 2000) is flexible, and the parameters of the piece-wise-linear relationship can be adjusted to capture the exponential decay function introduced here. Hence, in absence of field data, the exponential relations in Equations 3.16 and 3.17 with parameters from Tables 3.2 and 3.3 can be used by numerical modelers simulating ground water flow under landscapes with heterogeneous vegetative cover.

3.4.3.1 Field Assessment of Proposed Equations

While total *ET* can be estimated reasonably well with existing (e.g., Priestly and Taylor 1972) and newly proposed (e.g., Nachabe et al. 2005) techniques, resolving the *GWET* fraction can be a challenge. The *GWET* estimated by White's method was normalized by the *PET* and plotted against the d_{WT} in Figure 3.6. The solid line in this figure is the plot of Equation 3.17 with parameters from Table 3.3 for loamy sand and grass (shallow rooted) land cover. These conditions best reflected soil type and vegetation at our site. Equation 3.17 captures reasonably well the decline of *GWET*/*PET* with d_{WT}. Two observations are worthy of note. First, the number of field data points available was limited for this study due to the large number of storms in west-central

Florida. This restricted significantly the number of days of data that can be analyzed with White's equation. Secondly, though a pattern of decline of *GWET*/*PET* with d_{WT} can be identified, data points generated with White's equation are scattered widely.

The scatter on Figure 3.6 can be attributed to a number of factors. Recently, Loheide et al. (2005) did a comprehensive analysis of the ground water *ET* estimates obtained using the White (1932) methodology. The authors found that the largest source of error in the White (1932) equation is the uncertainty in the specific yield. Specific yield which is a non-linear function of d_{WT} is influenced by hysteresis and transient pore drainage (Nachabe 2002). While the non-linear dependence of specific yield on d_{WT} is captured in Equation 3.15 (Said et al. 2005), hysteresis is more difficult to estimate because it stems from the cycles of wetting and drying during shallow water table diurnal fluctuations. The specific yield also is transient (varies with time) because pore drainage (during water table decline), or imbibition (during water table surge), are time dependent processes. In other words, these processes are not instantaneous with observed water table fluctuation. Recognized as 'delayed yield' in the literature (e.g., Nachabe 2002), the relation calibrated by Said et al. (2005) does not account for the transient aspect of specific yield.

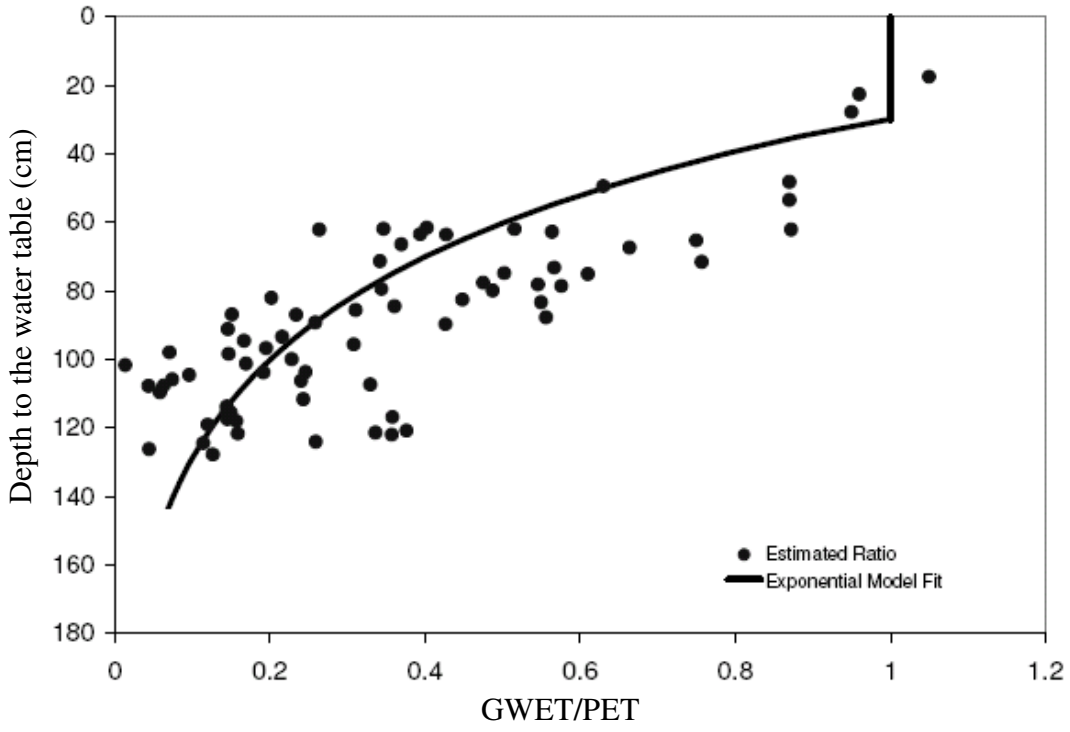

Figure 3.6 Estimated *GWET*/*PET* versus DTWT from White (1932). The Solid Line is the Proposed Theoretical Model, Equation 3.17, with Parameters from Table 3.3 for Loamy Sand with a Grass Land Cover.

In summary, while total *ET* can be estimated reasonably well using various methodologies, partitioning *ET* into *GWET* fraction and *VZET* can be a challenge because of the non-linear hydraulic connection between the two domains, the complex root distribution system, and hysteresis. Despite the large scatter of the data, the method by White (1932) did show the decline of *GWET* with increasing d_{WT}. This decline was captured reasonably well with the equations and parameters suggested in this study. Thus, this initial assessment indicates that an exponential decay relationship is consistent with the field data.

Table 3.2 Parameters for Equation 3.16. The r^2 Shows the Goodness of Fit of the Exponential Model to Simulated Results.

Soil Type	Land Cover Type								
	Bare Soil			Grassland			Forest		
	d' cm	b cm^{-1}	r^2 %	d' cm	b cm^{-1}	r^2 %	d' cm	b cm^{-1}	r^2 %
Sand	18	0.170	99	30	0.043	99	39	0.017	99
Loamy Sand	22	0.115	99	38	0.041	99	51	0.017	99
Sandy Loam	40	0.074	99	60	0.039	99	82	0.016	99
Sandy Clay Loam	35	0.055	99	70	0.031	99	102	0.014	99
Sandy Clay	26	0.078	98	66	0.028	97	145	0.016	99
Loam	55	0.04	97	85	0.026	99	128	0.014	99
Silty Clay	37	0.030	97	90	0.026	98	181	0.018	97
Clay Loam	50	0.032	98	92	0.020	98	159	0.012	99
Silt Loam	72	0.034	97	110	0.019	99	167	0.012	99
Silt	70	0.038	96	104	0.017	98	109	0.012	99
Silty Clay Loam	50	0.040	97	94	0.018	97	182	0.011	99
Clay	54	0.130	88	88	0.014	95	186	0.011	97

Table 3.3 Parameters for Equation 3.17. The r^2 Shows the Goodness of Fit of the Exponential Model to Simulated Results.

Soil Type	Land Cover Type											
	Bare Soil				Grassland				Forest			
	d" cm	y_0	b cm^{-1}	r^2 %	d" cm	y_0	b cm^{-1}	r^2 %	d" cm	y_0	b cm^{-1}	r^2 %
Sand	16	0	0.171	97	27	-0.012	0.036	99	31	-0.052	0.013	99
Loamy Sand	21	0.002	0.13	99	29	-0.018	0.031	98	36	-0.048	0.013	98
Sandy Loam	30	0.004	0.065	99	35	-0.013	0.022	97	50	-0.044	0.011	97
Sandy Clay Loam	30	0.006	0.046	98	31	-0.003	0.020	98	56	-0.014	0.012	98
Sandy Clay	20	0.005	0.042	99	35	0.005	0.028	99	87	0	0.017	99
Loam	33	0.004	0.028	98	39	-0.007	0.015	97	66	-0.017	0.010	98
Silty Clay	37	0.007	0.046	91	78	0.003	0.020	90	158	0.004	0.035	91
Clay Loam	33	0.008	0.027	98	35	0.004	0.014	99	84	0.001	0.011	99
Silt Loam	38	0.006	0.019	99	40	-0.003	0.011	98	82	-0.008	0.010	99
Silt	31	0.007	0.021	97	49	0.009	0.021	95	94	0.006	0.010	99
Silty Clay Loam	40	0.007	0.021	97	49	0.009	0.017	95	94	0.006	0.013	99
Clay	45	0.006	0.019	96	70	0.007	0.017	83	96	0.006	0.012	98

3.5 Conclusions

The process of *ET* extinction was studied in detail and a quantitative evaluation of the factors affecting it (considering soil retention and vegetative rooting depths) was carried out. Simulations of variable saturation flow suggested that an exponential decay better describes the decline of *ET* and ground water *ET* with increasing depth to the water table than the commonly used linear relationships. The exponential functions derived here can be easily used to describe the *ET* characteristics for different soil and vegetation

types. The soil and root parameters in the study, however, represent average conditions that can be used in the absence of site-specific data.

The simulations conducted here assumed continuous drying, and thus the vadose zone contribution was determined assuming a dry climate. An intermittent precipitation event or wetter antecedent moisture conditions would increase the vadose zone contribution. Hence the results of this study are mainly applicable for arid or semi-arid areas with little irrigation or rainfall. Another limitation for this study is that the extinction depth was assumed to be reached when *ET*/*PET* is 0.5%. Most vegetation will wilt if transpiration is too low. For these cases, the plant physiological response should be considered before setting a threshold value for extinction.

Equations 3.16 and 3.17 can be easily adopted as they require just two and three parameters respectively. Hence, these equations can guide numerical ground water modelers in simulating *GWET*. A field assessment of one equation showed that it was consistent with the field data. More field testing, however, should be carried out to evaluate the robustness of the model for different soil types and a variety of land covers.

Chapter 4: Conceptualization of Vadose Zone Processes to Account for Evapotranspiration Distribution

4.1 Introduction

From Chapter 3, it is evident that depending on the water table depth (shallower than the extinction depth), contributions from the vadose zone and ground water are highly variable. For watershed scale models, numerical solution of Richard's equation may help in solving vadose zone soil moisture dynamics. However, for regional scale models use of Richard's equation becomes both computationally and data intensive. Hence, the use of Richard's equation for large regional scale hydrological models is infeasible. Vadose zone moisture dynamics and its affect on the water table, hence, need to be modeled using a more simplistic methodology.

Depending on the final objectives, modeling efforts may be aimed either at determining water table fluctuations without detailed modeling of vadose zone soil moisture or, in other cases, involve determination of both soil moisture in the unsaturated zone as well as the water table fluctuations. For the former type of modeling requirements, conceptualization of specific yield variability, incorporating effects of the vadose zone, needs to be made. The latter type of modeling can, however, be done using a threshold based approach.

The following sections focus on the concept of specific yield, its traditional use and development of variable specific yield curves for different types of boundary

conditions such as evapotranspiration, rainfall, and pumping. The next chapter discusses development and validation of a threshold based modeling approach to account for variable vadose zone and ground water contribution to evapotranspiration, which can be used for regional scale modeling.

4.2 Specific Yield

4.2.1 Background

Modeling of water table fluctuations is very important for predicting runoff and *ET* in coastal plain environments such as west-central Florida (Ross et al. 2005). Highly transient and complex flow patterns that result from water table variations have a significant effect on the transport of solutes (Novakowski and Gillham 1988). Therefore, a prerequisite for the success of any hydrologic modeling of shallow water table systems is the efficient and accurate representation of the dynamics of the water table.

Water table fluctuations and associated recharge to the water table are most commonly estimated using a parameter known as the specific yield (S_Y) (Healy and Cook 2002; Crosbie et al. 2005). The definition of specific yield, which can be found in any ground water hydrology text, is the volume of water that an aquifer releases from storage per unit surface area of aquifer per unit decline in the water table (e.g., Todd 1959; Freeze and Cherry 1979). Mathematically it can be written as

$$S_Y = \frac{V_w}{A \Delta Z} \tag{4.1}$$

where A [L^2] is the aquifer area and V_w [L^3] is the volume released/stored resulting from ΔZ [L] water table fluctuation (in either direction).

As pointed out by Duke (1972), the above definition is misleading as it renders the specific yield as a constant, by making it independent of soil water pressure. Several studies have acknowledged and described the spatiotemporal variability of specific yield in great detail (Gillham 1984; Jayatilika and Gillham 1996; Nachabe 2002; Said et al. 2005; Sumner 2007). Variable distribution of water content in the unsaturated zone of a soil column, results in variable available fillabale pore space and, depending on the depth to water table, this space may cause differential water table fluctuations for the same amount of soil water added or removed. For instance, if the tension saturated zone, referred to as the capillary fringe, is within close proximity of land surface, adding a small amount of water will cause a sudden surge in the water table elevation as compared to a little or no elevation rise in deeper conditions (Barlow et al. 2000).

Another important factor in the specific yield determination concerns the time frame of fluxes and observations. A column of soil, if allowed to drain for a day will release more water than when it is allowed to drain for couple of hours. This is known as delayed yield (Nwankwor et al. 1992). Nwankwor et al. (1984) found in a field experiment, that the specific yield values obtained by the type curve fitting to time-drawdown curves were an order of magnitude lower than laboratory derived values.

Overall, corroborating the observation of Duke (1972), it can be concluded that specific yield is not just a function of porous media, but is also a function of depth to water table (d_{WT}), duration of drainage and the antecedent moisture conditions. Said et al. (2005) showed that variability in S_Y is apparent in field data and indicated that an apparent different behavior was exhibited for wetting versus drying.

Over the last decade the specific yield behavior has been widely studied, however, only a few hydrologic models have incorporated the variable d_{WT} behavior and the associated dynamics from flow processes (Jayatilika and Gillham 1996, Ross et al. 2004). Most ground water models such as MODFLOW (Harbaugh 2005) use a constant parameter in modeling water table fluctuations in responses to natural fluxes such as recharge and evapotranspiration (*ET*) or vice-versa. The models inadvertently assume a constant specific yield value for any d_{WT} and ignore any early time or delayed drainage process. Ross et al. (2004) attempted to add variable S_Y in an integrated MODFLOW-HSPF application. They considered the S_Y to vary with d_{WT} and relative moisture conditions based on simple conceptualization of moisture retention. However, they acknowledge that more field and theoretical studies are needed to help elucidate this behavior.

Adding to this knowledge gap is the fact that the studies on variable specific yield have been primarily restricted to the variation in water released from an aquifer (Newman 1987; Nwankwor et al. 1992) and very few formal attempts (e.g., White 1932; Meyboom 1967; Sophocleous 1984; Loheide et al. 2005; Crosbie et al. 2005; Sumner 2007) have been made to identify its variation in response to different natural processes such as from evapotranspiration and recharge. In natural environments, especially in humid regions with shallow water table, such as west-central Florida, the dynamics of the water table control important fluxes including root water uptake, evaporation, and recharge to the ground water table (Troch et al. 1992; Nachabe et al. 2005). Studies by Gillham (1984) and Sophocleous (1984) have reported an error, ranging from 30 to 330 times the actual value, for cases when a constant value of specific yield was used for simulating recharge.

From the foregoing discussion it is clear that sound understanding of the variable specific yield behavior is fundamental to an accurate estimation of natural and anthropogenic stresses including pumping or transpiration uptake by plants (Novakowski and Gillham 1988; Loheide et al. 2005). Different studies have analyzed the role of recharge (Crosbie et al. 2005), evapotranspiration (Loheide et al. 2005) and proximity of the capillary fringe (Gillham 1984) to land surface in isolation and no efforts have been made to compare the relative magnitudes of specific yield variation for different combinations of depth to water table and variable stress boundary conditions.

4.2.2 Objectives and Scope

This section aims at improving understanding of this variability in specific yield for different anthropogenic and natural stresses. The scope of the present work involves analysis of the specific yield behavior using saturated/unsaturated flow simulations. The objectives of this paper are to: (a) analyze the variability of specific yield due to evapotranspiration, pumping, and recharge; (b) analyze the impact of redistribution time on the specific yield variations; and, (c) analyze and comment on the validity of a constant and/or equilibrium specific yield assumption.

The basic approach of the study is to perform numerical simulations on a conceptual one dimensional column and, from mass balance, determine the volume of water added or removed by a corresponding change in the water table elevation. Using different sets of boundary conditions, various fluxes including *ET*, water table recharge, and pumping can be simulated. The analysis results in a better understanding of specific yield for different depths to water table and for different imposed fluxes.

4.2.3 Materials and Methods

4.2.3.1 Numerical Model

HYDRUS-1D (Simunek et al. 2005) was used to simulate changes in soil water content under saturated/unsaturated vertical ground water flow (Refer to Chapter 2) for further details about HYDRUS-1D).

For this investigation, a homogenous, vertical, conceptual soil column 300 cm long was setup in HYDRUS-1D. The column was subdivided into 1001 (maximum number) zones to obtain the finest possible discretization. Three different sets of simulations were made incorporating the processes of evapotranspiration (*ET*), precipitation and pumping, individually. Each set was carried out by changing the initial and boundary conditions (described under the section of *Initial and Boundary Conditions*).

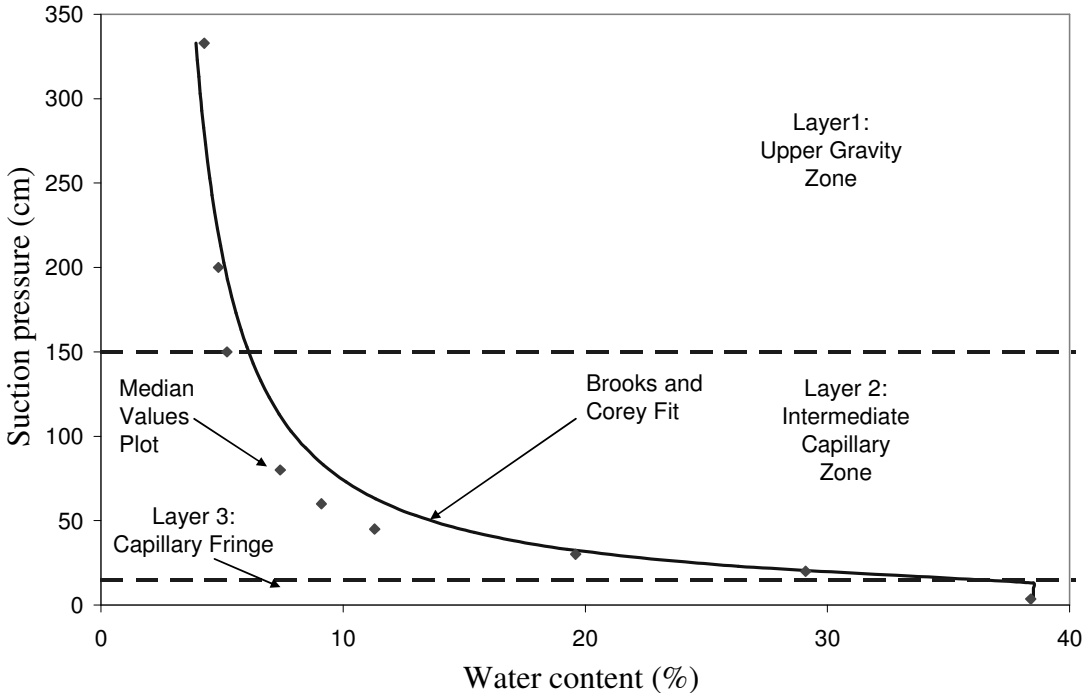

Figure 4.1 Median Values of the Observed Soil Water Retention Data Along with Best-Fit Brooks and Corey Model.

4.2.3.2 Soil Hydraulic Properties

Water retention data (soil water content versus capillary pressure) for the soils found in west-central Florida was obtained from a soil characterization survey published by the Institute of Food and Agricultural Sciences (IFAS), University of Florida (Carlisle et al. 1989). From this survey the median values of soil water content at different capillary pressures were derived (Figure 4.1). The idea behind selecting the median values is to get parameters which are most representative of soils found in west-central Florida (Figure 4.1)

The median soil data were described with an analytical model Brooks and Corey model, as given by Equations 4.2.1 and 4.2.2.

$$S_e(h) = \frac{\theta(h) - \theta_r}{\theta_s - \theta_r} = \begin{cases} \left(\frac{h_a}{h}\right)^{\lambda} & for \quad h \geq h_a \\ 1 & for \quad h < h_a \end{cases} \tag{4.2.1}$$

$$K(S_e) = K_S S_e^{\left(\frac{2}{\lambda} + l + 2\right)} \tag{4.2.2}$$

where S_e [L^3L^{-3}] is effective water content, K_s [LT^{-1}] is saturated hydraulic conductivity, θ_r [L^3L^{-3}]and θ_s [L^3L^{-3}] denotes residual and saturated water contents, respectively; h_a [L] is the air-entry pressure value (or bubbling pressure), λ [-] is a model parameter ,h [L]is the capillary pressure head and l [-] is a pore connectivity parameter assumed to be 1.0 as an average for many soils (Mualem 1976).

The IFAS data (Carlisle et al. 1989) do not list the water content for capillary pressures between 20 and 3.5 cm. From Figure 4.1, it can be inferred that the air entry pressure for the simulated soil lies somewhere between this range. Based on field experience for Florida fine sands (Trout and Ross 2004), the air entry pressure was

empirically set at 15 cm. Also, similar to the water content values, saturated hydraulic conductivity was set as the median of the saturated hydraulic conductivity values observed from the survey data. The parameter values used in the model were $\theta_s = 0.385$; $\theta_r = 0.02$; $h_a = 15$; $\lambda = 0.95$; $K_s = 9.5$ cm/hr.

4.2.3.3 Initial and Boundary Conditions

4.2.3.3.1 Initial Conditions

Numerical simulations using HYDRUS-1D for no ponding boundary conditions do not converge when the soil column is fully saturated. Hence, water table depths less than air entry pressure cannot be simulated. Therefore, the initial d_{WT} for *ET* and pumping stresses was defined at 20 cm below the land surface. For the case of infiltration and recharge simulation, the initial water table depth was set at 250 cm below land surface. Initial pressure distribution for all simulations was set as hydrostatic.

4.2.3.3.2 Boundary Conditions

In all three scenarios (*ET*, recharge, and pumping) the upper boundary condition was assumed to have no surface runoff and no ponding. A 'no-flow condition' (flux = 0) was defined at the lower boundary of the soil column for *ET* and precipitation scenarios. However, in order to simulate pumping, a lower boundary flux was set equal to the imposed pumping rate. Additionally, a uniform root zone of depth of 100 cm was defined to simulate transpiration out of the soil column.

As an average number for many regions in the U.S during the growing season, an *ET* of 0.5 cm/day was applied as a constant potential flux (e.g., Nachabe et al. 2005;

Linsley and Franzini 1972). Pumping rates were also set up at the same value to allow easy comparison and contrasting of the specific yield for different flux types. For the wetting phase, however, precipitation pulses of 5 cm and 2.5 cm for one hour were simulated with a prolonged redistribution time of 20 and 40 days. In Figure 4.2, the labels for wetting show pulse rate for one hour and the associated redistribution time (e.g., 2.5 cm/hr@40d means 2.5 cm pulse with redistribution time of 40 days). The purpose of simulating different redistribution times was to study the dependence of both rainfall intensity and redistribution time on the specific yield variability. All simulation sets were carried out independently, implying that only one of the three fluxes was active in any given simulation.

4.2.3.3 Root Water Uptake Model

The Sink term, *S*, as defined in HYDRUS-1D as:

$$S(h) = \alpha(h) S_p \tag{4.3}$$

where S(h) [$L^3L^{-3}T^{-1}$] is the actual root water uptake (RWU) from roots subjected to capillary pressure head '*h*', and S_p [$L^3L^{-3}T^{-1}$] is the potential RWU rate. For uniform root zone, S_p is defined as the ratio of potential transpiration rate and length of root zone. The α(h) is a root water uptake stress response function defined by Feddes et al. (1978). The values of α varies between 0 and 1 depending on the capillary pressure head 'h'.

4.2.4 Specific Yield Calculation

The HYDRUS-1D model solves for the pressure head and water content distributions in the domain subject to the boundary conditions described above. The

model results were used to track the evolution of the water table dynamics by tracking the elevation of the zero pressure head with time. The specific yield was subsequently determined from mass balance relationships and water table variation.

The first processing step included calculation of the simulated total soil moisture (TSM) across the entire soil profile for all specified time steps. The TSM is the total depth of water in the soil column and is calculated by integrating the water content along the soil column. Subtracting two sequential values of TSM at corresponding time steps yields the net volume of water (per unit area) leaving or entering the soil column. Equation 4.4 describes the mathematical form of the relation:

$$NetVolume\Big|_{t_i} = \int_{\zeta}^{0}(\theta)dz\Big|_{t_{i-1}} - \int_{\zeta}^{0}(\theta)dz\Big|_{t_i} \tag{4.4}$$

where θ [L^3L^{-3}] is the simulated water content at depth z [L] from the land surface at time t_i [T], with i being a running index for time and ζ [L] is the depth of soil profile. Depending on the direction of flow, net volume can be positive (water leaving the soil column) or negative (water entering the soil column).

As the simulations involve a one dimensional vertical column, the horizontal cross sectional area can be considered as unity. The specific yield can thus be computed by finding the ratio of net volume and water table elevation difference determined for the corresponding time steps as:

$$S_Y = \frac{NetVolume}{\Delta Z} \tag{4.5}$$

where $\Delta Z=Z_{i-1}-Z_i$ with Z_i [L] being the water table depth at any time t_i.

At any given d_{WT}, the most stable water content distribution occurs when there are no net fluxes in the soil column, in other words water content profile reaches equilibrium.

If this condition is disturbed by addition (e.g., infiltration) or removal (e.g., *ET*) of soil water, the soil column tends to equilibrate through redistribution of soil water content vertically, which ultimately involves water table movement.

However, in field conditions (Rahgozar et al. 2006) on a day to day basis, some limited variability in moisture content (departure from equilibrium) exists with no perceptible change in the water table elevation. Thus, the condition of a limited variability of actual water content profile with respect to equilibrium, be it dry or wet, will give an estimate of how much water can be added or removed (respectively) from the soil column without bringing about any significant changes in the d_{WT}. Stressing the moisture content beyond this limit rapidly (period of hours to days) manifests itself as a water table change as the profile progresses to re-equilibration. This limited departure from equilibrium hence quantifies storage that is not manifested as a water table change (over timescales of days to weeks), and herein is referred to as "Free Vadose Zone Storage" (γ).

Starting at any instant in time with a declining water table, if γ is zero or constant it means that all of water that is transpired out of the soil column is reflected as a water table change. On the other hand if the γ increases it means that the storage above water table is also contributing to *ET* and this contribution is not reflected as a water table change. The magnitude of γ thus gives an indication as to how much water can be cumulatively released from the storage above the water table without resulting in a water table fluctuation (within a limited time scale, e.g., a couple to tens of days). By subtracting the consecutive γ's, the loss of water from the vadose zone occurring within a given time can be estimated. Thus, the actual flux going out of the soil column can be

partitioned into that part which causes ground water fluctuation and that part which would not. As the latter flux is not contributed to directly (i.e., no vertical flux) from the water table, we will refer to it as the non-ground water flux (η). The non-ground water flux (η) results from *ET* drying of the vadose zone moisture beyond equilibrium down to the limit where no resulting water table decline occurs. To quantify η, the change in the Free Vadose Zone Storage (γ) must be evaluated. The change in γ, can be mathematically defined as

$$\Delta\gamma(t) = \Delta TSM_{eq}(t) - \Delta TSM_{model}(t) \tag{4.6}$$

where: TSM_{eq} is the total soil moisture above water table under equilibrium conditions, and TSM_{model} is the total soil moisture as calculated from the HYDRUS-1D model output i.e. the actual water content distribution. The ΔTSM_{eq} and ΔTSM_{model} are defined as:

$$\Delta TSM_{eq} = \int_{d_{WT}}^{0} \theta_{eq}\, dz\Big|_{t} - \int_{d_{WT}}^{0} \theta_{eq}\, dz\Big|_{t-1} \tag{4.7}$$

$$\Delta TSM_{model} = \int_{d_{WT}}^{0} \theta_{model}\, dz\Big|_{t} - \int_{d_{WT}}^{0} \theta_{model}\, dz\Big|_{t-1} \tag{4.8}$$

The contribution to total *ET* from the non-ground water flux can thus be calculated using Equation 4.9:

$$\eta(t) = \frac{\Delta\gamma(t)}{\Delta t} \tag{4.9}$$

From mass balance, ground water contribution (GWC) to *ET* and ground water flux (ψ) can be found using Equations 4.10 and 4.11

$$GWC = NetVolume - \Delta\gamma \tag{4.10}$$

$$\psi = \frac{GWC}{\Delta t} \tag{4.11}$$

Any flux occurring in the vadose zone, be it non ground water flux (η) or ground water flux (ψ), is governed by Darcy's Law, and hence its magnitude is directly proportional to the hydraulic conductivity of the unsaturated media. As the unsaturated hydraulic conductivity declines with increasing suction potential (see Equation 4.2) and, as the depth to water table increases, the time scale of soil water dynamics (e.g., water table recharge) increases dramatically (Hillel 1998). This results in what is known as delayed yield or release of more water from the aquifer as the time scale of observation is increased (Nwankwor et al. 1992). Hence, the time scale of observation for determining specific yield is very important. Past studies analyzing different natural processes have tackled this issue by fixing the time scale of calculations. Loheide et al. (2005), studying evapotranspiration by phreatophytes used the concept of 'readily available specific yield', introduced by Meyboom (1967) in which the time step of calculation was kept to less than 12 hours. Crosbie et al. (2005), in a different study calculated 'apparent specific yield' by assuming equilibrium conditions in the vadose zone 15 hours after a recharge event. For the current study, the time step of assessment was set at 24 hours for the simulation with boundary conditions of evapotranspiration and pumping. For recharge boundary conditions, two different time steps were used (20 and 40 days) to analyze the sensitivity of the time of redistribution on specific yield values.

4.2.4.1 Calculation of Equilibrium Specific Yield

Equilibrium specific yield is defined herein as the amount of water released/stored per unit decline or rise in the water table considering the water content profile remains at

equilibrium at all times. To determine equilibrium specific yield for any water table depth, equilibrium total soil moisture (Φ) for the whole column was calculated using as

$$\Phi = \int_{\zeta}^{0} \theta_{eq}(z)dz \tag{4.12}$$

where, ζ is the depth of soil profile, $\theta_{eq}(z)$ represents the equilibrium soil moisture content at any depth z, corresponding to a particular water table depth (d_{WT}). The ratio of the difference between the Φ and the difference in the corresponding water table depths yields the equilibrium specific yield value. Mathematically, this is expressed as

$$S_{Y_{eq}} = \frac{\left| \Phi_{i-1} - \Phi_i \right|}{\left| d_{WT_{i-1}} - d_{WT_i} \right|} \tag{4.13}$$

One important thing to note is that for the current study, as water table variations were not large, the specific yield obtained for a pair of initial and final water table conditions was assigned to the final water table depth.

Another point is that the drying simulation was carried out until the ratio of actual *ET* (calculated from Equation 4.4) and assumed potential *ET* (*PET*) became less than one percent. This value was arbitrarily chosen as the limit of effective *ET*. Also, the d_{WT} decline shows an asymptotic behavior with time. Thus, the simulation involving pumping of ground water was terminated at the same d_{WT}.

Before considering the results and inferences drawn from them, it is important to point out the reliability of the model to the field conditions. Shah et al. (2007) and Desilva et al. (2007) performed extensive calibration and verification of the HYDRUS model to west-central Florida field data with Myakka fine sand as the dominant soil type at their study site. Both studies showed that the HYDRUS simulation was highly

successful in mimicking observed water table and soil moisture profiles for multiple-year records. The reader is directed to those studies for demonstration of model validity, calibration and sensitivity.

4.3 Results and Discussion

Specific yield obtained by carrying out different simulations is shown in Figure 4.2. It becomes clear that specific yield varies with water table depth for all stresses: wetting, drying or pumping, as well as no stress condition, i.e., equilibrium. What follows is a detailed discussion on the evolution of variable specific yield and the soil physics governing this variation for different types of fluxes.

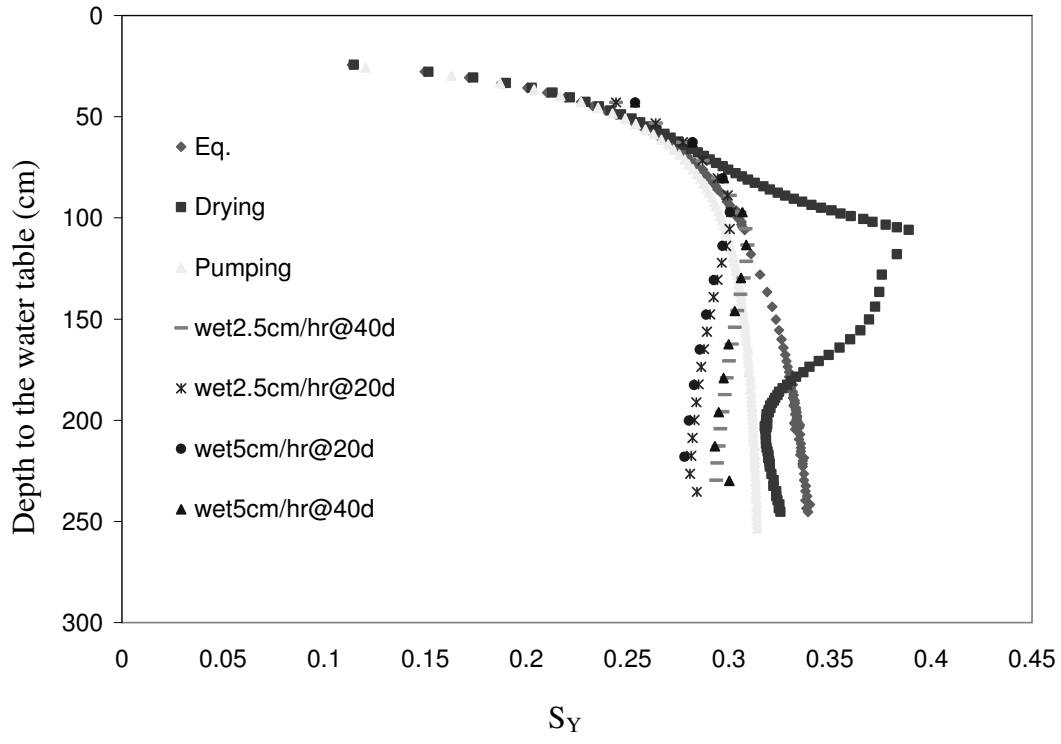

Figure 4.2 Variation of Specific Yield in Response to Different Stresses.

4.3.1 Drying Specific Yield

Investigation of variability of the specific yield under drying conditions shows irregular behavior. To understand this behavior, the non-ground water flux (η), ground water flux (ψ), and the actual *ET* flux going out of the column were plotted against the depth to water table (Figure 4.3). Initially when all *ET* is coupled to the water table (all ground water *ET*), the specific yield corresponds to equilibrium specific yield (which is also very small). However, as the depth to water table increases, free vadose zone storage (γ) commences to contribute to the net *ET* from the soil column keeping the *ET* at potential. This implies that, for this period, the *ET* flux is still at potential but due to decrease in the ψ the rate of water table decline decreases, causing a sharp increase in specific yield (as calculated from Equation 4.5). As ψ decreases, the η continuously increases to maintain the net *ET* flux at potential. Since, the water content in the vadose zone is limited, after reaching a maximum, η ultimately declines as moisture content approaches residual water content value. This causes the actual *ET* to decline below the imposed potential value (Figure 4.3). From this point onwards as actual *ET* values start to decrease the net volume leaving the soil column also declines, causing the specific yield values to decline.

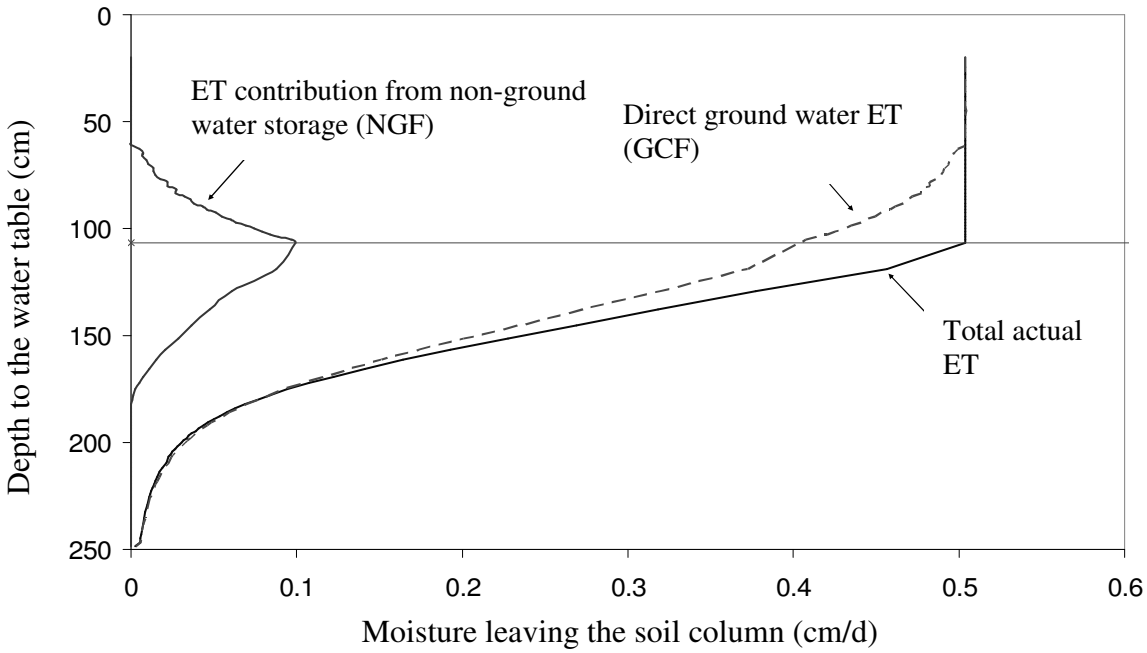

Figure 4.3 *ET* Contribution from Direct Ground Water (Water Table) and from the Non-Coupled Soil Water Storage Above the Water Table.

Figure 4.4 shows the variability of free vadose zone storage versus depth to water table. With increasing d_{WT}, the free storage in the soil column continuously increases indicating the contribution of η and justifying relatively higher values of S_Y as compared to the equilibrium values. However at approximately 170 cm below the land surface γ becomes constant showing zero contribution from non-ground water flux. From Figure 4.3 it can be seen that this is the point where the drying specific yield values coincides with the equilibrium value. From this point onwards saturated ground water is fully contributing to the actual *ET* (see Figure 4.3). However, as the soil moisture condition is much drier than the equilibrium condition, the flux from the soil is small and effectively negligible (Figure 4.3). This has been shown to be a practical limit of extinction (Shah et

al. 2007). This causes the drying specific yield values to decrease with respect to the equilibrium S_Y values.

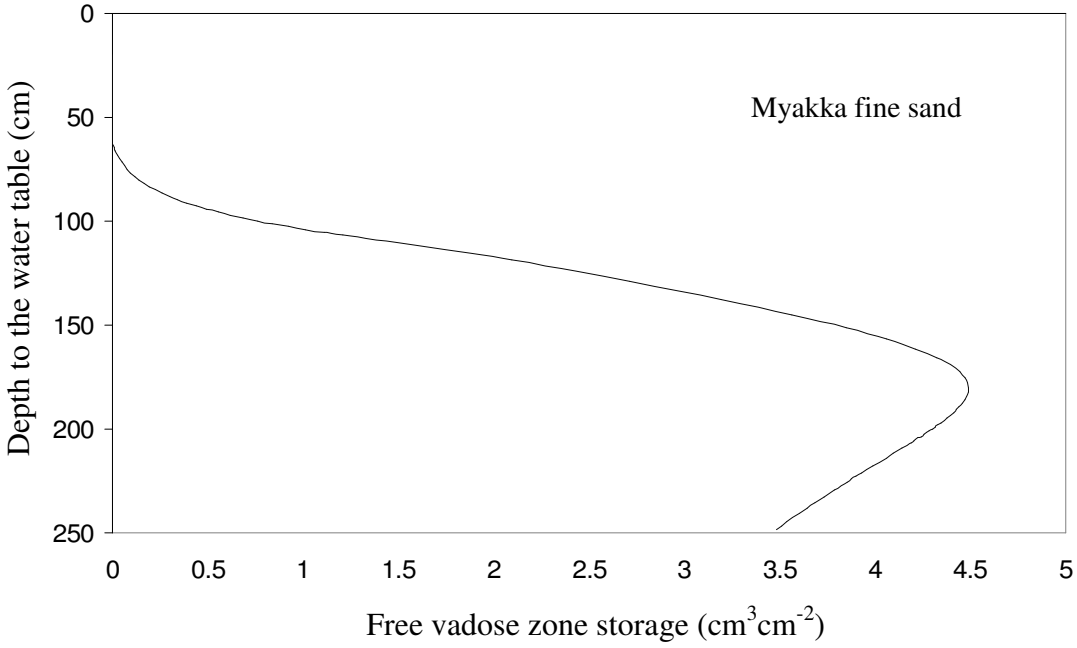

Figure 4.4 Available Free Vadose Zone Storage for Variable Depth to Water Table.

4.3.2 Specific Yield under Pumping Conditions

For pumping simulation, the explanation for having the specific yield values less than equilibrium, is more straightforward. Initially, when the water table is shallow (the water table is strongly coupled to with the vadose zone), the moisture condition is near equilibrium and the specific yield of pumping corresponds to the equilibrium specific yield. However, with increasing time and decreasing water table this coupling weakens. As water is continuously withdrawn from the water table via pumping, it takes increasingly more time for soil moisture in the vadose zone to redistribute vertical head gradients and non-equilibrium conditions persist. The net result under pumping is that,

the moisture conditions in the vadose zone are always elevated, with respect to the equilibrium (see Figure 4.5). This means less moisture (as compared to equilibrium conditions) is removed from the soil column rendering a specific yield value less than the corresponding equilibrium value. Over time, however, a sort of quasi-equilibrium is established with the amount of moisture uptake and moisture addition to an expanding vadose zone due to water table decline become roughly equal. Hence the specific yield over time becomes a constant value even though it remains less than equilibrium value. The simulation with a higher pumping rate shifts the specific yield values slightly to the left (further reduction). However this effect is minor and can be neglected, indicating that specific yield is not especially sensitive to the pumping rate.

For pumping conditions a common assumption is that specific yield values always follow the equilibrium specific yield curve (McWhorter and Sunada 1977; Nachabe 2002). However, contradicting this assumption, the current study clearly indicates that the specific yield values for pumping (in this case 0.5 cm/day) followed an equilibrium curve only until the d_{WT} of is about 50 cm. Beyond this depth the pumping S_Y was consistently smaller than the equilibrium specific yield.

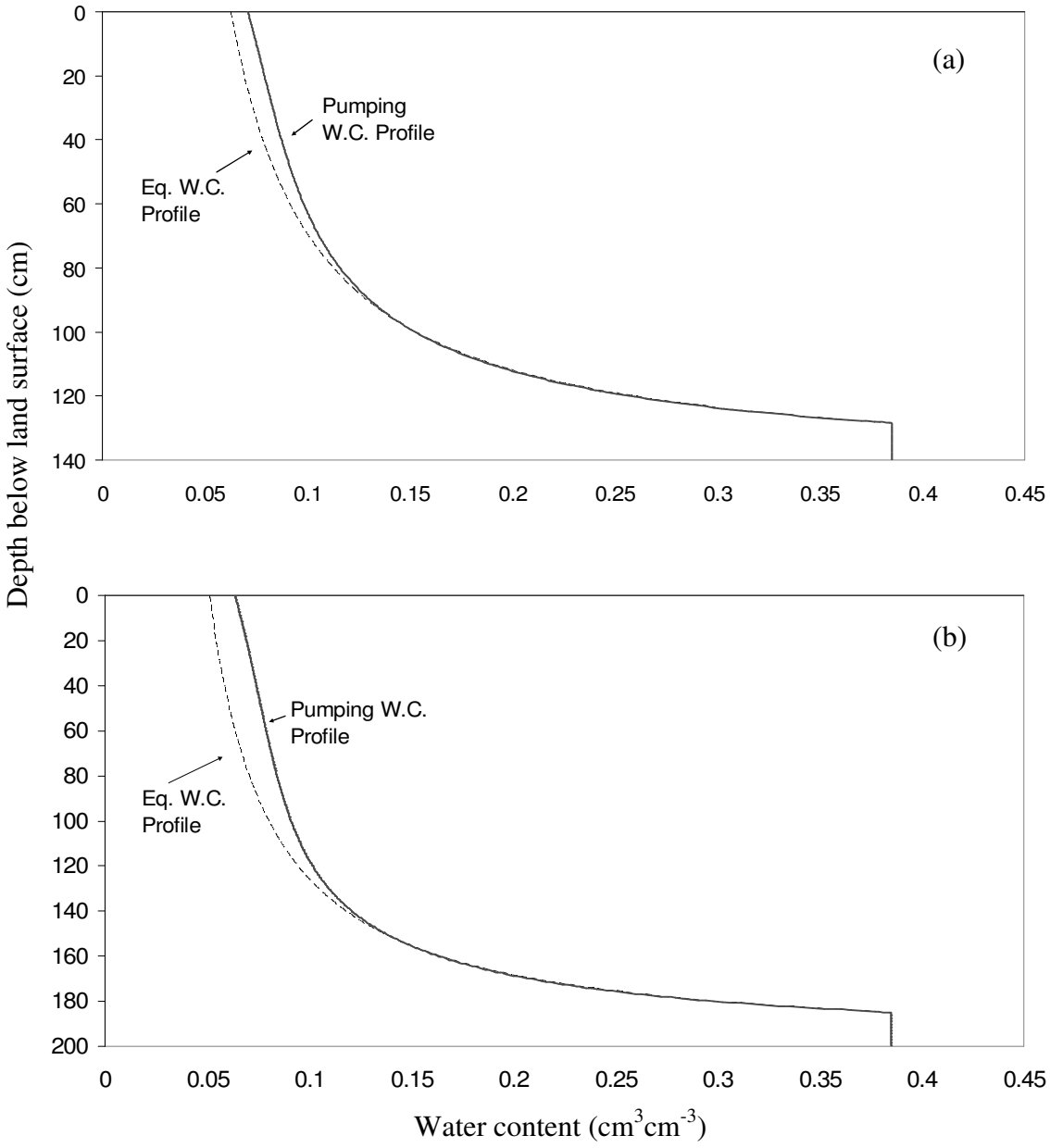

Figure 4.5 Actual Water Content Profile for Pumping and Equilibrium After (a) 60 and (b) 100 Days of Pumping.

4.3.3 Specific Yield under Wetting Conditions

In this set of simulations, the initial depth to water table was set to 250 cm below the land surface and the evolution of specific yield from d_{WT} equal to 250 cm up to the land surface was examined from infiltration wetting. When the water table is deep (250 cm), due to weak coupling, the wetting fronts take considerable time (~10-15 days) to make it to the zone of saturation. Hence, within this time frame of couple of weeks the water table rise is primarily due to redistribution of earlier wetting fronts. However, once the water table rises to a certain level (<1 m), the vadose zone and water table get strongly coupled again. With rising water table elevation, infiltration fluxes increasingly create more responsive recharge behavior. The reason for this is simply that the wetting front has to travel a shorter distance and also the rising water table encounters (and helps maintain) elevated moisture conditions in the vadose zone (Figure 4.6). Hence, the specific yield values again decrease with shallower water table and the profile appears more like the equilibrium distribution as can be inferred from Figure 4.2.

The time to redistribute can be considered analogous to the time for complete drainage which is also called delayed drainage (Nwankwor et al. 1992). Nachabe (2002) quantitatively defined this time as a function of soil properties and found it to decrease with decrease in water table depth. It is for this reason that the curves corresponding to greater redistribution time are closer to the equilibrium specific yield for both rainfall rates. It also appears that redistribution time is not a function of rainfall depths (rate). An interesting fact can be seen from the wetting curves in Figure 4.2. For the same redistribution time, even if the precipitation rate is doubled, specific yield behavior remains essentially the same. This suggests specific yield variability is just a function of

redistribution time. However, if a simulation is made with very high infiltration rates (~10cm/hr) the water table rise is so great within the time frame of observation that the model is not able to capture the actual variability of specific yield. Anything short of this critical threshold high rainfall rate results in essentially similar specific yield behavior.

4.4 Comparison with Other Studies

Variability in the specific yield is not a new concept; however, such detailed analysis of its variability does not exist in the literature. The ensuing paragraphs describe the current study put in perspective with the past studies on this topic. A discussion about how the current results corroborates or contradicts previous studies is also provided.

Healy and Cook (2002) in their thorough review of field and laboratory methods for determining specific yield pointed out that the estimate of specific yield suggested by dos Santos and Youngs (1969) and Duke (1972) provides a good starting point, to which further adjustments have to be applied to account for hysteresis, field scale heterogeneity and other variables. The suggested relationship is

$$S_Y = \phi - \theta(h) \tag{4.14}$$

where ϕ [L^3L^{-3}] is the saturated water content and $\theta(h)$ [L^3L^{-3}] is the water content at the land surface for any given depth to water table h [L] and S_Y is the specific yield value. A big limitation of this relationship is that Equation 4.14 is valid only when the initial and final water contents are at equilibrium value. Comparison of Equation 4.14 with the equilibrium specific yield values calculated using Equation 4.13 showed an exact overlap in the calculated specific yield values for the entire range of water table depths. This

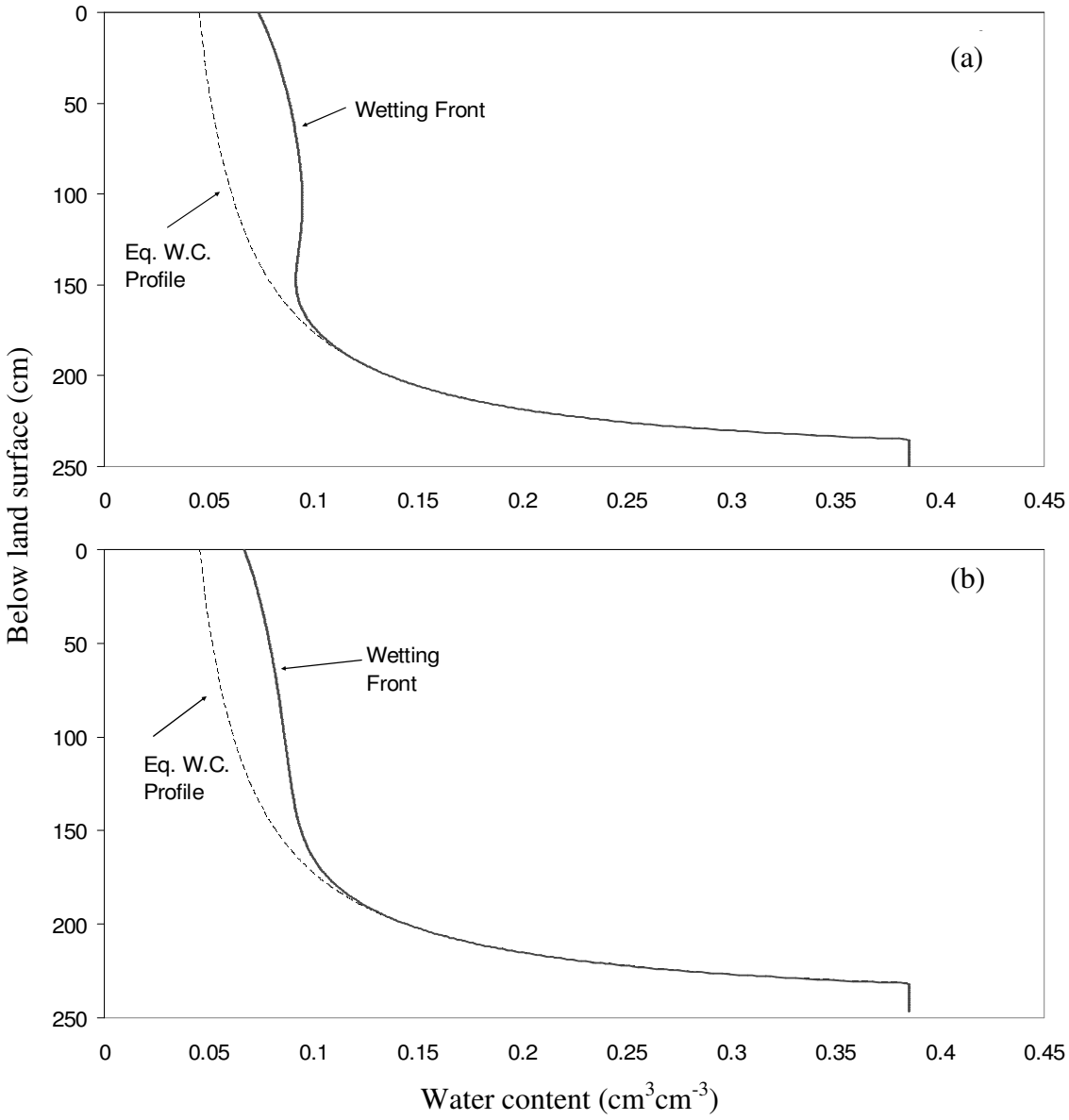

Figure 4.6 Wetting Front and the Equilibrium Water Content Profile After (a) 20 and (b) 40 Days of the Pulsing Soil Column with 5cm/hr Rainfall Infiltration for One Hour.

supports the premise that if the conditions are in equilibrium this simple equation can be effectively used for specific yield calculation. However, as can be seen from Figure 4.2, for imposed wetting, drying, and pumping boundary conditions, the specific yield values

depart from the equilibrium specific yield (in some cases considerably) as the water table becomes deep.

Therefore, assuming equilibrium specific yield values for all stresses can cause, in some cases, considerable error in the estimation of water table fluctuations or fluxes such as evapotranspiration (Loheide et al. 2005). Loheide et al. (2005) referred to the above relationship (Equation 4.14) as depth compensated specific yield, while Crosbie et al. (2005) called the same relationship apparent specific yield. As the initial and final conditions, warranting the validity of the above equations have to be equilibrium water content and the results match exactly to equilibrium specific yield values (Equation 4.13) derived from comprehensive mass balance analysis, it is more intuitive to refer to Equation 4.13 as equilibrium specific yield ($S_{Y_{eq}}$) and use it as a common terminology for all the processes such as recharge and evapotranspiration.

A more common method used for calculation of specific yield, especially for deep water table environments (d_{WT} >2 m), is the difference between the saturated water content (θ_S) and the water content at field capacity (θ_{fc}) (e.g., McWhorter and Sunada 1977).

$$S_{Y_0} = \theta_s - \theta_r \tag{4.15}$$

The field capacity is often defined as the moisture retention for drained soil at 1/3 bar pressures (Jamison and Kroth 1958). For the soil used in the HYDRUS investigation S_{Y_0} is about 0.34, which is the value of the equilibrium specific yield at water table depth of about 200 cm below the land surface. Thus, it is clear that using a constant value of specific yield for analysis involving shallow water table will result in significant error

and dampened ground water fluctuation. For deep water table environments, however, Equation 4.15 is a reasonable estimate of specific yield value for normally mild soil fluxes (< 1 cm/day). Also, further supported by this study is the case of S_Y for a very shallow water table, when the capillary fringe intersects the land surface. Due to limitation of HYDRUS, and the use of Brooks and Corey moisture retention model, specific yield values were not calculated for water table shallower than capillary fringe value. However, results of Crosbie et al. (2005) and Gillham (1984) can be easily used to show that the specific yield continues to decline with decreasing water table depths and ultimately becomes zero as the capillary fringe comes up to the land surface. For conditions of d_{WT} shallower than capillary fringe, a negligible release or addition of water would be required to significantly change water level. The latter phenomenon, known as the reverse Wieringermeer effect, was first modeled by Gillham (1984) and later observed in the field by Helitois and Dewitt (1987).

The water content profiles by Loheide et al. (2005) present an interesting contradiction when compared to the water content profiles obtained under drying conditions. Figure 4.7(a and b) show the simulated water content under drying to be smaller than the equilibrium water content, which is totally contrary to what Loheide et al. (2005), simulated (see Figure 9 in Loheide et al. 2005). The reason for this discrepancy is that root water uptake in the current study is both from the vadose zone and ground water as opposed to just ground water in Loheide et al. (2005). Therefore, the simulated root uptake conditions for their study correspond to a pumping simulation where all the demand is met from ground water. Hence, the water content profiles for pumping (Figure 4.6) closely match those obtained by Loheide et al. In other words the

specific yield values obtained by Loheide et al. (2005) for evapotranspiration will always be lower than the equilibrium specific yield, contrary to the corresponding specific yield values obtained in the current study.

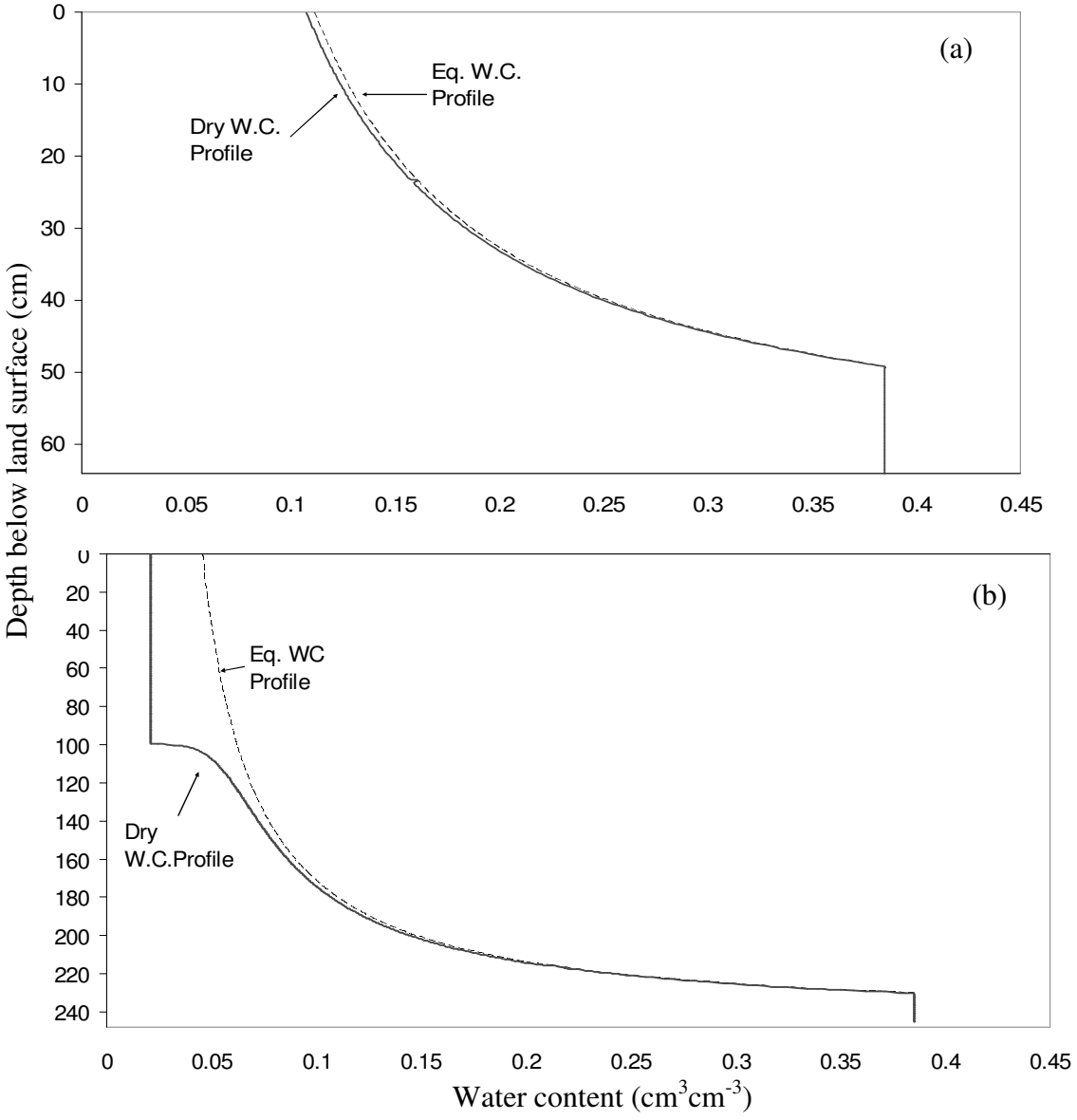

Figure 4.7 Departure of Drying Water Content Profile from the Equilibrium with Increasing Water Table Depths. (a) Near Equilibrium for Shallow Water Table (b) Following Water Table Decline.

One of the biggest implications of this observation is that the specific yield values calculated by Loheide et al. may be only applicable to phreatophytes and the tri-linear diagram obtained by them will be valid only if the roots are extracting water solely from the ground water.

4.5 Conclusions

Numerical simulations were done to analyze the variability in specific yield under different stresses: wetting, drying, and pumping, as well as equilibrium. It was found that there is significant variation in the specific yield values depending on the water table depth and the stresses involved. The value of specific yield was found to be lower than equilibrium for wetting conditions while for drying it was higher. *ET* rate as well as redistribution time was found to play a major role in deciding the value of specific yield for any depth to the water table

An important conclusion that comes from this analysis and corroborates previous theories is that the assumption of a constant specific yield is erroneous and may cause large error in the calculation, especially in shallow water table environments ($d_{WT} < 2m$). For pumping scenarios it was found that, contrary to the assumption of most models (e.g., MODFLOW), S_Y deviated from equilibrium conditions substantially. In addition, for wetting scenarios it was observed that the redistribution time was the main factor governing the specific yield variability and that recharge and the corresponding water table response can lag behind the infiltration event significantly (> 40 days) even in modest water table depths (< 2 m). In a field setting with plant water demand, most of the

delayed recharge would undoubtedly be taken up by the *ET* during inter event periods throughout the root zone.

From the point of view of potential error introduced, it can be concluded that the for deep water table conditions (> 2m) the S_Y values tend to converge within 10-15% of equilibrium, implying that the assumption of constant/equilibrium specific yield can be used as a good approximation for simulating water table fluctuation under these conditions. It should be noted that hysteresis was not simulated in the HYDRUS-1D runs, yet strong specific yield variability was obtained. Therefore, it can be concluded that variability in specific yield is not just an artifact of hysteresis; its presence, however, will enhance variability in S_Y.

The above sets of simulations were done only for fine sandy soil characteristic of the coastal plain and in particular, west-central Florida. The main objective was to discuss the qualitative behavior of the specific yield with water table stress. Depending on the site and specific soil parameters, the quantitative behavior may change significantly. However the implications for and possible errors in, predictive models of the water table in alluvial, wetland and other shallow water table settings is significant.

Chapter 5: Vadose Zone Evapotranspiration Distribution and Conceptualization for Integrated Modeling

5.1 Introduction

The vadose zone is an intrinsic part of the hydrologic cycle, essentially controlling interrelationships between precipitation, infiltration, surface runoff, evapotranspiration (*ET*) and ground water recharge. The vadose zone regulates the transfer of water from the land surface to ground water and vice versa, while providing protection, screening, filtering, transfer, and attenuation of potential ground water contaminants that are delivered via the land surface. Yet, unlike the ground water below and surface water resources above, the dynamics of the vadose zone have not been quantified as well (Harter and Hopmans 2004). The potential for continuous capillary rise maintains *ET* at potential rates long after other parts of the landscape dry out (Gardner 1958).

The vadose zone receives water from rainfall and capillary rise, and delivers water through *ET*. *ET* is an important element of the hydrologic cycle and is the dominant component of the annual rainfall of a region (e.g., 70 or 80 percent in Florida Bidlake et al. 1993; Knowles 1996; Sumner 2001). Unfortunately, *ET* can be the most difficult hydrologic process to analyze.

Of several different approaches of quantifying the distribution of *ET* stress (e.g., Bicknell et al. 2001; Banta 2000) in the unsaturated and saturated zone, the approach involving solution of Richard's equation for unsaturated flow can provide a more precise method of determining water movement between the soil surface and the ground water table. However, due to the computational burden and data requirements of this approach, most of the watershed models use simple approximations or empirical algorithms to allocate evapotranspiration to different regions in the vadose zone. *ET* distribution plays a critical role in integrated models which combine the surface water and ground water processes via vadose zone. The uncertainties in the source of *ET*, whether supported by water table, or the vadose zone, can introduce error in simulations of water table in recharge and base flow.

A number of integrated models have been developed in the past 10 to 20 years including, FHM (Ross et al. 1997), WASIM-ETH (Schulla and Jasper 2000) and the Integrated Hydrologic Model (IHM) (Ross et al. 2003). Different integrated models use different approaches to partition *ET* stress between saturated and unsaturated zones. For instance, IHM distributes *ET* using a three-layer soil water concept (Ross et al. 2005). The three-layer concept defines four thresholds controlling vadose zone and ground water contribution to *ET*. Based on these thresholds, *ET* demand from the vadose zone/ground water (water table) can be satisfied: (a) entirely by the vadose zone, (b) partially from both vadose zone and ground water, (c) by direct evaporation from the soil, or (d) entirely by ground water at open-water evaporation rates.

5.1.1 Objectives and Scope

Though the origin of the above mentioned three-layer soil water concept lies in the conceptualization of *ET* processes in one of the most commonly used surface water model, Hydrologic Simulation Program-FORTRAN (HSPF) (Bicknell et al. 2001), it has never been rigorously tested using the saturated-unsaturated theoretical flow equations. The objectives of this chapter are thus: (a) To use a theoretical framework to determine the distribution of *ET* stress between the vadose zone and ground water and (b) compare and contrast the results obtained with the three layer concept used in IHM.

5.2 Materials and Methods

The simulation technique and the type of soil used are same as that used in Chapter 5 on specific yield. However, as the interest now is to find out thresholds that control vadose zone and ground water components of the total *ET* flux, different initial and boundary conditions were defined.

5.2.1 Initial and Boundary Conditions

Two simulations were done by changing the initial and boundary conditions to simulate the process of evapotranspiration in as much detail as possible. The first simulation was set initially to have depth to the water table (d_{WT}) at 20 cm below land surface, while d_{WT} of 250 cm below land surface was set up for the second simulation. To facilitate easy reference, the simulations can be named as simulation A and simulation B, respectively. The initial conditions in the soil column were set up to be hydrostatic in both sets. In both scenarios, the upper boundary was assumed to have no surface runoff

and the land surface was open to the atmosphere. In addition, a no flux boundary (constant flux = 0) was assumed as the lower boundary of the soil column.

A 100 cm uniform root zone was assumed for the simulations to facilitate transpiration out of the soil column. As an average number for many regions in the U.S during the growing season, an *ET* of 0.5 cm/day was applied as a constant potential stress (e.g., Nachabe et al. 2005; Linsley and Franzini 1972).

The post processing of the HYDRUS output was carried out in the exact same steps as described in Chapter 4. Free vadose zone storage, non-ground water flux and ground water flux were consequently determined for both simulations A and B.

What follows is a brief discussion about the three-layer concept used in IHM for *ET* partitioning. The purpose of the discussion is to provide a background to help in the discussion of results. Detailed information about IHM and/or *ET* conceptualization in IHM can be found in (Ross et al. 2005).

5.2.2 Three-Layer/Two Zones Concept

The Integrated Hydrologic Model (IHM) was developed to simulate surface and ground interaction - especially in shallow water table systems (Ross et al., 2005). IHM couples surface and ground water processes in a unique integration of the Hydrological Simulation Program-FORTRAN (HSPF) (Bicknell, et al. 2001) and MODFLOW (McDonald and Harbaugh 1996) respectively.

In HSPF (Bicknell et al. 2001), the unsaturated zone between the land surface and water table is divided into two regions, the upper zone (top 10-15 cm) and the lower zone (remainder of the vadose zone) as shown in Figure 5.1. The upper zone is comprised of

'*A*' horizon (shallow soil), and surface depressions, including small isolated wetlands, ponds, and small lakes, not "routed" in the model. The lower zone represents the remainder of unsaturated zone down to the shallower of the extinction elevation or the water table elevation. It is the lower zone which is responsible for sustained moisture availability and dry period root zone evapotranspiration (Bicknell et al. 2001).

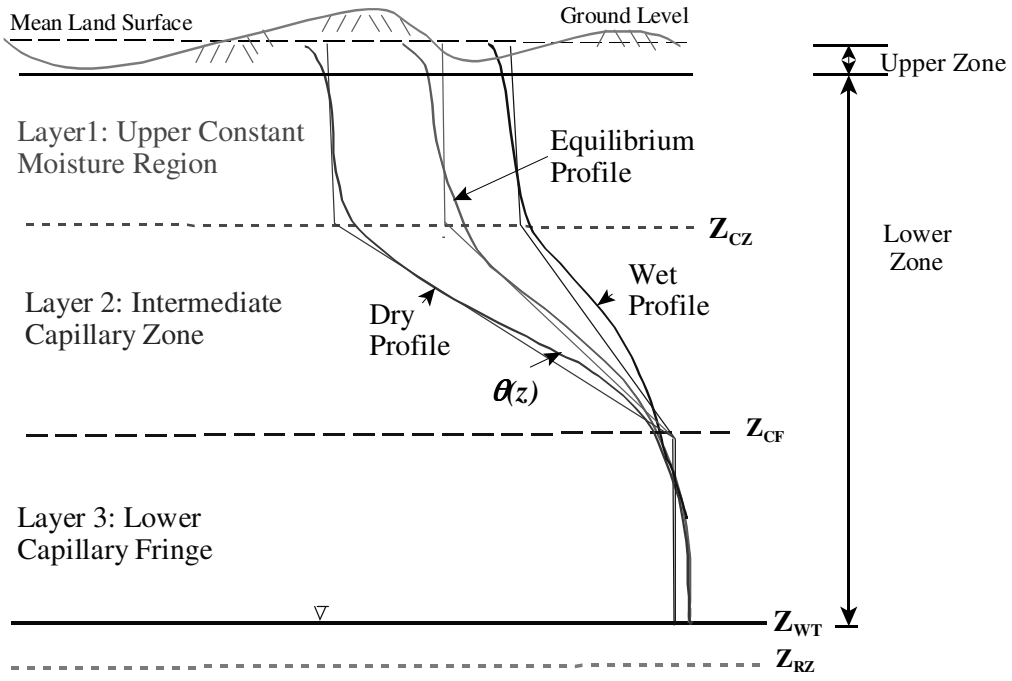

Figure 5.1 Three-Layer Water Content Concept Used in IHM.

IHM partitions the water within the saturated and unsaturated zones using a three layer soil water retention profile. This assumption is considered to be a significant improvement over the simple uniform moisture profile assumption of the integrated models (e.g., MIKE-SHE (Ross et al. 1997)), in the approach of integrated modeling. The three-layer concept has lead to four threshold conditions that illustrate transition points in

the distribution of *ET*. Based on these thresholds, *ET* demand from the vadose zone/ground water can be satisfied: (a) entirely by the vadose zone, (b) from both vadose zone and ground water, (c) from the soil (direct evaporation), or (d) entirely from ground water at fractional potential evaporation rates.

In IHM, for analyzing soil water variability, the lower zone is divided into three layers; the upper gravity region, the intermediate capillary zone, and the lower capillary zone (capillary fringe) as shown in Figure 5.1. Lower zone storage as defined in IHM is the moisture available to the root zone for any given water table elevation that is above the wilting point, or driest profile. For deep water table conditions, the lower zone storage can exhibit the largest values incorporating a range of variable soil water retention to an effective depth below the root zone (assumed to be the soil intermediate capillary zone thickness). This follows the plant behavior within the root zone, i.e., the ability of plants to reduce soil water content to near wilting value and indirectly bringing about a reduction in the soil water content.

The deepest layer, right above the water table, represents the near-saturation capillary fringe. This layer is followed by the intermediate layer of capillary rise. This intermediate layer shows maximum variation of soil water with depths. Both layers are assumed to be fixed by the soil type. For deep water table conditions ($d_{WT} > \zeta_x$), the uppermost layer (close to land surface) represents the nearly uniform soil water region above the capillary rise (capillary zone). For shallower conditions of water table this layer of uniform soil water content may be totally absent. Three profiles are shown in Figure 5.1, corresponding to dry, equilibrium and wet soil moisture conditions of a mildly sorptive soil (e.g., loamy sand). The thick lines on the figure represent the actual profiles

in a uniform soil and the thin lines represent a stepwise, linear approximate profile developed for computational efficiency.

Because evapotranspiration (*ET*) represents a dominant process in the water cycle (second only to rainfall) and controls the partitioning of energy and water fluxes at the land surface, it is used in this study to test the three-layer approach. Four threshold conditions (case a-case d), shown in Figure 5.2, illustrate transition points in the distribution of *ET* from one region of vadose zone or ground water to another. All elevations, z, are relative to a common datum (e.g., the National Geodetic Vertical Datum of 1927, NGVD) including land surface (z_{LS}), capillary zone (z_{CZ}), capillary fringe (z_{CF}), root zone (z_{RZ}), and water table (z_{WT}).

5.3 Results and Discussion

5.3.1 Numerical Simulation

Results from the HYDRUS-1D model that were used to determine the actual *ET* leaving the soil column simulation showed that the extinction depth was about 250 cm (based on *ET*/*PET* of 0.5%) for the root zone of 100 cm. Based on the Brooks and Corey function fitted to retention data for Myakka fine sand, the thickness of the capillary zone (a region of pronounced elevated retention) comes out to be approximately 150 cm. Thus, the extinction depth is consistent with the IHM definition of capillary zone plus root zone. On looking closely at Figure 4.1 and comparing it with Figure 5.1, distinct three-layer behavior for the soil types found in west-central Florida can be easily observed. Also shown in Figure 4.1, the capillary zone of the median water retention characteristics is approximately 150 cm. Thus, HYDRUS 1D solutions support the IHM definition of

extinction depths and also the three layer soil water retention behavior can be clearly observed.

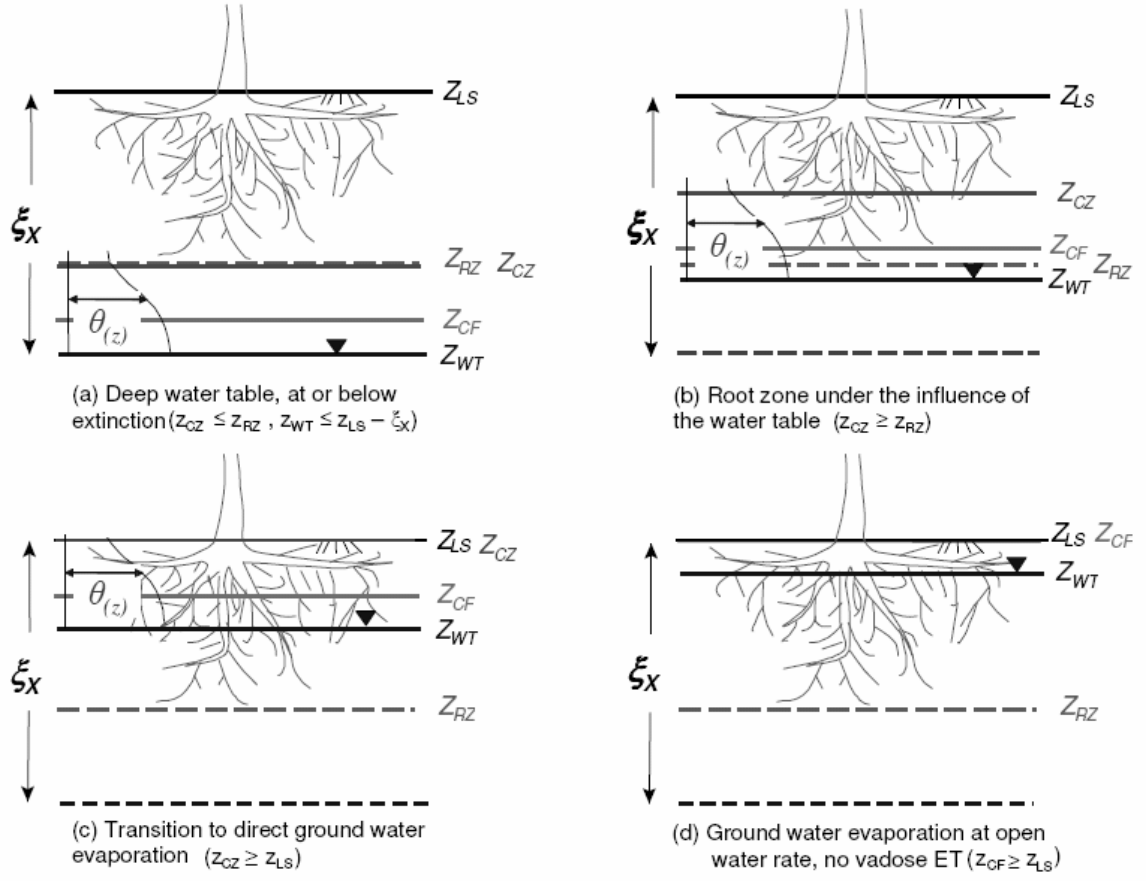

Figure 5.2 Thresholds Used in IHM for Distribution of *ET* between Vadose Zone and Ground Water.

5.3.2 *ET* Thresholds Conditions

5.3.2.1 Case A

As conceptualized in IHM that if water table is at or below extinction, all the contribution will be from the vadose zone, i.e., all the *ET* will be supported by free vadose zone storage. The simulation of HYDRUS-1D with water table at 250 cm below

land surface with initial conditions being hydrostatic showed that even after 10 days of *ET* stress, the water table did not decline further and all flux came from the storage above the water table (vadose zone *ET*). Figure 5.3 shows that the initial equilibrium profile has shifted over to the dry profile. However, there was no movement in the water table and the actual *ET* rate declined very fast to a value below 0.5% of *PET* after 10 days, the working definition of extinction depths.

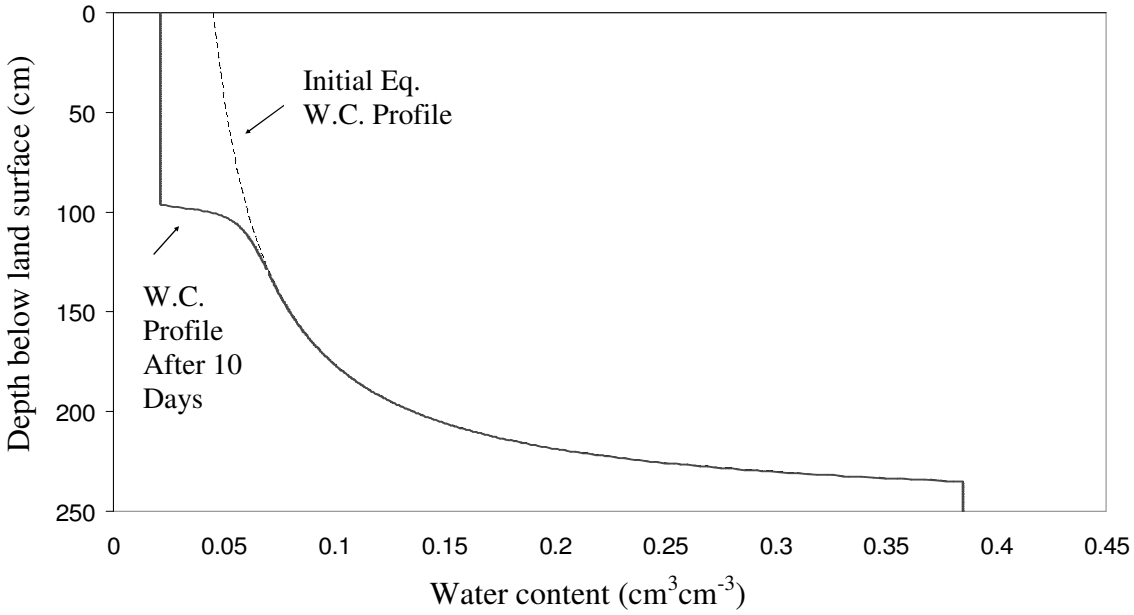

Figure 5.3 Water Content Profiles for Equilibrium and Dry Conditions after 10 Days of *ET* with Water Table at the Extinction Depth.

5.3.2.2 Case D

To validate case D, the simulation was done starting with the water table depth of 20 cm below ground water. However, as in Figure 4.3, the ground water supports all the *ET* at potential rate, up to a depth of around 60 cm, which is about four times the magnitude of capillary fringe (15 cm). The reason for this can be explained by the

weakening of the hydraulic connection with the water table for depth below 60 cm, where the water transpired by roots cannot be replenished at the same rate by ground water. Deep roots can extract water directly from the ground water up to greater depths, thus ground water contribution remains at potential to a greater vertical extent. Therefore, depth to water table at capillary fringe depth is a reasonable threshold for complete ground water *PET* support (all ground water *ET*) however, HYDRUS 1D solution indicate that the potential *ET* is satisfied from ground water contribution up to 60 cm.

5.3.2.3 Case B and Case C

For cases B and C, for d_{WT} greater than 60 cm the contribution from the storage in the vadose zone becomes important and hence, as shown in Figure 4.3 in Chapter 4, as the ground water contribution decreases the free vadose zone *ET* flux increases. The combined vadose zone plus ground water flux supports the *PET* rate to a depth of 1 m. If water table continues to drop (from case D to cases B and C) after the initial transition, *ET* will be supported by ground water *ET* and partially vadose zone *ET* contribution as conceptualized in IHM. Once the water table drops below the root zone, the free vadose zone flux will start to decrease and rapidly tend to zero.

As mentioned earlier due to the kind of boundary conditions set up the simulation renders the vadose zone conditions to be driest possible state for any d_{WT} at the given *ET* stress. To determine the effect of wetter vadose zone conditions on the *ET* distribution simulations with different initial d_{WT} under hydrostatic conditions were done, the results were compared with the original simulation. Figure 5.4(a) shows total soil moisture above the water table plotted versus corresponding d_{WT}. The change in the *TSM* above

the water table can be considered as an indicator of the contribution from the vadose zone while the water table decline shows the saturated ground water contribution. From Figure 5.4(a) it is clear that the equilibrium and the soil moisture values obtained from the initial simulation sort of blanket out the soil moisture variation in the vadose zone, hence corroborating the earlier statements about driest condition and maximum γ (Free vadose zone storage).

Two main characteristics as seen in Figure 5.4(a) are, (a) at any d_{WT} the initial conditions starts from the equilibrium (as set up in the model) and ultimately transitions to the moisture profile of the original simulation and (b) the rate of decline of the d_{WT} in the transitions keeps on decreasing as the initial d_{WT} keeps on increasing. These observations indicate that non-coupled flux increases proportionally with the degree of wetness of vadose zone profile. A close analysis of Figure 5.4(a) show the above 60 cm vadose zone conditions don't play a role as they are always at equilibrium. Around 100 cm, both the vadose zone and the ground water storage are actively supporting the *ET* stress however the loss of vadose zone soil moisture now is clearly greater than the initial simulation, showing greater magnitude of η (Non ground-water flux). For deeper water table (d_{WT} >150) it can be seen that all the *ET* stress is supported by vadose zone until the soil moisture conditions transitions to the driest possible profile after which the water table contribution becomes active. At or beyond extinction all the extra moisture of vadose zone is lost and then *ET* virtually stops without bringing about any changes in the d_{WT} (as previously noted in Figure 5.3). The above observations prove that the thresholds of *ET* remain unchanged for different antecedent moisture conditions; however the magnitude of contribution coming from saturated ground water and vadose zone is highly

dependent on prior conditions. To test for water content profile wetter than equilibrium two different simulations involving rainfall for some time, followed by the *ET* stress were done. The results are plotted in Figure 5.4(b). As expected from the γ concept all the extra moisture beyond equilibrium was first dried up without any water table change and then the transition to the driest profiles begins exactly similar to what was observed in earlier simulation (Figure 5.4(a)).

5.4 Limitations

Although the above results and discussion showed that the concept of the three layer model can be verified using the HYDRUS-1D model, there are certain limitations to this verification as well as some differences between the two models. Rigorous three-layer concept in IHM is a simple approach requiring no flux-stress model.

The problem with Brooks and Corey model is that the thickness of the capillary fringe layer that has to be defined explicitly. In this study, a thickness of 15 cm was pre-defined. The comparisons between the two models showed that the qualitative definition for the layer thicknesses can lead to overestimation or underestimation of the threshold thicknesses as in case D.

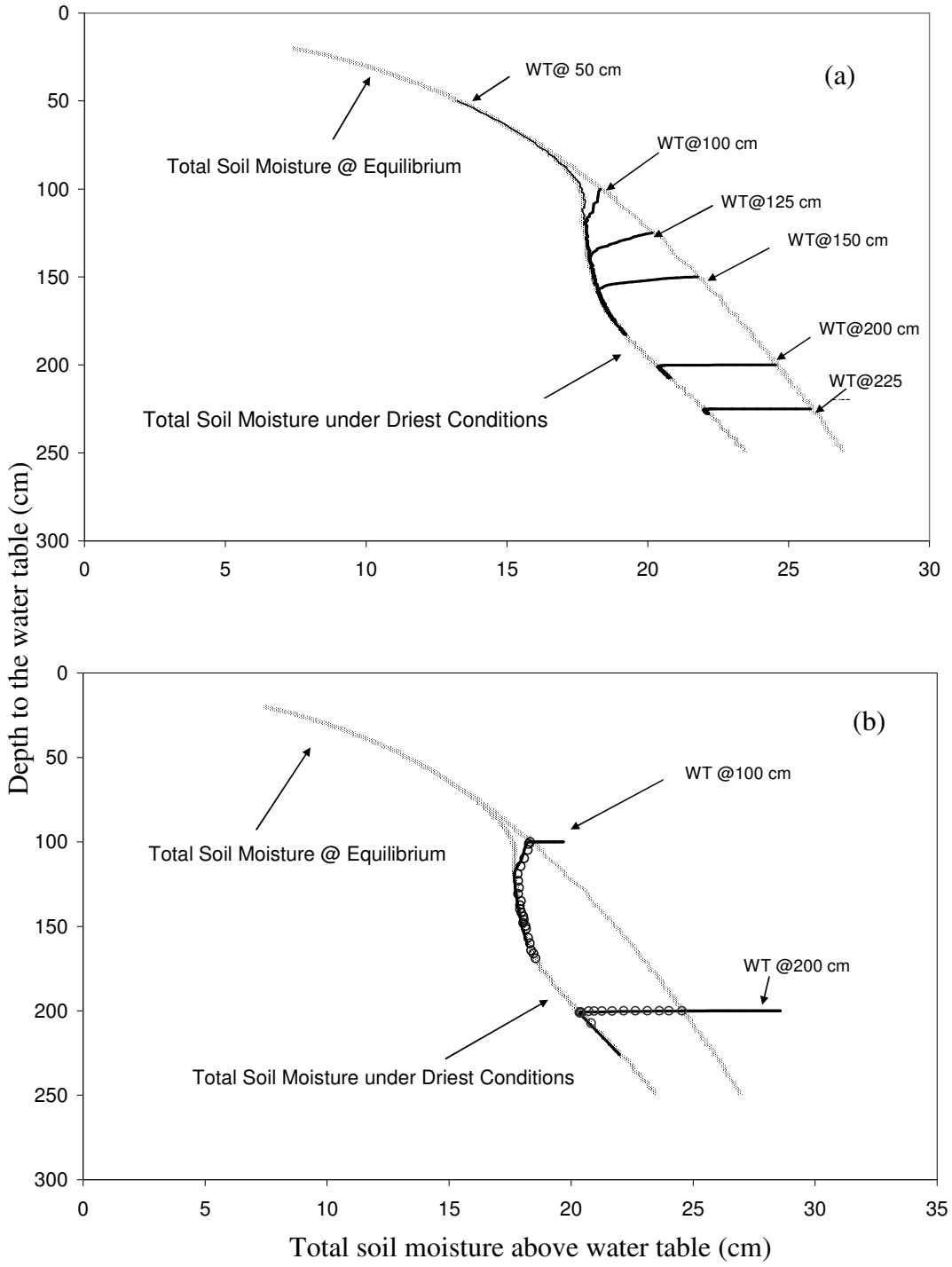

Figure 5.4 Variation of Total Soil Moisture above the Water Table under Different Initial Water Table Depths or Initial Water Content Conditions at (a) Equilibrium (b) Wetter than Equilibrium.

The three-layer model verification using the theoretical equations is a sort of qualitative analysis dealing with the thresholds controlling the *ET* partitioning to the vadose zone and ground water. The calculation of exact quantitative description is difficult as it is highly dependent on the antecedent moisture conditions, which are really dynamic in nature.

5.5 Conclusions

The HYDRUS-1D model was used to numerically solve the Richard's equation, with imported plant *ET* stress and was subjected to several "what if" investigations. The Brooks and Corey and van Genuchten models were fitted to the median water retention characteristics curve of the soil types found in west-central Florida. The Brooks and Corey model was found to be superior to the van Genuchten retention model, reproducing observed data and describing the observation well from the raw record.

The simulated and fitted data clearly support the approach of IHM. The definition of the extinction depth is not strict and depends on soil type and retention character. However, in this paper, the extinction depth was defined as the depth at which *ET* rate declined to become less than 0.5% of its initial value. Comparing the observed data and fitted data indicates similar three layer behavior.

Four thresholds cases were checked for validity using HYDRUS-1D model. In the first three cases (deep water table, root zone close to water table, and transition to direct ground water evaporation), there were close matches between the two models. In the fourth case (ground water evaporation at open water), potential *ET* can be satisfied from ground water contribution for a depth greater than capillary fringe.

Although there are similarities in both HYDRUS-1D and IHM, the two models have a different perspective at representing the vadose zone. While HYDRUS-1D can be applied for small-scale cases, site-scale, IHM is typically applied at regional or watershed scales. The three-layer model used in IHM and the threshold conditions presented appear to be theoretically sound and simplify the approach.

Chapter 6: Determination of Root Water Uptake: Calculation from Soil Moisture Data and Conceptualization for Modeling

6.1 Introduction

Simulating root water uptake is an integral component of modeling evapotranspiration using any hydrological model. Traditionally used models and concepts, however, make over simplifying assumptions about plants (Shah et al. 2007b), hence casting a doubt on the model results. Hence, what needs to be done is to try and combine land cover characteristics in the root water uptake models to produce more reliable results.

The current chapter discusses a new branch of study called 'Eco-Hydrology' which aims at progressing the interdisciplinary work on ecology and hydrology with an objective of improving hydrological modeling capabilities. The chapter also presents a methodology involving use of soil moisture and water table data to calculate root water uptake and how the observation of root water uptake contradict the assumptions commonly used root water uptake models. The second part of the chapter will take a step further and propose a modeling framework wherein land cover characteristics can be used to model root water uptake.

6.2 Background

Over the past two centuries, rapid increase in human population coupled with unplanned water management activities has resulted in severe degradation of ecosystems on a global scale (Zalewiski 2000). Several studies have shown that the mechanisms of interaction of the biota with their surroundings contribute to their spatiotemporal patterns (Rodriguez-Iturbe and Porporato 2004). Hence, knowledge about species specific interaction with its environment is of utmost importance for successful restoration efforts.

Historically, hydrology and ecology have evolved as two distinct sciences with little or no connection with each other (Baird and Wilby 1999). As an example, for a hydrologist, plants on the river bed have never been more than a Manning's roughness coefficient; similarly for an ecologist, the soil is no different than a reservoir of water. It is this difference in perspectives that has limited our ability to forecast changes, assess impacts and develop mitigation strategies. Traditional relationships used for quantifying hydrological processes, though very useful, are based more on empiricism rather than actual experimental approaches. Estimating evapotranspiration from pan measurements (Doorenbos and Pruitt 1977), specifying extinction depths based on qualitative rules (Anderson and Woessner 1991), and estimation of recharge to ground water as a calibration parameter (e.g., MODFLOW (Harbaugh et al. 2000)) are some of the relationships that have been in use in hydrology primarily because the plants physiology has been ignored. Recent studies, like that of Shah et al. (2007) and Nachabe et al. (2005), have shown that processes like evapotranspiration, recharge, etc. are strongly a function of the type of vegetation cover and climate. Ignoring the land cover effects can hence lead to erroneous estimate of these fluxes.

To cater to this need, interdisciplinary work in ecology and hydrology has been initiated. Zalewiski et al. (1997), Rodriguez-Iturbe and Porporato (2004) have shown promising results from seminal research in this new area called 'Eco-hydrology', thereby increasing confidence in the use of ecohydrological framework for understanding species dynamics. Despite the recent progress, our knowledge about species interaction, especially that of plants in ecotones and response of an ecosystem to the change in ambient conditions remains limited.

An important gap that remains in the eco-hydrological framework is the ability to successfully simulate the spatial and temporal patterns of root zone soil moisture. Fundamental to the modeling of the soil moisture dynamics in the root zone is the knowledge of the water uptake patterns by roots. Two major classes of root water uptake models that are in use are the microscopic scale models (Steudle 2000), where water movement along single root hair is modeled, and the other is the macroscopic model where instead of a root hair, a section of roots is considered (e.g., Feddes et al. 1978). The former class of models, even though more accurate, require more information and hence become infeasible while modeling on the watershed scale (~10 km^2); the latter class of models are empirical and even though they can be applied on large scales do not consider plant physiology and hence cannot be used with confidence for modeling purposes.

Analytical watershed scale models based on soil physics have the capability to simulate the moisture conditions in the unsaturated vadose zone, incorporating variability in soil and atmospheric conditions. However, empirical conceptualization of root water uptake in these models cast a doubt on the validity of the model results.

6.2.1 Objectives and Scope

The objective of this paper is thus to: (a) discuss the empirical root water uptake models used, (b) to describe a methodology involving field data to calculate root water uptake, (c) use field data to compute root water uptake values, (d) compare and contrast the model derived estimated from those derived from field data, and (e) propose a modeling framework involving plant physiological characteristics to model root water uptake

6.3 Theory

The governing equation for soil moisture dynamics in the unsaturated soil zone is the Richard's equation (Richard 1931). Richard's equation is derived from Darcy's law and the continuity equation. What follows is a brief description of Richard's equation and how can it incorporates root water uptake. For more detailed information about the formulation of Richard's equation, including its derivation in three dimensions, the readers are directed to any text book on soil physics e.g., Hillel (1998).

Due to ease of measurement and conceptualization, energy of water (E) is represented in terms of height of liquid column and is called the hydraulic head (h). It is defined as the total energy of water per unit weight. Mathematically hydraulic head, h, can be represented as

$$h = \frac{E}{\rho_W g} \tag{6.1}$$

where ρ_W is the density of water and g is the acceleration due to gravity. The flow of water always occurs along decreasing head. In soil physics, the fundamental equation

used to model the flow of water along a head gradient is known as Darcy's Law (Hillel 1998). Mathematically the equation can be written as

$$q = K\frac{\Delta h}{l} \tag{6.2}$$

where q [$L^3L^{-2}T^{-1}$] is known as the specific discharge and is defined as the flow per unit cross-sectional area, K [LT^{-1}] is termed as the hydraulic conductivity, which indicates ease of flow, Δh [L] is the head difference between the points of interest and l [L] is the distance between them. Darcy's Law is analogous to Ohm's law with head gradient being analogous to the potential difference and, current being analogous to specific discharge and hydraulic conductivity being similar to the conductance of a wire.

The second component of Richard's equation is the equation of continuity. The continuity equation is based on the law of mass conservation, and for any given volume it states that the net increase in storage in the given volume is inflow minus the sum of outflow and any sink present in the volume of soil. Mathematically it is this sink term that allows the modeling of water extracted from the given volume of soil.

In one dimension, for flow occurring in the vertical direction (z axis is positive downwards), Richard's equation can be written as

$$\left(\frac{\partial\theta}{\partial t}\right)=\left(\frac{\partial}{\partial z}K\left(\frac{\partial h}{\partial z}+1\right)\right)-S \tag{6.3}$$

where θ is the water content, defined as the ratio of volume of water present and total volume of the soil element , t is time, S represents the sink term while other terms are as defined before.

If flow in lateral directions is also considered, Richard's equation in three dimensions can be derived. Solution of the partial differential equation derived above can, hence, theoretically provide the spatial and temporal variability of moisture in the soil. However, due to the high degree of non linearity of the equation, no analytical solution exists for Richard's equation and numerical techniques are used to solve it. For a numerical solution of Richard's equation, two essential properties that need to be defined a-priori are, (a) relationship between soil water content and hydraulic head, also known as, soil moisture retention curves and (b) a model that relates hydraulic head to root water uptake. While much of literature and field data exist describing the soil moisture retention curves, relatively less information exists about root water uptake models. The root water uptake models generally used, especially on a watershed scale, are mostly empirical and lack any field verification. The main reason for this can be attributed to the fact that, until recently, plant physiology was ignored in hydrological modeling. Details about the soil moisture retention curves and numerical techniques used to solve Richard's equation can be found in Simunek et al. (2005). The focus of this paper will be on root water uptake models and field data that contradict the existing models.

6.3.1 Root Water Uptake Model

The most common approach used to model root water uptake is to define sink term S as a function of hydraulic head using the following equation

$$S(h) = \alpha(h) S_p \tag{6.4}$$

where S(h) [$L^3L^{-3}T^{-1}$] is the actual root water uptake (RWU) from roots subjected to hydraulic or capillary pressure head '*h*'. On the right hand side of the equation S_p [$L^3L^{-3}T^{-1}$] is the maximum (also known as potential) uptake of water by the roots. The $\alpha(h)$ is a root water uptake stress response function, with its values varying between 0 and 1.

The idea behind the conceptualization of Equation 6.4 is based on three basic assumptions. The first assumption being that as the soil becomes dryer, the amount of water that can be extracted decreases proportionally. Secondly, the amount of water extracted by the roots is affected by the ambient climatic conditions. Drier and hotter conditions result in more water loss through the stomata of leaves, hence, initiating more water extraction from the soil. The third and final assumption is that the uptake of water from a particular section of a root is directly proportional to the amount of roots present.

The root water stress response function (α) is a result of the first assumption. Two models commonly used to define α are the Feddes model (Feddes et al. 1978) and the van Genuchten model (van Genuchten 1987). Figure 6.1(a and b, respectively) show the variation of α with decreasing hydraulic head, which is same as decreasing water content or increasing soil dryness. Both models for α are empirical and do not involve any plant physiology to define the thresholds for the water stress response function. An interesting contrast, due to empiricism that is clearly evident is the value of α during saturated conditions. While the Feddes model predict the value of α to decrease to zero van Genuchten model predicts the opposite response with α rising to become unity under saturated conditions.

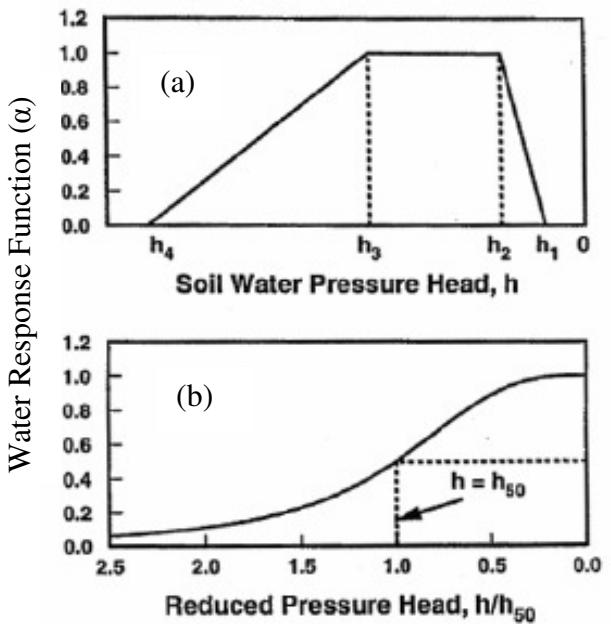

Figure 6.1 Water Stress Response Function as Conceptualized by (a) Feddes et al. (1978) and (b) van Genuchten (1980) [Adapted from Simunek et al. 2005].

Recently a couple of different models (Li et al. 2001; Li et al. 2006) have been presented to overcome the empiricism in α; however, these models are more a result of observation fitting and fail to bring in the plant physiology, which is what causing the changes in the water uptake rate due to variation in soil moisture conditions.

Combining the second and the third assumptions in Equation 6.4 results in the definition of S_p. S_p for any section of roots is defined as the product of root fraction in that section and the maximum possible water loss by the plant which is also known as the potential evapotranspiration. Potential evapotranspiration is a function of ambient atmospheric conditions and standard models like Penman-Monteith (Allen et al. 1998) are used to calculate the potential evapotranspiration rate. For any given value of potential evapotranspiration rate, limiting the value of S_p by the fraction of roots restricts the amount of water that can be extracted from a particular section. This, as will shown

later using field data, is a big limitation especially during dry period when the top soil with maximum roots get dry while the deep soil layer with lesser root mass still has soil moisture available for extraction.

6.4 Materials and Methods

6.4.1 Study Site

For the current chapter, field data from the study site described in Chapter 2 is used. Soil moisture and water table data from well location PS-43 and PS-40 were used to determine root water uptake from forested versus grassed land cover. The well PS-43 is referred to as Site A while PS-40 will be called Site B. Hourly averaged data at a four hour time step were used for the analysis in this chapter.

Extensive soil investigations including in situ and laboratory analysis were performed for the study site. The soil in the study area is primarily sandy marine sediments with high permeability in the surface and subsurface layers. Detailed information about soil and site characteristics can be found in Said et al. (2005), and Trout and Ross (2005). Data for the period of record January 2003 to December 2003 were used in this analysis.

6.4.2 Methodology

Soil matrix has voids which can be filled with water or air. In soil physics, the ratio of the volume of voids and total volume of soil matrix is defined as porosity. If all the pores (or voids) are filled with water the soil matrix is termed as saturated and the water content in the soil matrix is called saturated water content and is represented as θ_s.

As the soil starts drying up the water content (θ) in the soil matrix starts reducing below θ_s. It is known that as the small pores in the soil matrix do not necessarily make a continuous network not all of the water can be removed from the soil under natural conditions (Hillel 1998). Hence, even under extremely dry conditions, soils do not get completely dry. The minimum water content that remains is called the residual water content and is represented by θ_r.

A common technique used to represent the observed water content is to normalize it using Equation 6.5, hence confining the values between 0 and 1.

$$S_e = \frac{\theta - \theta_r}{\theta_s - \theta_r} \tag{6.5}$$

Here S_e is called the normalized water content, varying between 0 and 1. θ is the observed water content, while θ_r and θ_s are the residual and saturated water content values, respectively.

An important implication of varying water content, which greatly affects the soil moisture dynamics, is the fluctuations in the value of hydraulic conductivity of soil. When the soil is saturated all the pores are well connected and hence the water can flow thorough the soil matrix easily. However, as the soil starts drying, the path gets blocked due to intermittent air pockets that develop due to evaporation of water from the pores. The net result is that the water carrying capacity of soil is reduced, which is manifested as the reduced hydraulic conductivity (Jury et al. 1991).

Hence, with increasing soil dryness, which increases soil suction head, both water content and hydraulic conductivity are reduced. van Genuchten (1980) proposed a model

relating the water content and hydraulic conductivity with the suction head and is represented by the following equations

$$h(\theta) = \frac{(S_e^{\frac{1}{m}} - 1)^{\frac{1}{n}}}{\phi} \tag{6.6}$$

$$K(h) = \begin{cases} K_S S_e^l [1 - (1 - S_e^{1/m})^m & h < 0 \\ K_S & h \geq 0 \end{cases} \tag{6.7}$$

where m = 1 – 1/n for n > 1, S_e [-] is the normalized water content, K_S [LT^{-1}] is the hydraulic conductivity when the soil matrix is saturated, l [-] is the pore connectivity parameter assumed to be 0.5 as an average for most soils (Mualem 1976), and ϕ [L^{-1}], n [-] and m [-] are the van Genuchten empirical parameters. Negative values of hydraulic head means the water content in the soil matrix is less that saturated water content while the positive values indicate saturated conditions. From Equations 6.6 and 6.7, it is clear that for each type of soil, five parameters, namely, K_S, n, ϕ, θ_r and θ_s have to be determined to uniquely define the relationship of hydraulic conductivity and water content with soil suction head.

Before the discussion about the how the parameters values were determined, it is essential to get a grasp of the system we are dealing with. Figure 6.2 show the schematics of the vertical soil column which is monitored using eight soil moisture sensors and a pressure transducer measuring water table elevation, at each of the two locations. Shown also in Figure 6.2 is the zone of influence of each sensor along with the elevation of water table and arrows showing possible flow directions.

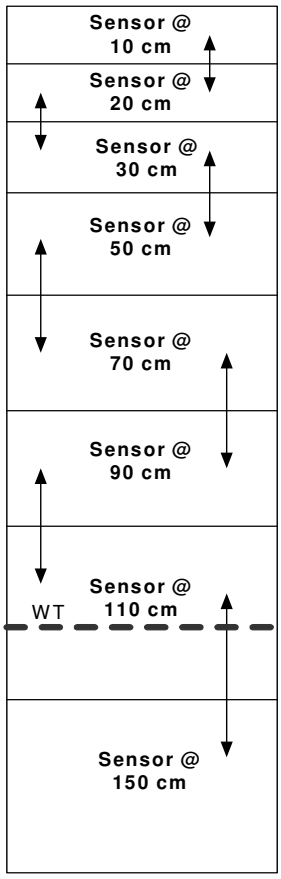

Figure 6.2 Schematics of the Vertical Soil Column with Location of the Soil Moisture Sensors and Water Table.

For the purpose of defining moisture retention and hydraulic conductivity curves, each section is treated as a different soil layer and was independently parameterized. Hence, for each of the two locations for this particular study eight, soil cores from depths corresponding to the zone of influence of each sensor were taken and analyzed using the methods described below.

6.4.2.1 Saturated and Residual Water Content

Actual water content measurements for all the eight locations were available for each of the two sites, for around two years, with well pronounced wet and dry seasons. Hence, from the observed data, the maximum and minimum water content was set up as saturated and residual water content, respectively.

6.4.2.2 Saturated Hydraulic Conductivity

Saturated hydraulic conductivity (K_S) for different soil layers at the study locations was calculated using falling head permeameter analysis as described in Das (2002). Falling head permeameter test is a standard technique to determine the saturated hydraulic conductivity. Multiple tests were done and the results were averaged to determine the most appropriate value of saturated hydraulic conductivity for each of the soil layers at both the study locations.

6.4.2.3 van Genuchten Parameters

To determine the values of parameters n, ϕ the soil cores taken out were saturated and rotated in a centrifuge. Rotating the sample cores generated outward centrifugal force that created suction forces in the soil sample and caused the loss of water from the sample. For each revolution per minute (RPM) setting, the soil sample was weighed and depending on the saturated weight and water content the new water content value was determined. Moisture retention curves from the measure data were then plotted and fitted with Equation 6.6 and the best fit values of $n, \phi,$ were taken as the parameter value for the respective soil layer.

The method to determine moisture retention curve has been used in the past by Carlisle et al. (1989) as a part of comprehensive soil survey of Floridian soils. Table 6.1(a) and (b) shows the parameters values that were obtained following the all the soil tests.

Table 6.1 Soil Parameters for Study Locations in (a) Grassland and (b) Forested Area.

(a)

Sensor Location below land surface (cm)	θs (%)	θr (%)	$\Phi(cm^{-1})$	n (-)	K_S (cm/hr)
10	38	3	0.02	1.35	0.0100
20	34	3	0.03	1.35	0.0100
30	31	3	0.03	1.35	0.0100
50	31	3	0.07	1.90	0.0100
70	31	3	0.20	2.20	0.0100
90	31	3	0.20	2.20	0.0004
110	33	3	0.20	2.20	0.0004
150	35	3	0.20	2.10	0.0012

(b)

Sensor Location below land surface (cm)	θs (%)	θr (%)	$\Phi(cm^{-1})$	n (-)	K_S (cm/hr)
10	35	3	0.03	1.85	4.212
20	35	3	0.07	1.7	2.520
30	32	3	0.07	1.7	2.520
50	34	3	0.03	1.6	0.803
70	31	3	0.03	1.6	0.005
90	32	3	0.05	1.9	0.005
110	32	3	0.05	1.8	0.005
150	30	3	0.05	1.8	0.001

6.4.2.4 Calculation of Root Water Uptake

Once the soil parameterization is complete, root water uptake from each section can be calculated. For any given soil layer in the vertical soil column (Figure 6.2), above the observed water table, observed water content and Equation 6.6 can be used to calculate the hydraulic head. For soil layers below the water table, hydraulic head is the same as the depth of soil layer below the water table due to assumption of hydrostatic pressure. Similarly using Equation 6.7, hydraulic conductivity can be calculated. Hence, at any instant in time, hydraulic head in each of the eight soil layers can be calculated. To determine total head, gravity head, which is the height of the soil layer above a common datum, has to be added to the hydraulic head. For this particular study, the datum was arbitrarily selected as 2000 cm below the land surface. Water flow along decreasing head, hence, depending on total head values of the adjacent layers and the direction of water flow for a given soil layer is determined.

To quantify flow across each soil layer, Darcy's Law (Equation 6.2) is used. Average head values between two consecutive time steps are used to determine the head difference. Also, flow across different soil layers is assumed to be occurring between the midpoints of one layer to another, hence, to determine the head gradient ($\Delta h/l$) the distance between the midpoints of each soil layer is used. The last component needed to solve Darcy's Law is the value of hydraulic conductivity. For flow occurring between layers of different hydraulic conductivities equivalent hydraulic conductivity is calculated by taking the harmonic mean of the hydraulic conductivities of both the layers (Freeze and Cherry 1979). Hence, for each time step, harmonically (Equation 6.8) averaged hydraulic conductivity values were used to calculate the flow across soil layers.

$$K_{eq} = \frac{2K_1K_2}{K_1 + K_2} \tag{6.8}$$

where K_1 [LT^{-1}]and K_2 [LT^{-1}]are the two hydraulic conductivity values for any two adjacent soil layers and K_{eq} [LT^{-1}]is the equivalent hydraulic conductivity for flow occurring between those two layers.

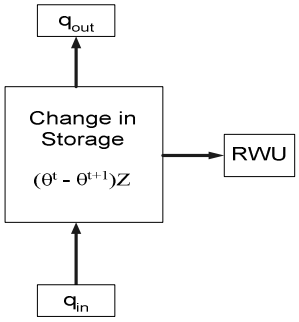

Figure 6.3 Schematics of a Section of Vertical Soil Column Showing Fluxes and Change in Storage.

Figure 6.3 shows a typical flow layer with inflow and outflow marked. Now using simple mass balance, changes in water content at two consecutive time steps can be attributed to net inflow minus the root water uptake (assuming no other sink is present). Equation 6.9 can hence be used to determine root water uptake from any given soil layer with thickness Z cm

$$RWU = (\theta^t - \theta^{t+1})Z - (q_{out} - q_{in}) \tag{6.9}$$

Using the described methodology, one can determine the root water uptake from each soil layer at both study locations (site A and site B).

Time step for calculation of the root water uptake was set as four hours and the root water uptake values obtained were summed up to get a daily value for each soil layer. The results section describes the finding of the study.

6.5 Results

Using the above methodology, root water uptake was calculated from each section of roots for tree and grass land cover from January to December 2003 at a daily time step. Figure 6.4(a and c) shows the variation of root water uptake for a representative period from May 1st to May 15th, 2003. This particular period was selected as the conditions were dry and there was no rainfall. Graphs in Figure 6.4(a and c) show the root water uptake variation corresponding to each section. Also plotted on the graphs is the normalized water content, which gives an indication of water, lost from the section.

Figure 6.4(a) shows the root water uptake from grassed site while the panel of graphs in Figure 6.4(c) plots RWU from the forested area. From Figure 6.4(a and c) it can be seen that in both the cases of grass and forest the root water uptake varies with water content and when the top layers starts to get dry, then the water uptake from the lower layer increases so as to keep the root water uptake constant clearly indicating that compensation do take place and hence the models need to account for it. Another important point to note is that, in Figure 6.4(a), root water uptake from the top three layers accounts for the almost all the water uptake while in Figure 6.4(b) the contribution from fourth and fifth layers is also significant. Also, as will be shown later (Figure 6.6), in the case of forested land cover, root water uptake is observed from the sections that are even deeper than 70 cm below land surface. This is expected owing to the differences in

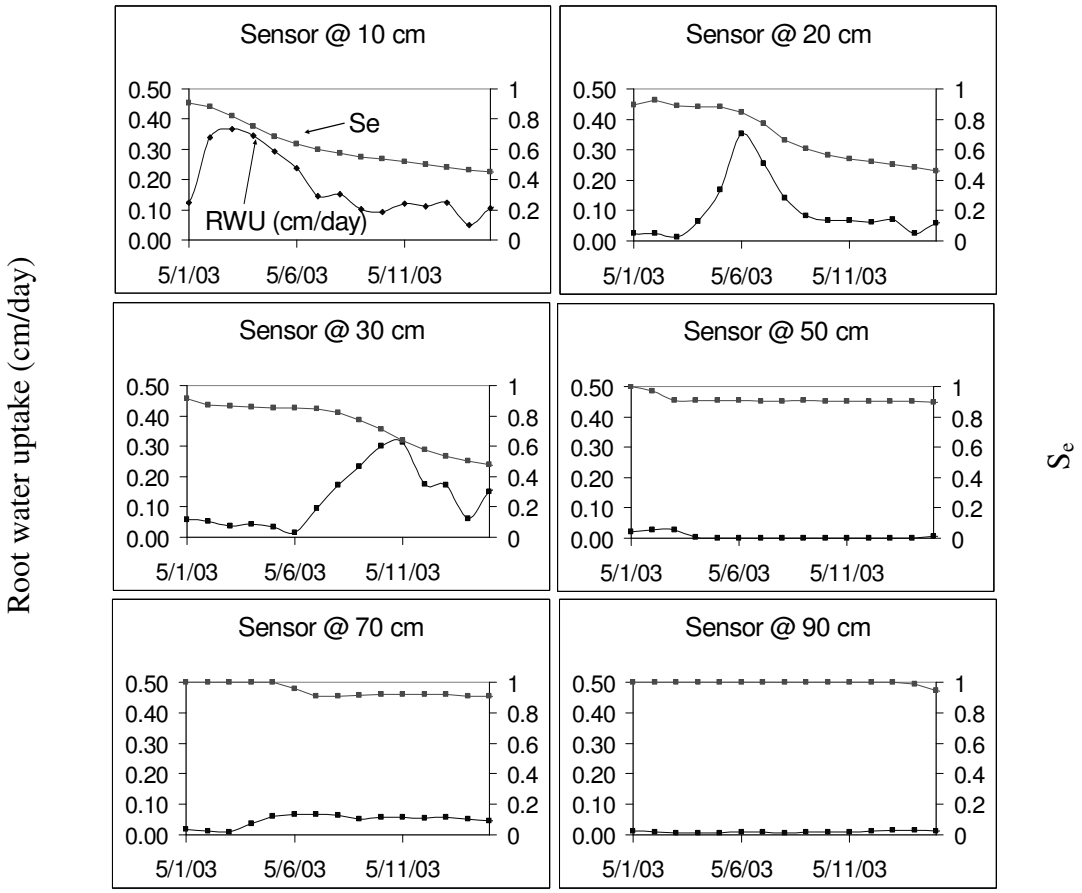

(a)

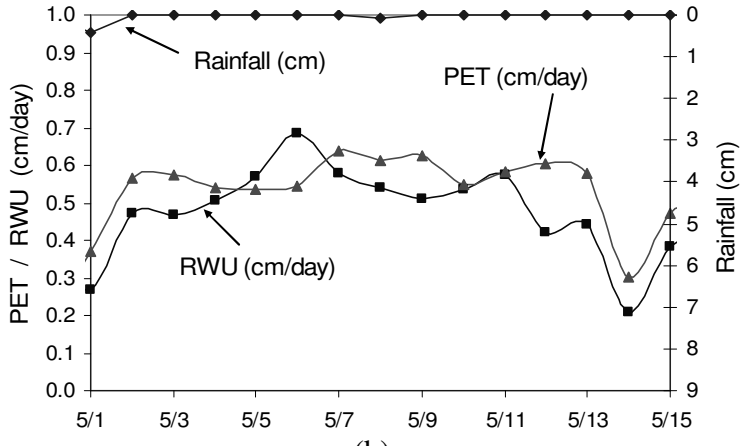

(b)

Figure 6.4 Root Water Uptake from Sections of Soil Corresponding to Each Sensor on the Soil Moisture Instrument for (a and b) Grass Land and (c and d) Forest Land Cover.

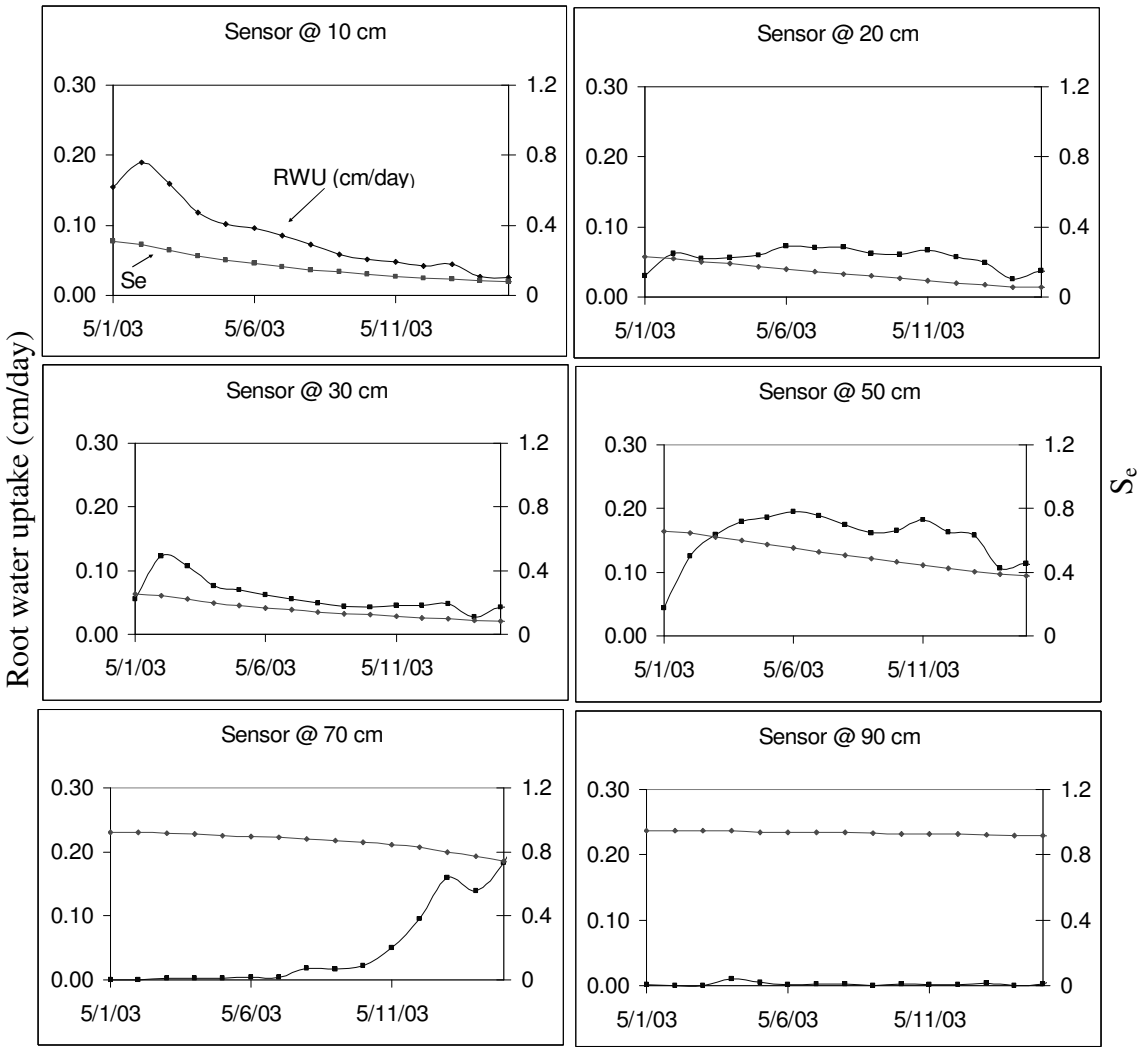

(c)

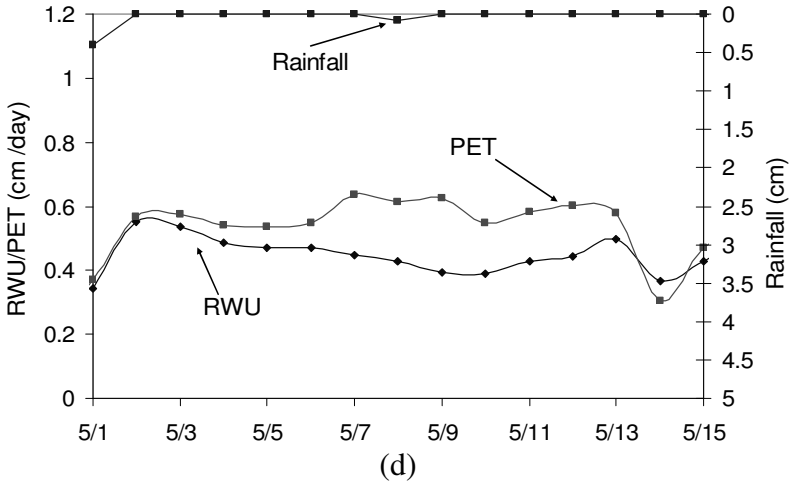

(d)

Figure 6.4 (Continued)

the root systems of both land cover types. While grasses have shallow roots, forest trees tend to put their roots deeper into the soil to meet their high water consumptive use.

Figure 6.4(b and d) shows the values of potential *ET* (*PET*) plotted along with the observed values of root water uptake. On comparing grass versus forested graphs it is evident that the grassland is still evapotranspiring at values close to *PET*, root water uptake from forested land covers is occurring at less than potential. This behavior can be explained by the fact that water content in the grassed region (as shown by the normalized water content graph), due to shallower water table (not shown in the figure), is more than that of the forest and even though the 70 cm sensor shows significant contribution the uptake is still not sufficient to meet the potential demand.

Figure 6.5 shows an interesting scenario when a rainfall event occurs right after a long dry stretch that caused the upper soil layers to dry out. Figure 6.5(a) shows the root water uptake profile on May 18th, 2003 for the forested land cover with maximum water being taken from section of soil profile corresponding to 70 cm below the land surface. A rainfall event of 1inch took place on May 19th, 2003 and, as can be clearly seen in Figure 6.5(b), the maximum water uptake shifts right back up to 10 cm below the land surface, clearly showing that the ambient water content directly and instantaneously affects the root water uptake distribution. Figure 6.5(c) shows the snapshot on May 20th, 2003 a day after the rainfall where the root water uptake starts redistributing and shifting toward deeper wetter layers. In fact this kind of behavior was observed for all the data analyzed for the period of record for both the grass land and forested land cover. With roots taking water from deeper wetter layers and, as soon as the shallower layer becomes wet the uptakes shift to the top layers. Figure 6.6(a and b) show a long duration of record

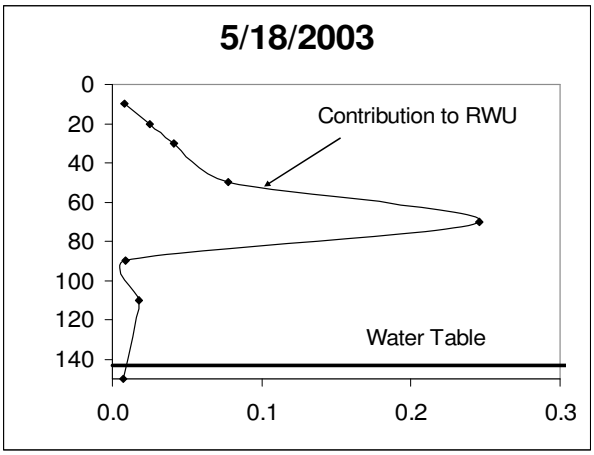

(a)

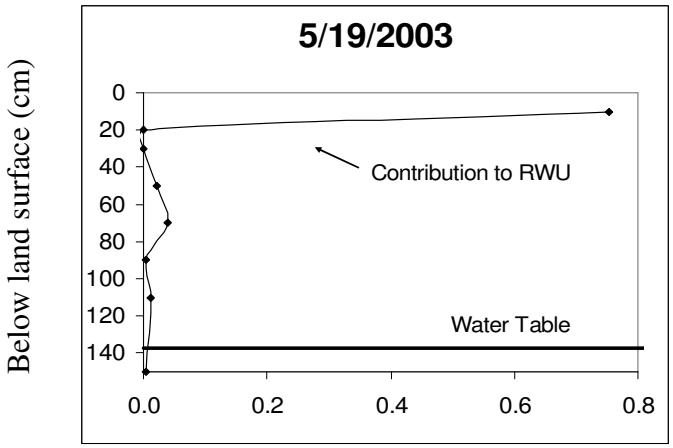

(b)

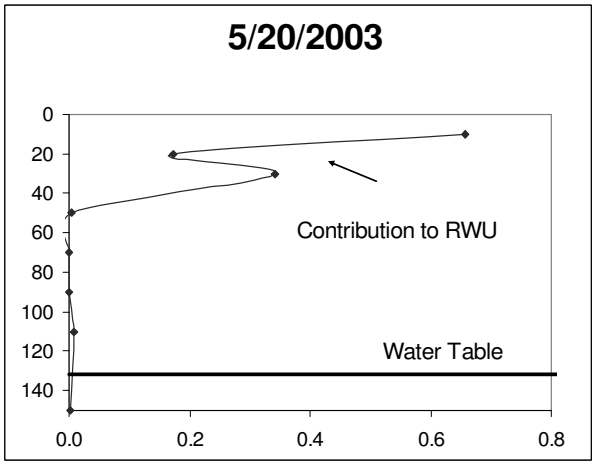

(c)

Root water uptake (cm/day)

Figure 6.5 Root Water Uptake Variation Due to an Inch of Rainfall Event

spanning two months (starting October to end November), with the whiter shade indicating higher root water uptake. From both the figures it is reiterated that water uptake significantly shifts away from drier soil layers, especially in the case of forest land cover (Figure 6.6(b)), while in the case of the grass land, uptake is primarily concentrated in the top layers.

As a quick summary, the results indicate that:

(a) Assuming RWU as directly proportional to root density may not be a good approximation.

(b) Plants adjust to seek out water over the root zone.

(c) In case of wet conditions, preferential RWU from upper soil horizons may take place.

(d) In case of low *ET* demands, the distribution of *ET* was found to be occurring as per the root distribution, assuming an exponential root distribution.

Hence, traditionally used models are not adequate as such, to model this behavior. Changes in regard to the modeling techniques as well as conceptualizations, hence, need to be done. Plant physiology is one area that needs to be looked into to see what plant properties affect the water uptake and how can they be modeled mathematically. The next section discusses a modeling framework based on plant root characteristics which can be employed to model the aforesaid observations.

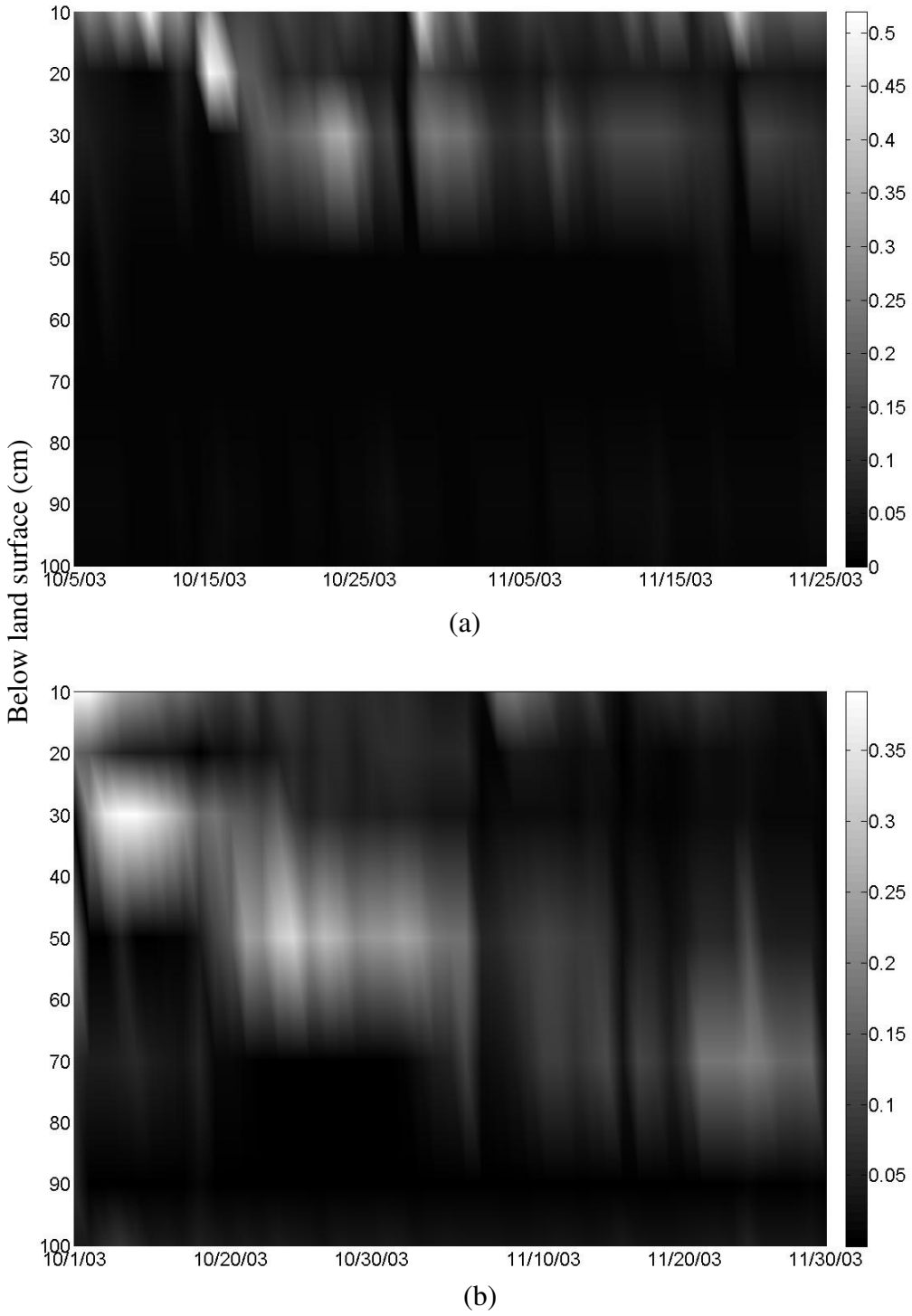

Figure 6.6 Daily Root Water Uptake Variation from October to November 2003 for (a) Grass Land Cover and (b) Forested Land Cover.

6.6 Incorporation of Plant Physiology

Any framework to model root water uptake dynamically, will have to explicitly account for all the four points listed above. The dynamic model should be able to adjust the uptake pattern based on root density as well as available water across the root zone. The model should use physically based parameters so as to remove empiricism from the formulation of the equations. For a given distribution of water content along the root zone (observed or modeled), knowledge of root distribution as well as hydraulic characteristics of roots is hence essential to develop a physically based root uptake model. The following two sections will describe how root distributions can be modeled as well as how do roots need to be characterized to model uptake from root's perspective.

6.6.1 Root Distribution

Schenk and Jackson (2002) expanded an earlier work of Jackson et al. (1996) to develop a global root database having 475 observed root profiles from different geographic regions of the world. It was found that by varying parameter values the root distribution model given by Gale and Grigal (1987) can be used with good accuracy to describe the observed root distributions. Equation 6.10 describes the root distribution model.

$$Y = 1 - \beta^d \tag{6.10}$$

where Y is the cumulative fraction of roots from the surface to depth d, and β is a numerical index of rooting distribution which depends on vegetation type. Figure 6.7 shows the observed distribution (shown by data points) versus the fitted distribution using Equation 6.10 for different vegetation types. The figure clearly indicates the goodness of

fit of the above model. Hence, for a given type of vegetation a suitable β can be used to describe the root distribution.

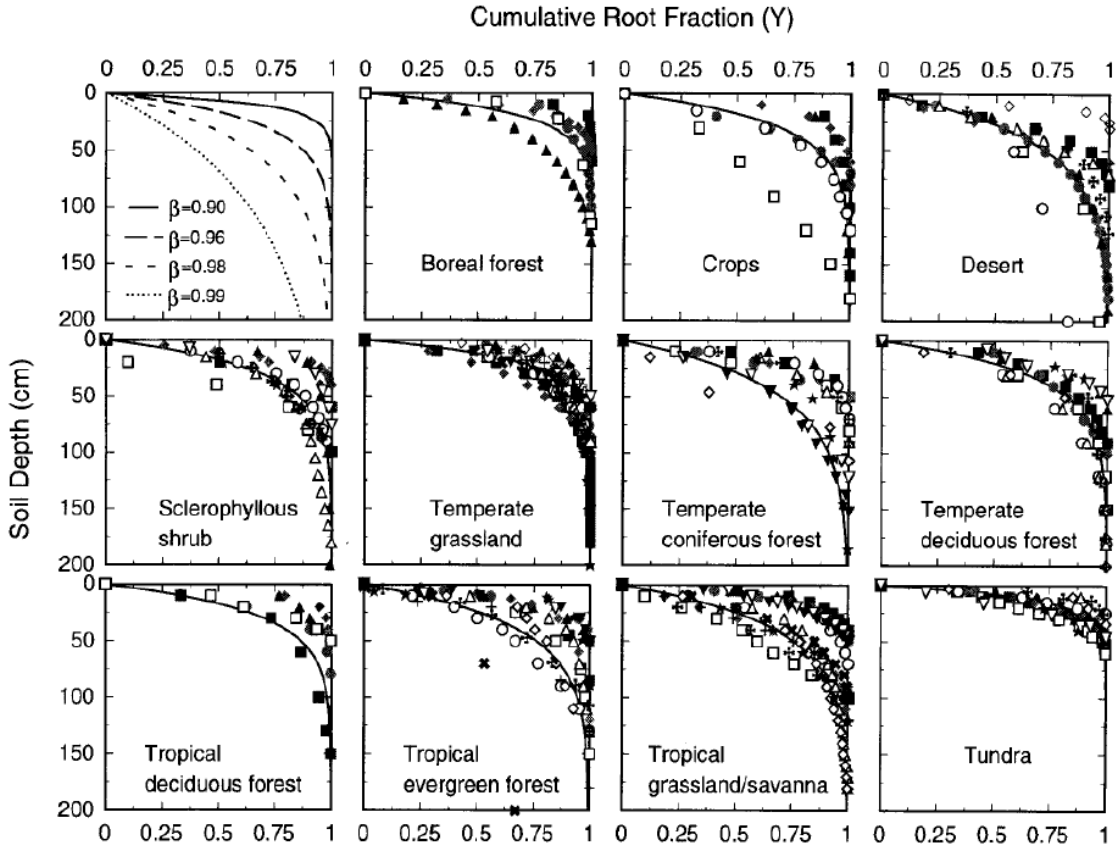

Figure 6.7 Observed and Fitted Root Distribution for Different Type of Land Covers [Adapted from Jackson et al. 1996].

6.6.2 Hydraulic Characterization of Roots

Hydraulically, soil and xylem are similar as they both show a decrease in hydraulic conductivity with reduction in soil moisture (increase in soil suction). For xylem, the relationship between hydraulic conductivity and soil suction pressure is called the 'vulnerability curve' (Sperry et al. 2003) (see Figure 6.8). The curves are drawn as a percentage loss in conductivity rather than absolute value of conductivity due to the ease

of determination of former. Tyree et al. (1994) and Hacke et al. (2000) have described methods for determination of vulnerability curves for different types of vegetation. Commonly, the stems and/or root segments are spun to generate negative xylem pressure (as a result of centrifugal force) which results in loss of hydraulic conductivity due to air seeding into the xylem vessels (Pammenter and Willigen 1998). This loss of hydraulic conductivity is plotted against the xylem pressure to get the desired vulnerability curve.For different plant species the vulnerability curve follows an S-Shape function, see Figure 6.8 (Tyree 1999).

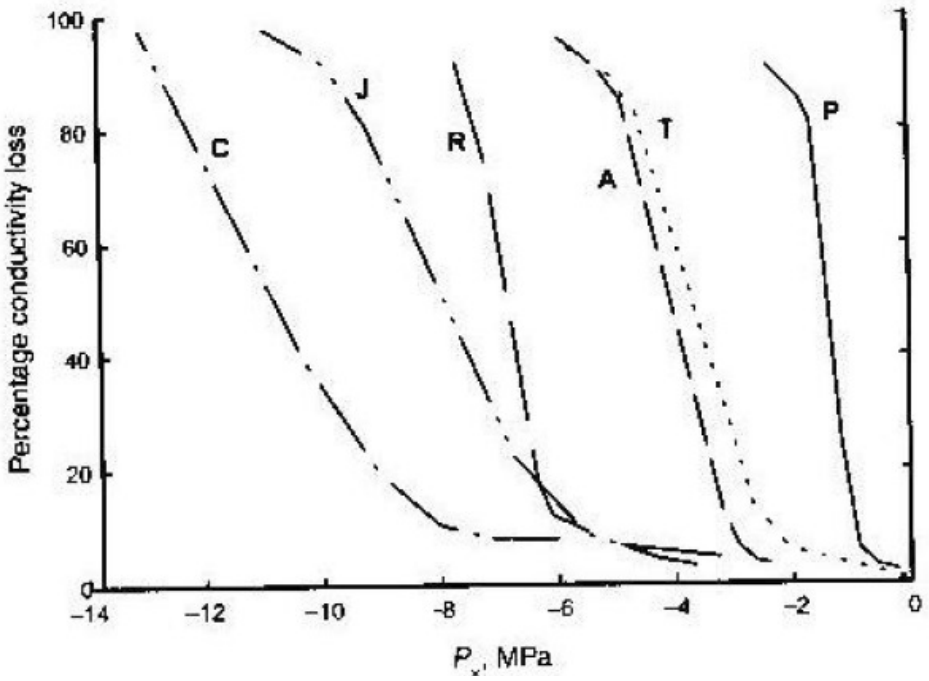

Figure 6.8 Vulnerability Curves for Various Species [Adapted from Tyree 1999].

In Figure 6.8, y-axis is percentage loss of hydraulic conductivity induced by the xylem pressure potential P_x, shown on the x-axis. C= Ceanothus megacarpus, J = Juniperus virginiana, R = Rhizphora mangel, A = Acer saccharum, T= Thuja occidentalis, P = Populus deltoids.

Pammenter and Willigen (1998) came up with an equation to model the vulnerability curve by parametrizing the equation for different plant species. Equation 6.11 describes the model mathematically.

$$PLC = \frac{100}{1 + e^{a.(P - P_{50\,PLC})}} \tag{6.11}$$

where PLC denotes the percentage loss of conductivity P_{50PLC} denotes the negative pressure causing 50% loss in the hydraulic conductivity of xylems, P represents the negative pressure and a is a plant based parameter. Figure 6.9 shows the model plotted against the data points for different plants. Oliveras et al. (2003) and references cited therein have parameterized the model for different types of pine and oak trees and found the model to be successful in modeling the vulnerability characteristics of xylem.

The knowledge of hydraulic conductivity loss can be used analogous to the water stress response function α (Equation 6.4) by scaling *PLC* from 0 to 1 and converting the suction pressure to water head. The advantage of using vulnerability curves instead of the Feddes or van Genuchten models is that vulnerability curves are based on xylem hydraulics and hence can be physically characterized for each plant species.

6.6.3 Development of a Physically Based Root Water Uptake Model

The current model development is based on the model conceptualization proposed by Jarvis (1989); however, the parameters for the current model are physically defined and include plant physiological characteristics.

For a given land cover type, Equations 6.10 and 6.11 can be parameterized to determine the root fraction for any given segment in root zone and percentage loss of

conductivity for a given soil suction pressure. For consistency of representation, percentage loss of conductivity will be hence forth represented by α (scaled between 0 and 1) and will be called stress index.

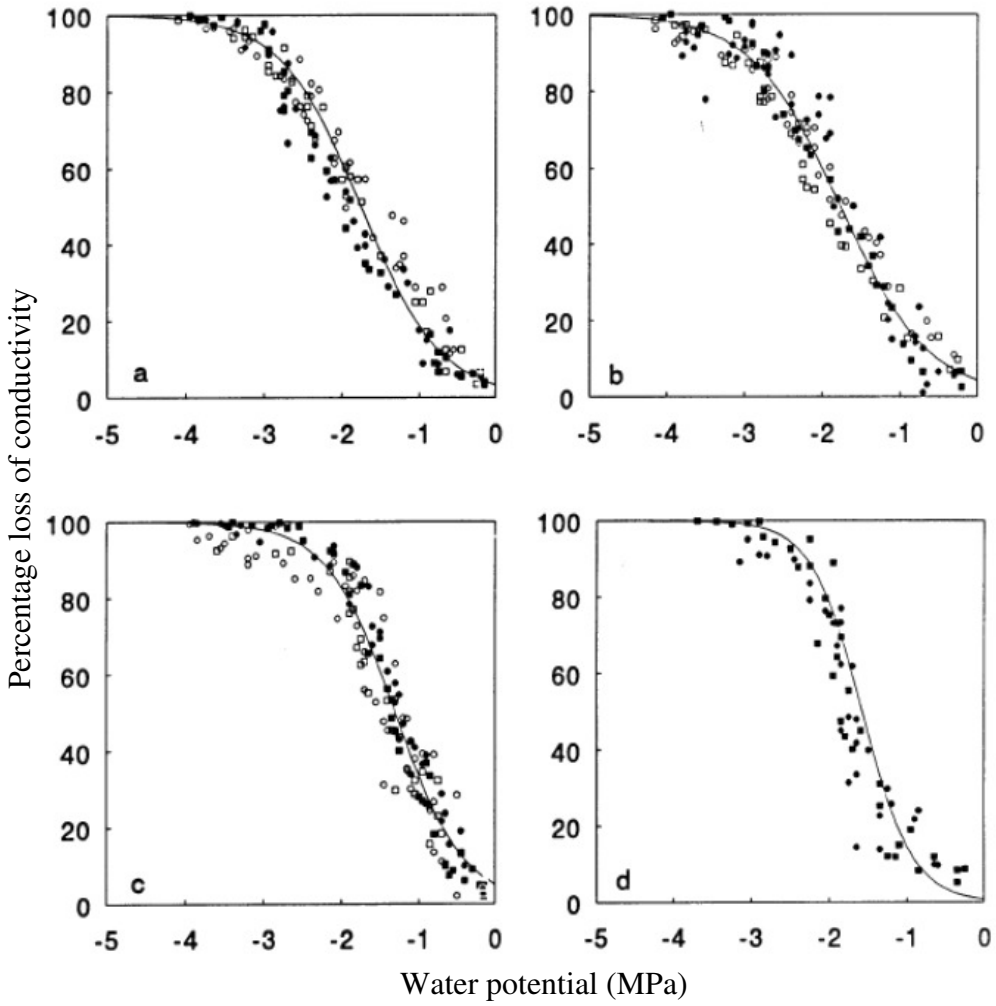

Figure 6.9 Observed Values and Fitted Vulnerability Curve for Roots and Stem Sections of Different Eucylaptus Trees [Adapted from Pammenter and Willigen 1998].

For any section of root zone, say i^{th} section, the root fraction can be written as R_i and the stress index, determined from vulnerability curve and ambient soil moisture condition, can be written as α_i. The average stress level $\bar{\alpha}$ over the root zone can be defined as the

$$\bar{\alpha} = \sum_{i=1}^{n} R_i \alpha_i \tag{6.12}$$

where n represents the number of soil layers and other symbols as previously defined. Thus, as can be seen from Equation 6.12, the average stress level $\bar{\alpha}$ combines the effect of both root distribution and available water content (via vulnerability curve).

As shown in Figure 6.6(b), if there is available moisture in the root zone, plants can transpire at potential by increasing the uptake from the lower wetter section of the roots. In terms of modeling it can be conceptualized that above a certain critical average stress level ($\bar{\alpha}_C$), plants can transpire at potential and below $\bar{\alpha}_C$ the value of total evapotranspiration decreases. The decrease in the *ET* value can be modeled linearly as shown by Liao et al. (2001). The graph of average stress level versus *ET* (expressed as a ratio with potential *ET* rate) can hence be plotted as shown in Figure 6.10. In 6.10, ET_a is the actual *ET* out of the soil column while ET_p is the potential value of *ET*. Figure 6.10 can be used to determine the value of actual *ET* for any given average stress level.

Once the actual *ET* value is known, contributions from individual section can be modeled depending on the weighted stress index using the relationship defined by

$$S_i = \left(\frac{E_a}{\Delta Z_i} \right) \left(\frac{R_i \alpha_i}{\bar{\alpha}} \right) \tag{6.13}$$

where S_i defined as the water uptake from the i^{th} section, ΔZi is the depth of i^{th} section and other symbols are as previously defined.

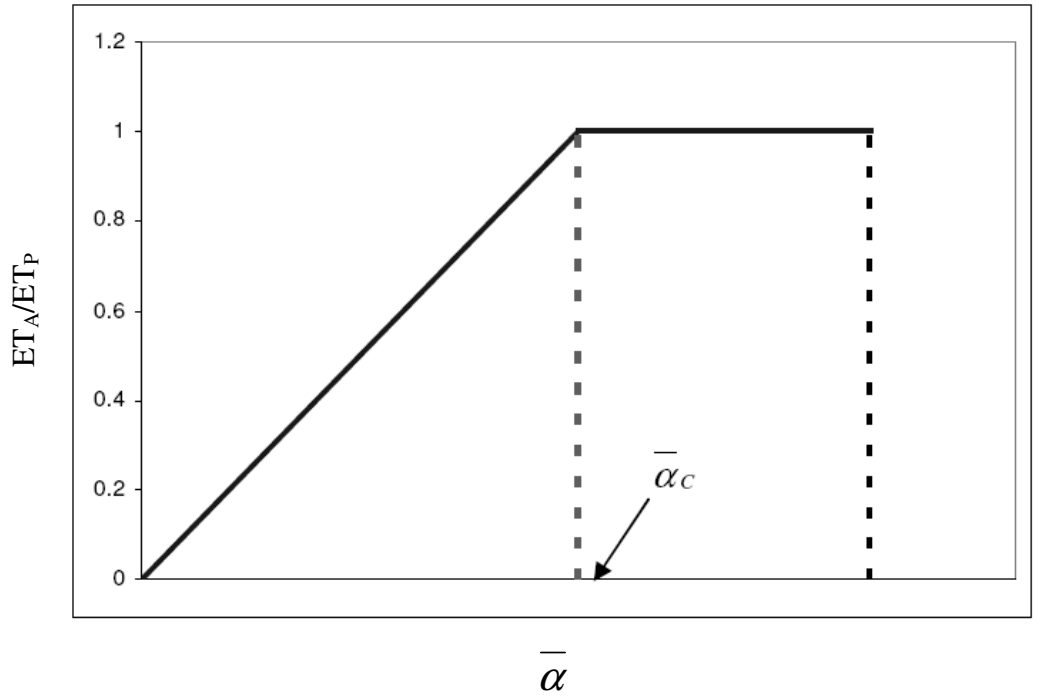

Figure 6.10 Variation of Ratio of Actual to Potential *ET* with Location of the Critical Stress Level.

Jarvis (1989) used empirical values to simulate the behavior of the above function and Figure 6.11 shows the result of root water uptake obtained from his simulation. The values next to each curve in Figure 6.11 represent the day after the start of simulation and actual *ET* rate as expressed in mm/day. On comparison with Figure 6.6, the model successfully reproduced the shift in root water uptake pattern with the uptake being close to potential value (ET_P = 5.0 mm/d) for about a month from the start of simulation. The decline in *ET* rate occurred long after the start of the simulation in accordance with the

observed values. The model hence was successful not only in simulating peak but also in the observed magnitude of the root water uptake.

The advantage of the above described approach in modeling root water uptake is that the parameters and the characteristics are physically based and hence less susceptible to empiricism and, unlike the traditionally used model, it takes into account not only the root distribution but also the available water content in determining the root water uptake.

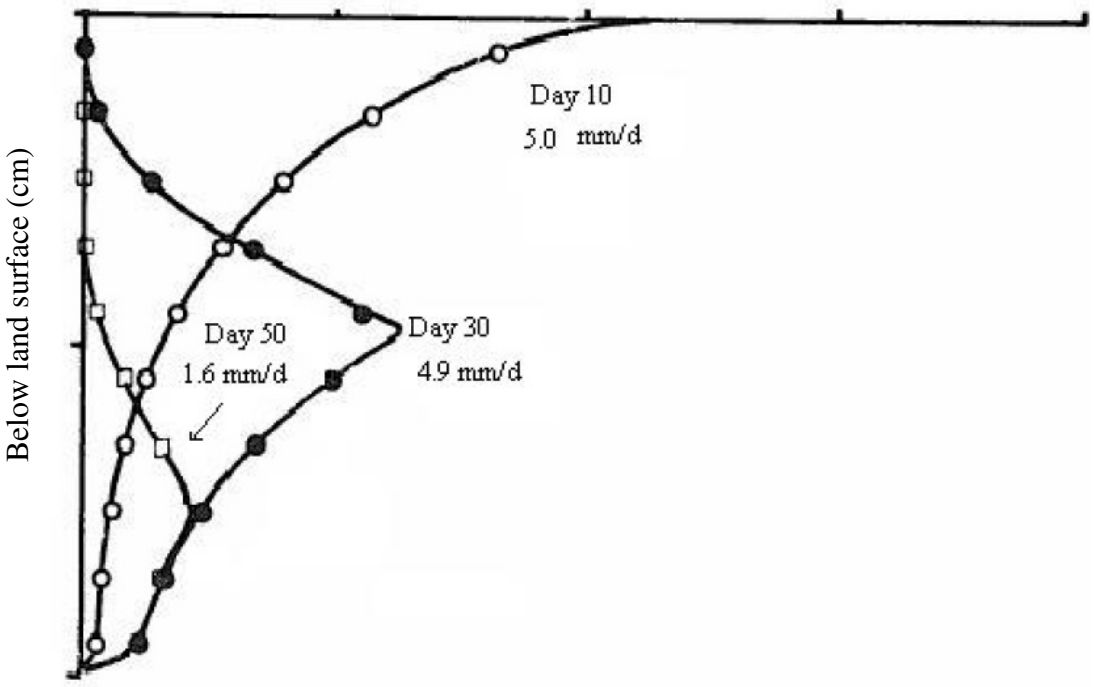

Figure 6.11 Variation in the Vertical Distribution of Root Water Uptake at Different Times [Adapted from Jarvis 1989].

6.7 Conclusions

The methodology presented here elucidates the non linear variation of root water uptake. It also revealed that the water uptake is not just directly proportional to amount of the roots but also depends on the ambient water content and under dry conditions roots can easily take water from deeper wetter soil layers.

Traditionally used models are not adequate as such, to model this behavior. Changes in regard to the modeling techniques as well as conceptualizations, hence, need to be done. Plant physiology is one area that needs to be looked into to see what plant properties affect the water uptake and how can they be modeled mathematically.

Also discussed is a framework which makes use of xylem vulnerability curves to provide a physical basis to model root water uptake. Simulation results have shown promise for the framework to provide a robust model of root water uptake. However further work needs to be done to determine the vulnerability curves and root distributions for Site A and Site B and then use the recommended model to validate observed versus simulated values.

The methodology described in this chapter involves initial laboratory analysis to determine the hydraulic characteristics of plant xylems; however, once a particular plant species is characterized then the parameters can be used for that specie elsewhere under similar conditions. The eco-hydrological framework approach has great potential for improving predictive hydrological modeling.

Chapter 7: Long Term Air Entrapment Affecting Runoff and Water Table Observations

7.1 Introduction

This final chapter discusses a phenomenon that exists in shallow water table environments and may under intense rainfall effect the water level observed in observation well that are screened below the water table elevation. The phenomenon is the air entrapment, which occurs when an intense rainfall event effectively seals the surface soil layer thus trapping the soil air below the advancing wetting front. Due to the compression of air the pressure at the surface of water table becomes greater than atmospheric and hence the observation wells that are vented to atmosphere show a sudden jump in water levels, hence erroneously indicating recharge even though the wetting front is still way above water table. A modeling strategy using vertical soil moisture profiles and some preliminary results are discussed in this chapter.

7.2 Background

The role of air entrapment in inhibiting infiltration has long been recognized (e.g., Adrian and Franzini 1966; Morel-Seytoux and Khanji 1974; Vachaud et al. 1974; Parlange and Hill, 1979). Several theoretical and experimental studies e.g., Youngs and Peck (1964) and McWhorter (1971), have quantitatively defined the impact of air compression on infiltration. These studies found that, air compression ahead of a wetting

front, in some water table conditions, brings about a sharp decrease in the infiltration rate. However, as pointed out by Parlange and Hill (1979) and observed by Wang et al. (1998), air compressibility has been generally considered negligible, when the air is free to move ahead of the wetting front. Hence, the importance of air compression in an unconfined aquifer with deep water table is considered negligible. However, for shallow water table environments (depth to water table <2 m) air compression plays a significant role in determining infiltration in many soils (Touma et al. 1984).

Another phenomenon found in shallow water table environments is a rapid rise in the water level of observation wells screened below the water table during high intensity rainfall events. The process, known as the Lisse Effect (Weeks 2002), as the wetting front advances, pressurization of the soil air occurs. As a result of this increased air pressure, observation wells which are screened below the water table show a rapid rise in their water level, despite the fact that the actual water table (elevation of saturation) is essentially unchanged. As mentioned in Weeks (2002) the effect was noted as early as 1932 by Thal Larsen in the village of Lisse, Holland and was given its name by Hooghoudt (1947).

Heliotis and DeWitt (1987) and Meyboom (1967) have reported observations of Lisse effect in water table hydrographs; however, their explanation is more from the point of view of identifying anomalies in water table observations rather than a way to quantify air pressurization. Weeks (2002) attempted to mathematically link air pressurization to the anomalous water level rise in observation wells, but his analysis was overly simplistic and proved useful only for calculating the maximum possible water level rise for a

specific soil type. Nonetheless the effort provides a background relating air entrapment and water table fluctuations.

Because air entrapment in shallow water table environments reduces infiltration and causes artificial rise in the water table, it has significant implications for estimating ground water recharge. Healy and Cook (2002) presented a thorough review of methodologies to estimate recharge using ground water levels, but commented that one of the major limitations of any method for shallow unconfined aquifer was the Lisse effect. As the artificial rise in the water table is difficult to identify and it can easily be mistaken for recharge (Healy and Cook 2002).

Accurate estimation of soil air pressure is thus of great importance for modeling runoff and water table recharge. Mathematical solutions derived from laboratories studies e.g., Wang et al. (1997, 1998) provide very useful insight into the process of air entrapment, however the use of the laboratory derived equations have not been adequately tested under field conditions. Latifi et al. (1994) concluded that air pressure buildup was more pronounced in soil columns of two layers than in a soil monolith. Zhang and Ross (2007) discuss the importance and prevalence of soil layering in most coastal plane soils. Natural soil layering introduces uncertainty in the applicability of laboratory results, derived under homogenous soil conditions.

Another important aspect to note is that most of the theoretical/experimental work or field observations have been limited to an event based approach wherein the effects of single rainfall event on air pressurization/ water table fluctuation are noted and analyzed for only short duration. For the purpose of long term modeling of stream flow and aquifer recharge a continuous monitoring and analysis is needed. For field conditions subjected

to multiple events and varying antecedent conditions, air effects may become compounded and/or prolonged. Recently, Crosbie et al. (2005) proposed a time series approach to infer ground water recharge using a water table fluctuation method. The approach tried to overcome the limitations mentioned in Healy and Cook (2002) and was reported to be applicable to long term records of precipitation and water table elevation. Even though the proposed model by Crosbie et al. (2005) was innovative in its and accounting for air pressurization, the model eliminated all water level rise, if the assumed criteria for Lisse effect (see Crosbie et al. 2005, Equation 2) is satisfied. This may, during long continual rainfall events, neglect the actual water table rise due to wetting fronts reaching the water table.

7.2.1 Objectives and Scope

The above discussion clearly illustrates the need for a more physically based analysis of air entrapment over long term (multi-event) records. The current study attempts to address this need by using shallow water table elevation records in conjunction with observed soil water content profiles that were measured during a field study. The specific objective of the investigation is to: (a) detect the presence of Lisse effect, (b) quantify the air pressurization values in field data, (c) use quantified air pressurization values to determine the location of true elevation of the water table, and (d) to elucidate the overall implication on modeling runoff and recharge.

The approach used in the study is to calibrate a Richard's equation model to observed water content profile and derive depth to water table from resultant pore water tension pressure, as it is unaffected by the air pressurization. The soil moisture behavior

can then be used to determine the true depth to water table. The difference between the observed and the true depth to water table will hence give the value of air pressurization.

7.3 Study Site and Data Collected

For the current study, field data were obtained from a study site described in Chapter 2. Soil moisture and water table data from well PS-43 located in the grassed area of the study site was used for the analysis. Hourly data from both soil water content probe and pressure transducer was used for analysis in this study. Rainfall data were obtained from a tipping bucket rain gauge housed in a weather station established in the study area.

7.4 Methodology

Due to air entrapment traditional rainfall infiltration models like Green and Ampt (1911), tend to over predict infiltration with physical soil parameters in shallow water table environments. In this case, infiltration can be derived from volume changes since soil water content was explicitly measured. Assuming a one dimensional soil column, integration of the soil water content values will give the total water content (TWC) per unit area of soil column at any instant in time. Subtraction of two consecutive values will, hence, give an estimate of net infiltration or net evapotranspiration (*ET*) (depending on the algebraic sign of the difference) in units of length. For the purposes of this study, net infiltration or net *ET* refers to all inflow and outflow respectively (including lateral flows) for details of the approach one is directed to Rahgozar et al. (2005). Nachabe et al. (2005) used a similar approach to determine *ET* and found the methodology to give a very good match with calculated values from other methods. For this particular study, given the

spatial distribution of the soil moisture sensors, a simple numerical integration (trapezoidal rule) was done to calculate TWC for the soil column of length 1.5 m. The mathematical equation used is

$$TWC = \sum_{1}^{8} z_i \theta_i \tag{7.1}$$

where z_i [L] is the depth associated with each sensors (see Table 7.2), and θ_i [L^3L^{-3}]is the water content values at the corresponding sensor.

7.4.1 Numerical Model

Soil water content profiles were modeled using a single phase, one dimensional Richard's equation model known as HYDRUS -1D (version 3) (Simunek et al. 2005). HYDRUS was previously used by Hammecker et al. (2003) to try and quantify the effect of air compression. The approach they used was to apply Dirichlet conditions, namely the upper boundary given by the ponding water level in the plot and the lower boundary given by the depth of the water table as the two boundary conditions. The lack of match with the observed data was attributed to the air compression, as all the other processes were assumed to be accounted for in HYDRUS. No further analysis was done to quantify the air entrapment from the numerical solution.

As described in Hillel (1998), due to air entrapment, the soil water content does not attain total saturation but some maximal value lower than saturation, which he called satiation. Satiation can be taken into account by considering that the maximum water content in a soil only reaches to a value smaller than porosity, more commonly referred to as natural saturation or effective porosity (Charbeneau 2000). Hence, laboratory

determination of soil saturation water content normally overestimates the values found in situ. This phenomenon was considered in the calibration of soil parameters.

For the current investigation data for two months (May and June) in 2002 and another two months (April and May) in 2003 were analyzed, and modeled numerically using HYDRUS. This period of record was selected because it represented the transitional months when conditions changed from very dry to very wet. Hence, a good contrast between the conditions with and without air pressurization can be expected. Due to hysteresis, the effective porosity shows a long term seasonal behavior as listed in Table 7.1. Hence, for calibration purposes, saturated water content values that are used correspond to the maximum water content values observed during the period of record. As expected the values were found to be less than the laboratory determined porosity, by as much as 7-8%.

Table 7.1 Differences in Observed Maximum Water Content (Water Table at the Land Surface) for Different Period of Records.

Sensor Location Below Land Surface (cm)	Maximum Water Content for Period (2001- 2004) %	Maximum Water Content (May-June 2002) %	Maximum Water Content (April –May 2003) %
10	42.3	33.9	37.3
20	37.6	34.8	32.9
30	31.4	31.3	29.5
50	30.8	29.3	29.4
70	30.3	28.3	29.3
90	30.9	28.7	29.5
110	32.7	29.9	32.0
150	36.9	36.6	34.4

7.4.1.1 Model Setup

It is known that under heterogeneous conditions air pressure buildup is more pronounced than under homogenous conditions (Latifi et al. 1994). Field observations of water content values obtained from the soil moisture sensors show that the soil profile is far from homogenous even at a vertical scale of 1.5 m. (Figure 7.1), also noted by Zhang and Ross (2007). Hence, with the purpose of making the model representative of actual soil column at the study location, the simulated soil column was setup with eight different soil layers, each corresponding to a soil moisture sensor. It is worth noting that the objective of the model setup is to mimic as closely as possible the observed water content. To make the numerical model highly resolved, it was discritized into 1001 numerical nodes, which corresponds to maximum spatial discretization allowed in HYDRUS. HYDRUS calculates the value of pressure head and water content at each of the nodal location. Hence, an almost smooth water content profile can be obtained from this highly resolved discretization.

Of special interest is the actual depth to water table which, due to air pressurization, can be lower than observed. Therefore, a conservative column length of 200 cm was used even though the observed maximum value of observed depth to water table (d_{WT}) never exceeded approximately 140 cm. For the given sensor distribution the depth and location of each soil layer is given in Table 7.2.

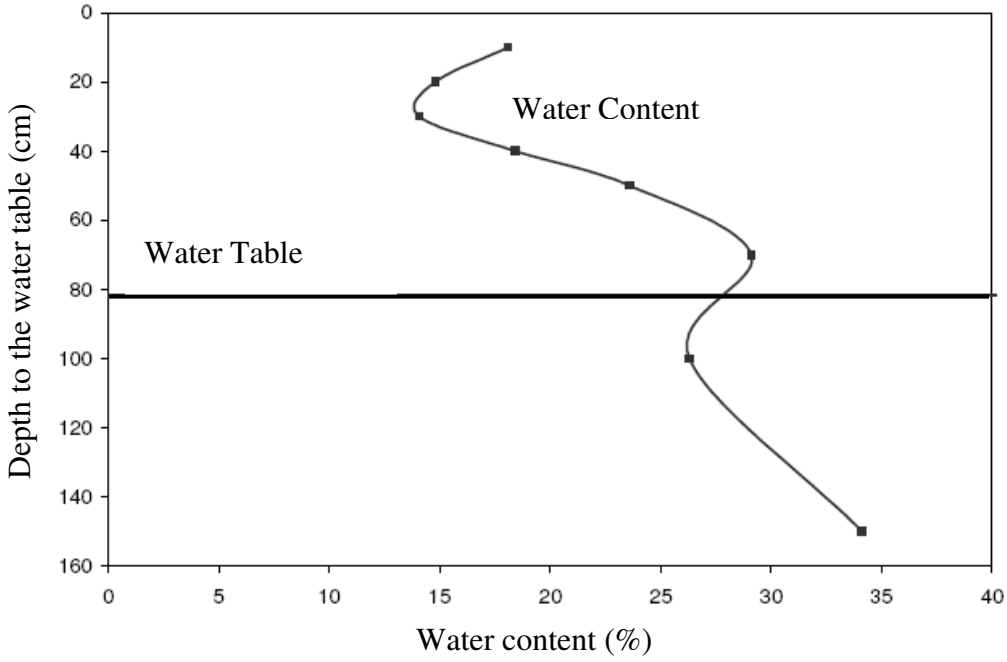

Figure 7.1 Snapshot of Water Content Variation Along the Vertical Soil Profile.

7.4.1.2 Soil Hydraulic Properties

For the purposes of numerical solution of Richard's equation, the relationship between soil water content and suction pressure head has to be defined. Out of many different models found in literature, the Brooks and Corey (1964) model was selected. Mathematically the model is defined by Equations 7.2 and 7.3.

$$S_e(h) = \frac{\theta(h) - \theta_r}{\theta_s - \theta_r} = \begin{cases} \left(\frac{h_a}{h}\right)^{\lambda} & for \quad h \geq h_a \\ 1 & for \quad h < h_a \end{cases} \tag{7.2}$$

$$K(S_e) = K_s S_e^{\frac{2}{\lambda}+l+2} \tag{7.3}$$

where S_e [L^3L^{-3}] is effective water content, K_s [LT^{-1}] is saturated hydraulic conductivity, θ_r [L^3L^{-3}]and θ_s [L^3L^{-3}] denotes residual and saturated water contents, respectively; h_a [L] is the air-entry pressure value (or bubbling pressure), λ [-] is a model parameter, h [L]is

the capillary suction pressure and l [-] is a pore connectivity parameter assumed to be 1.0 as an average for many soils (Mualem 1976). The soil parameters thus needing to be defined in HYDRUS are the residual and saturated water content, bubbling pressure, saturated hydraulic conductivity and the model parameter λ.

Soil parameters, taken from a soil survey published by the Institute of Food and Agricultural Science, University of Florida (Carlisle et al. 1989), for an area very close to the study site serve as the base for calibration of soil hydraulic properties. From the soil survey data it was clear that the soil profile in the region (in and around the study area) comprises of six to eight different horizons characteristic of Myakka fine sand with the thickness closing matching to the ones observed in the field and assumed in the numerical model.

7.4.1.3 Initial and Boundary Conditions

As part of the model setup, initial and boundary conditions were defined based on observed field data. As mentioned before, two periods from May 4th to June 30th, 2002, and April 1st to May 30th, 2003 were analyzed. To accomplish this, two sets of simulations with similar initial and boundary conditions were setup.

7.4.1.3.1 Initial Conditions

As both period of records were preceded with very dry conditions (more than 10 days of no rainfall), no initial air pressurization was assumed and soil water content distribution was assumed to be at equilibrium (i.e., water pressure distribution was assumed hydrostatic). Hence, the observed value of d_{WT} can be assumed to closely match

the zero water pressure elevation (i.e., true depth to water table). For the first simulation starting from May 4th, 2002, the initial d_{WT} was thus set at 100 cm. For the second simulation, starting on April 1st, 2003, the initial d_{WT} was established at 80 cm.

7.4.1.3.2 Boundary Conditions

The 1D numerical soil column (for both simulations) was set up with a no-flow boundary condition at the bottom. At the top, atmospheric boundary conditions with no surface runoff were defined. Changes in observed TWC were used to define the imposed stress of rainfall and potential evapotranspiration. The variable boundary conditions (defining the stresses) were set up at an hourly interval with, depending on the result of Equation 7.1, either net *ET* or net precipitation defined one at a time. HYDRUS-1D does not allow specification of actual evapotranspiration explicitly. Instead, the code determines values and contribution from the soil profile using the specified potential transpiration values (see the following paragraph for details). The net *ET* was later compared to the actual *ET* that was observed in the field. This served as a validation that the imposed boundary conditions were similar to that observed in the field. Further details are discussed in the results section.

Evapotranspiration is simulated via the sink term S [$L^3L^{-3}T^{-1}$] shown on the right side of Richard's equation. This sink term modeled as modeled in HYDRUS-1D is distributed through the root zone to reflect the plant root distribution in the domain as follows:

$$S(x) = \alpha(h)\, S_p(x) \tag{7.4}$$

where $\alpha(h)$ [-] is root water uptake stress response function ($0 \leq \alpha(h) \leq 1$), as defined by Feddes et al. (1978), and $S_p(x)$ [T^{-1}] is the spatial distribution of the potential transpiration rate over the soil profile as a function of depth x [L]. The potential transpiration rate is the water uptake rate when the plant is not experiencing any water stress; $\alpha(h) = 1$. For vegetated cover, the potential *ET* is distributed through the subsurface root system according to a distribution function. The distribution function used is:

$$S_p(x) = b'(x)\, T_p \tag{7.5}$$

where T_p [LT^{-1}] is the potential *ET* and $b'(x)$ [L^{-1}] is the relative fraction of roots at any depth x. Jackson et al. (1996) compiled data on the distribution of roots as determined by large number of field studies and found that the model proposed by Gale and Grigal (1987) was very successful in describing the root distribution. The model of root distribution is:

$$Y = 1 - \gamma^{d} \tag{7.6}$$

where Y is the cumulative fraction of roots from the land surface to depth d, and γ is a numerical index of rooting distribution which depends on vegetation type. This relationship was used in the numerical simulation, to specify relative root density at each node, with γ equals to 0.952 for grass (Jackson et al. 1996), the predominant land cover at the study location. The root zone thickness was specified as 1 meter consistent for grass in this environment (Jackson et al. 1996).

7.4.2 Calibration to Observed Period of Record

The whole calibration process was done as a two step process. In the first step hydraulic characteristics of top three soil layer were calibrated using the inverse solution

tool in HYDRUS 1D, while the parameters for other soil layers were kept at the values given in Carlisle et al. (1989). Secondly the parameters of the bottom layers were adjusted manually to get the best match to the soil water content variation.

The inverse solution tool in HYDRUS uses the Marquardt-Levenberg algorithm to determine the best fit soil parameters, based on specified observed values. The limitation with the inverse tool is that it can accept only about 7000 records as observed values, and 15 parameters as the maximum that can be calibrated. Owing to this limitation, parameters for only top three soil layers were calibrated using the inverse solution tool, with about a month of data (May 4th-May 30th, 2002)). The remaining parameters of soil layers values were manually calibrated, and some fine adjustment was made to the earlier calibrated parameters, for another month of data (May 30th-June 30th, 2002). Overall for this analysis, observed water content values from the period of record for the first simulation (i.e., May 4th-June 30th, 2002) were used as input values. As previously discussed, from observation of maximum values, it is clear that, as a result of air entrapment, saturated water content in the field data averages lower than ultimate porosity. As a result, the only constraint that was placed in the inverse solution was that saturated water content value be fixed as the maximum observed water content at the corresponding sensor location for the period of record. Apart from saturated water content, other soil hydraulic properties are mostly unaffected by air entrapment. As such, the calibrated values from the first period of records were used unaltered for the second simulation. This was considered a simple validation for the calibrated soil hydraulic variables. Similar to the first simulation, the saturated water content values for the second run were also specified based on the maximum value (corresponding to water table at or

above land surface) observed for the period of record of the simulation. Table 7.2 lists the soil parameters used for the theoretical solution of Richard's equation.

7.4.3 Calculation of Excess Pressurization Using Ideal Gas Law

The difference between the d_{WT} obtained from theoretical solution (HYDRUS-1D) and field observations, gives a quantitative estimate of air pressurization. If the pressure of the entrapped air is atmospheric then the observed and the actual d_{WT} will be at the same location, void pressures above atmospheric will cause the two water table depth values to depart (observation will be higher). The pressure of the compressed air in excess of atmospheric, herein denoted as "excess pressure", is defined as the difference between the observed d_{WT} and the HYDRUS-1D generated d_{WT}. It is expressed in terms of depth of water column.

In an attempt to quantify the amount of excess pressure and, potential thresholds for air eruption, a simple spreadsheet-air-excess-pressure-analysis was set up. The maximum saturated water content for every sensor from the entire period of data collection was found. To this value 7.5% (Nachabe et al. 2004) was added to account for the residual air, crudely representing the actual soil porosity at each sensor. Multiplication of porosity by the depth associated with each sensor (as shown in Table 7.2) gives the available pore space in the soil column (per unit cross sectional area). Subtracting total soil water content obtained by integrating water content values along the soil profile (like in Equation 7.1) from the porosity gives the amount of pores filled with air in the soil column.

Table 7.2 Calibrated Parameters and Extent of Soil Layers Below the Land Surface.

Layer /Sensor No.	Depth Below Land Surface (cm)	Saturated Water Content		Residual Water Content	Soil Hydraulic Parameters for Brooks and Corey Model			
		2002 (%)	2003 (%)	(%)	λ [-]	h_b (cm)	K_s (cm/hr)	l [-]
1	0-15	33.9	37.3	1	1.1	25	20	1
2	15-25	34.8	32.9	1	1.1	25	20	1
3	25-40	31.3	29.5	1	1.2	25	20	1
4	40-60	29.3	29.4	5	0.7	25	10	1
5	60-80	28.3	29.3	5	0.7	25	10	1
6	80-100	28.7	29.5	5	0.7	25	10	1
7	100-125	29.9	32.0	5	0.7	25	10	1
8	125-200	36.6	34.4	5	0.7	25	10	1

It is important to know the inherent assumptions involved in the spreadsheet calculation of excess pressure. The first and possibly most important assumption is that all the entrapped air present between the wetting front and the water table has the same pressure. This limitation will be discussed later. The second assumption is that continuous counter flow of air during an event is neglected. Therefore, the only way the soil air can leave the soil column is via air eruption. Finally, the temperature is assumed to be constant and the Ideal Gas Law behavior is assumed under adiabatic conditions.

7.4.3.1 Implementation of the Spreadsheet Model

Morel-Seytoux and Khanji (1975) proposed a model for quantifying air compression using Boyle's law. As Boyle's law assumes the mass of the gas to be

constant, this methodology becomes invalid in case of air eruption. It is for this reason the Ideal Gas Law is used for the spreadsheet analysis, with the underlying assumption that air behaves like an ideal gas. Consistent with the HYDRUS solution, hourly time steps were used for pressure calculations. Thus, hourly values of total soil water content were used to determine the changes in the volume from which the void air pressure is derived.

Mathematically, the Ideal Gas Law can be defined as

$$PV = nRT \tag{7.7}$$

where P is the absolute pressure (N/cm^2), T is absolute temperature (K) assumed constant at 298K, V is volume of the void air (cm^3), n is the number of moles, and R is the gas constant (= 831.41 N-cm / (mol/ K)).

As mentioned earlier, both the simulation periods were preceded by dry conditions. Therefore, the initial pressure of the entrapped air is assumed to be atmospheric, P_0, i.e. 10.13 N/cm^2. The initial volume V_0 of entrapped air was determined by subtraction of observed total soil water content (initial value) from the total pore space (constant =68.92 cm^3). At the next hour the new volume of air (V_1) is similarly calculated, using the corresponding observed total soil water content. Assuming a constant temperature T, Equation 7.7, is used to determine the initial number of moles (n_0). Using n_0 and the volume at the next hour V_1 the pressure P_1 was found again using Equation 7.7.From this approach excess pressure (in centimeter of water column) is determined as follows

$$\Delta P = \frac{P_1 - P_0}{\rho g} \tag{7.8}$$

where ΔP is the excess pressure (cm), ρ is the density of water, and g is the acceleration due to gravity, and ρg is assumed as 0.00981 N/cm^3.Between consecutive time steps two processes are possible. First, due to net *ET*, the new volume of air is greater than the previous volume or secondly, due to net infiltration, voids are reduced and excess pressure ensues. It is important to note that at an hourly time step sufficient infiltration can occur to cause the excess pressure to become quite large. Therefore excess pressure may reach an upper limit where by rapid air eruption occurs. This breaking value (as defined in Wang et al. (1997) results in eruption and a lowered air pressure values is produced.

Consider the *ET* case where the volume of air increases. In this case the new value of air pressure will decrease, except that there is no wetting front to preclude air uptake by the soil from the atmospheric boundary. As a result the pressure cannot significantly decrease below atmospheric. Thus, during the spreadsheet analysis the new pressure value is made atmospheric if the solution of the Equation 7.7 results in sub atmospheric pressure during drying conditions. However, no adjustment is made if the new pressure comes out to be greater than atmospheric. One problem that remains is that Ideal Gas Law cannot be used to determine the air eruption thresholds. Also, as a consequence of air eruption, undeterminable numbers of moles of air are lost. Hence, for the infiltration case, to incorporate air breaking values threshold pressures must be set through observation of the data to constrain the maximum pressure.

In the absence of any other indicators, excess pressure determined from comparison of the HYDRUS solution with the field observation, was used to limit the excess pressure values calculated in the spreadsheet. Air eruption was evident in the

several events in both periods requiring constraining the maximum pressure. Thus, if the excess pressure calculated from Equation 7.8 exceeded the thresholds for air breaking derived by HYDRUS, the excess pressure was set at the threshold and the numbers of moles lost were calculated using Ideal Gas Law.

As will be seen later in the results section the excess pressures calculated using HYDRUS show large variations depending on the infiltration magnitude and the antecedent conditions. However critical thresholds were more consistent. This implies that, in order to determine air eruption for each event, different thresholds have to be set. To avoid this cumbersome approach, the analysis was done only on the events occurring in the month of May of 2002 and 2003.

7.5 Results

7.5.1 Calibration and Validation Results

The numerical soil column model, calibrated for 2002 and validated against 2003 data, gave values very close to the observed soil water content. Figure 7.2(a-d) shows observed and simulated water content values for both the simulations, during dry and wet conditions. The observed d_{WT} and HYDRUS d_{WT} are also plotted. As expected, during wet conditions the observed d_{WT} departs from the HYDRUS d_{WT} while they match almost exactly during the drying conditions. To compare the observed boundary conditions with those simulated in HYDRUS, the water content values obtained from the simulations were integrated using Equation 7.1 and plotted versus the observed total water content values. The data points were found to lie along a forty five degree line with and coefficient of regression value (r^2) of 0.997. The high value of r^2 indicates that the

numerical model is reasonably calibrated to the conditions and soil types observed in situ, thereby increasing confidence in numerical simulation results.

7.5.2 Numerical Solution

HYDRUS -1D was used to derive pressure head and water content values at each node in the soil column, continuously in time. The model was run at an hourly time step, but due to limitations in the maximum number of output, model results were saved every six hours. From the pressure distribution along the soil column, the d_{WT} was determined by noting the location of zero pressure head (Freeze and Cherry 1979). It has been deduced from the calibration and validation results, that the model describes the soil characteristics reasonably well and successfully reproduces the water content profiles and d_{WT} during drying periods. Therefore, d_{WT} determined above should represent the actual d_{WT} in absence of air pressurization.

Figure 7.3(a) and (b) show the variations of the observed d_{WT} and the HYDRUS d_{WT} with time. Also plotted on the secondary Y axis is the net infiltration (as obtained from Equation 7.1). As Figure 7.3 illustrates, the HYDRUS solution was very successful (given a tolerance of ±3 cm) in describing the water table during the drying periods and many wet periods. Therefore, departures from the actual (HYDRUS) d_{WT} during large infiltration events clearly indicate air entrapment and pressurization.

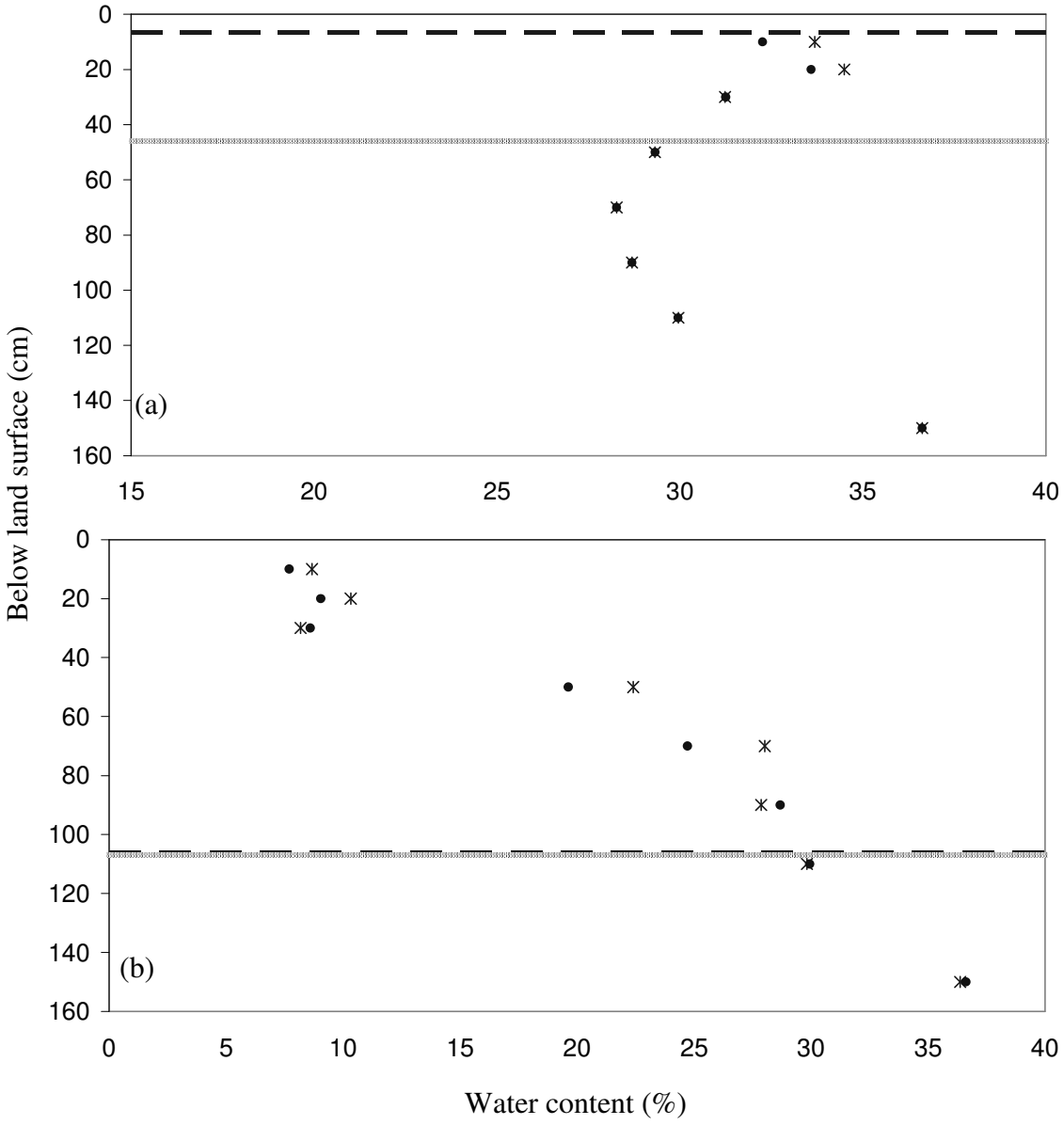

Figure 7.2 Snapshot of Calibration Results. Crosses Represent the Observed Water Content Values, while the Circles are the Calibrated Values. The Dashed Lines Represent the Observed d_{WT} and Solid Line Represents the d_{WT} calculated from HYDRUS. Water Content Distribution from 2002 (a) Wet Conditions (b) Dry Conditions, and 2003 (c) Wet Conditions (d) Dry Conditions.

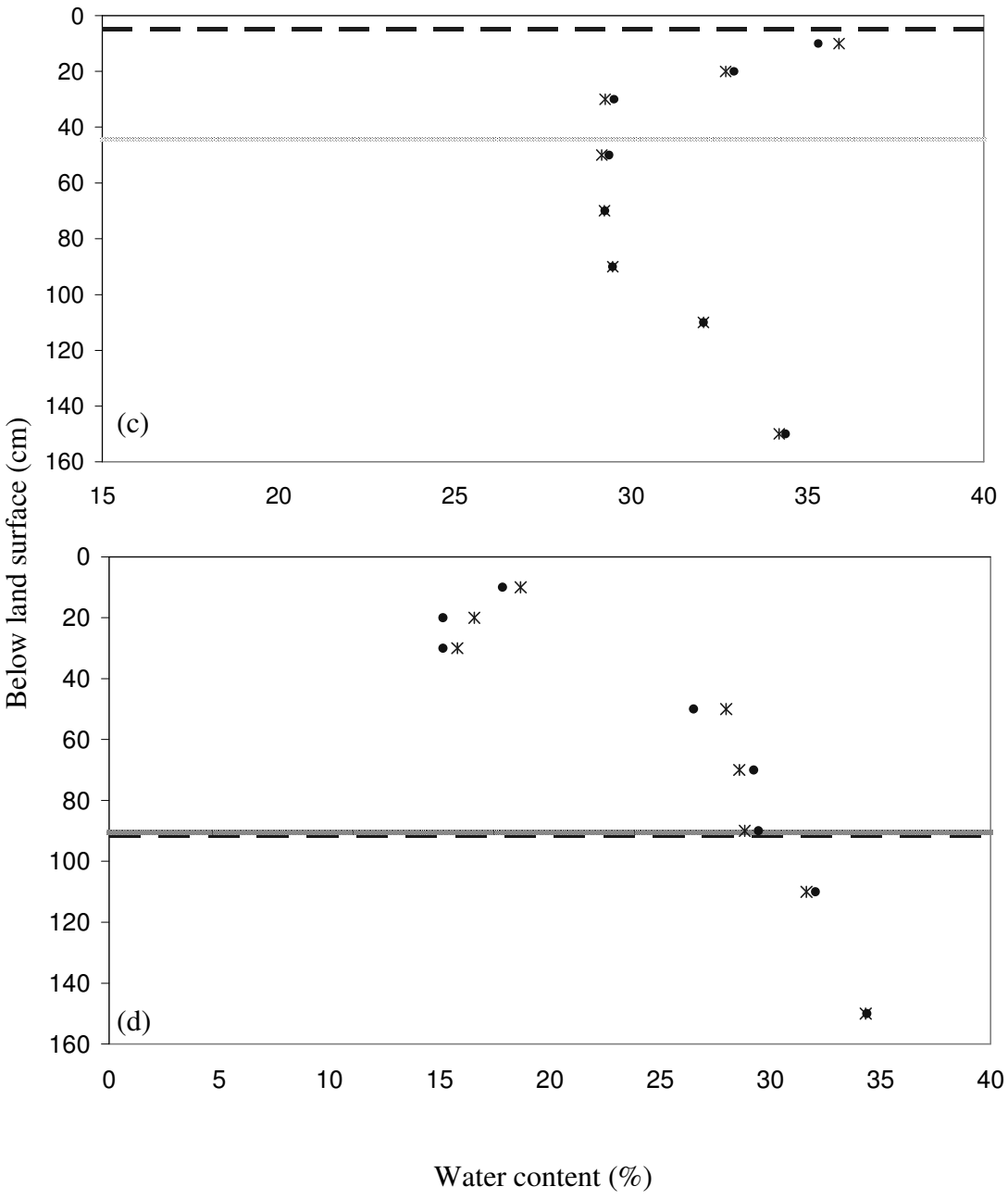

Figure 7.2 (Continued)

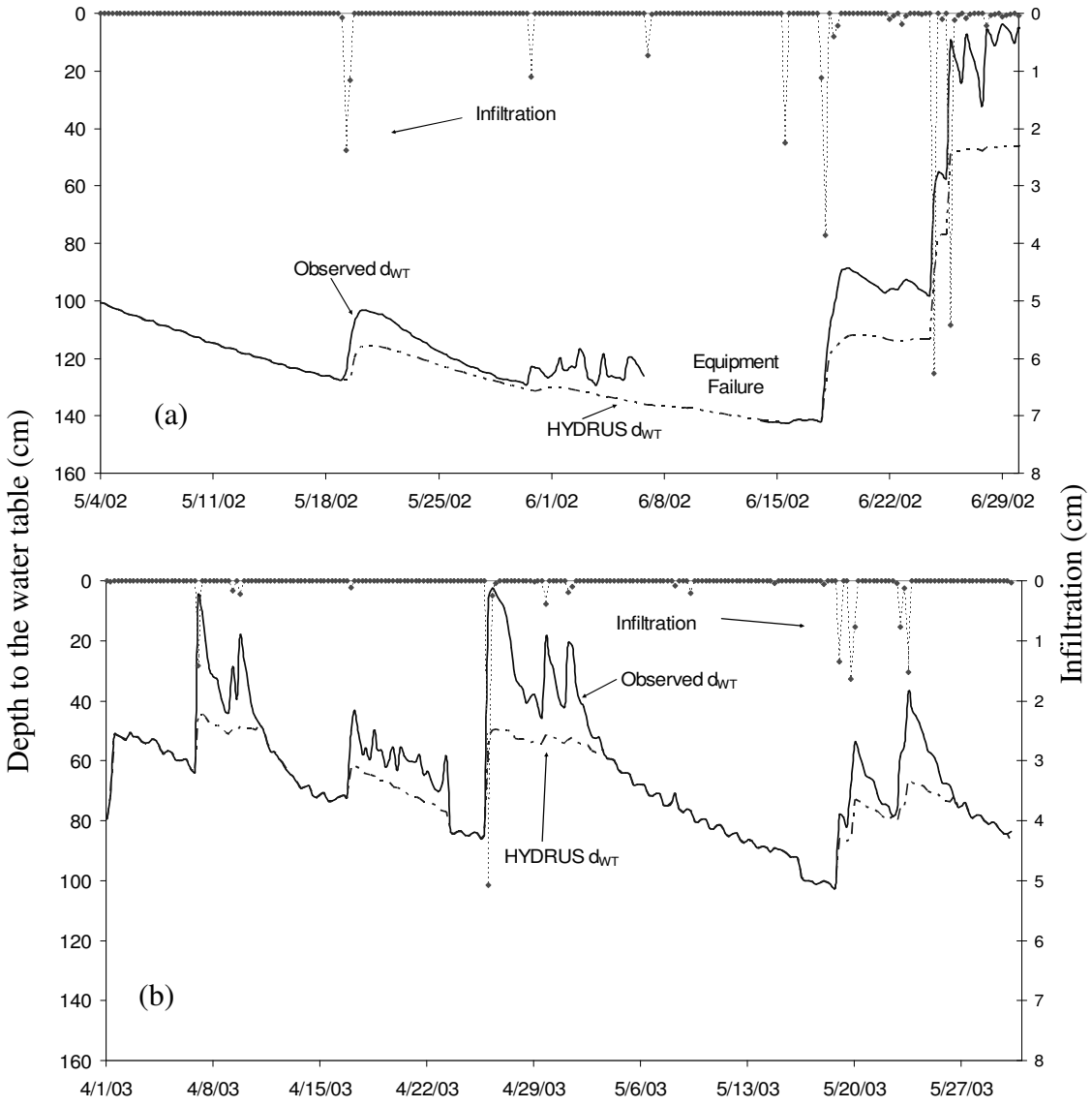

Figure 7.3 Actual d_{WT} Calculated from HYDRUS Plotted Against Observed d_{WT} for (a) May 2002-June 2002, (b) April 2003-May 2003.

From the results above, the magnitude of the excess pressure was found to be a function of actual d_{WT}. For example, the April 7th, 2003 1.4 cm infiltration event shown in Figure 7.4(b) produced an excess pressure of around 40 cm, while a May 19th, 2003

infiltration event of similar magnitude only produced 7 cm of excess pressure. As can be seen from the graph the antecedent conditions were very similar with the only difference being the d_{WT}. For the two events, d_{WT}, in former case was 60 cm while for the latter period it was 100 cm. In fact (from Figure 7.4) in 2002 on June 15th, 2002 an infiltration event of around 2.25 cm did not produce any excess pressure as the water table was deep at around 140 cm. Overall both graphs show that the actual water table fluctuations are smooth. However, due to the excess air pressure, the observed water table fluctuations appear more responsive.

To evaluate the role of air entrapment in controlling the runoff process, infiltration, as calculated using Equation 7.1, was plotted along with observed rainfall and the calculated excess pressure for the period of simulation in 2002 and 2003 (Figure 7.4(a) and (b)). From the graphical analysis it was found that the magnitude of the maximum excess pressure for both the simulations remained at around 45-47 cm, yet some differences in the periods existed. In 2002, the two months of simulation definitely produced some runoff, contrary to 2003 where all the rainfall infiltrated. The 2002 and 2003 simulations while representing similar seasonal period exhibit some notable difference in soil response reflecting difference in antecedent moisture condition (AMC). Several specific events from 2002 and 2003 are offered for discussion. On April 26th, 2003 and on June 25th, 2002 the excess pressure maximum was found to be around 45 cm. However, on April 26th, 2003 all rainfall infiltrated contrasting June 25th, 2002 where negligible infiltration took place. These differences are attributed to difference in AMC. From Figure 7.4 and 7.5 if the AMC prior to the rainfall events is considered, on April 26th, 2003 the actual d_{WT} was around 85 cm with dry antecedent condition (< 0.05 cm of

rainfall in previous 10 days) while on June 25th, 2002 the water table was high at 46 cm reflecting much wetter AMC. Another noteworthy observation is that on June 25th, 2002 the sizable infiltration event resulted in water table rise from 85 to 50 cm (below land surface) with excess pressure build of 45 cm, as against April 26th, 2003 where the water table remained pretty much stable. The most obvious question that results from these observations is how can one be so sure that the runoff produced is due to air pressurization?

To address this question the intensity of rainfall from the data were calculated and compared with the saturated hydraulic conductivity of the top layer of the soil. It was found that the during all four months of analysis the rainfall intensity was never greater than the infiltration capacity theoretically given by soil physics (i.e., Richard's equation neglecting air effect) as the vertical hydraulic conductivity and predicted by simple models such as Green and Ampt (1911) model. The clear conclusion is that runoff resulted solely due to air entrapment, investigated below through simple spreadsheet analysis of air pressurization.

7.5.3 Spreadsheet Analysis

Figure 7.5(a-d) shows the variation of excess pressure calculated from spreadsheet analysis of void air pressures using Ideal Gas Law along with the HYDRUS solution, and the observed d_{WT}. The number and variation of air moles are also included in the figure to demonstrate air eruption. A review of Figure 7.5(a) and (b) shows that rate of pressure decline calculated from the spreadsheet is significantly more than the decline calculated from HYDRUS. The results from the spreadsheet analysis hence raise

a big question, what is going on with air pressure in shallow d_{WT} and why are the air excess pressure periods so prolonged. Another conclusion might be that Richard's equation solution may not represent d_{WT} and infiltration behavior well enough in shallow water table settings to reasonably quantify runoff (Hortonian or saturation excess) and recharge processes. In an attempt to answer, this question and the bold statement, basic processes in porous gas behavior (i.e., spreadsheet) and soil moisture physics (neglecting air effects) needs to be examined.

Richard's equation as solved by HYDRUS ignores void air pressurization. Hence for all boundary conditions and soil moisture variation it solves for $d_{WT,}$ from which the excess pressure is derived. The spreadsheet solution on the other hand is highly dependent on the soil air volume changes from which the excess pressure is calculated. While, HYDRUS calculations incorporate soil properties from which pore water pressure distribution is calculated and d_{WT} determined, spreadsheet solution do not take any soil property into account. The only driving variable in the spreadsheet solution is the change in void air volume, which is inherently assumed to be occurring between the wetting front and the water table. The following paragraph tries to numerically explore the differences that are created due to the aforesaid difference in methodologies involving either HYDRUS or spreadsheet (Ideal Gas Law).

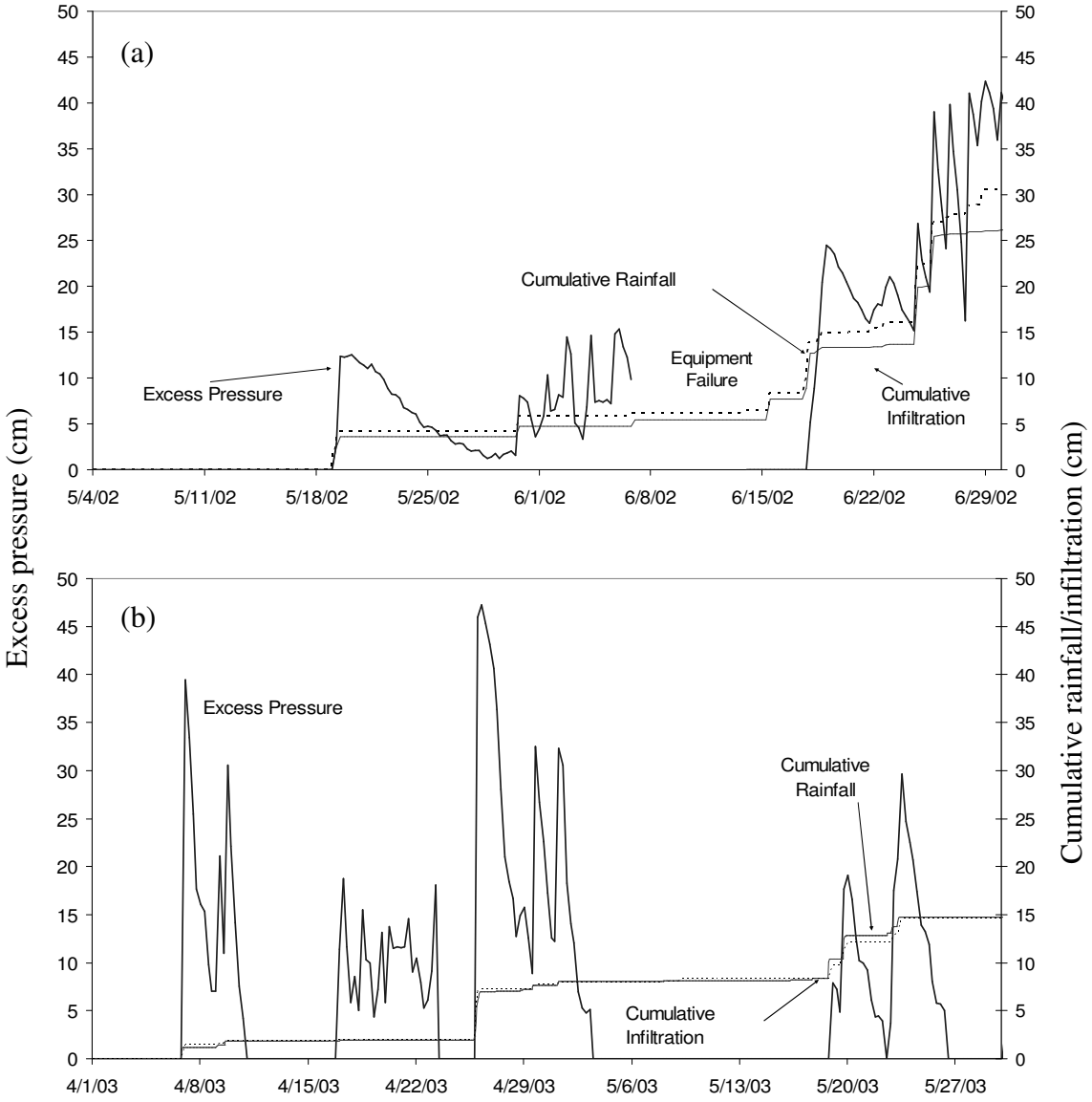

Figure 7.4 Rainfall and Infiltration Plotted Along with Excess Pressure for (a) May 2002-June 2002, (b) April 2003-May 2003.

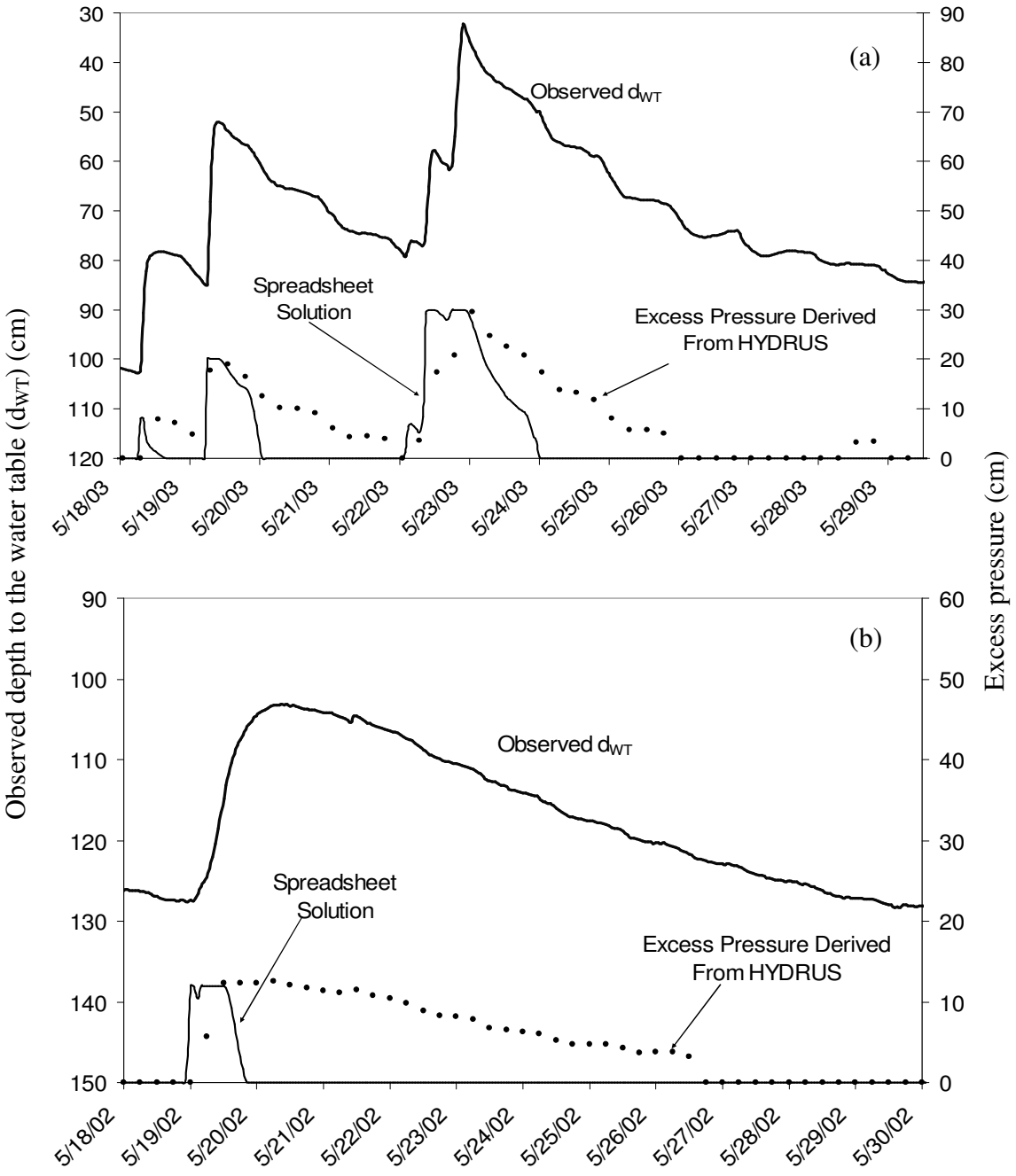

Figure 7.5 Excess Pressure as Calculated from Spreadsheet Model and HYDRUS Solution. (a) Shows the Variation of Pressure for May 2003, (b) Shows Variation of Pressure for May 2002, (c) and (d) Shows the Variation in the Number of Moles as Predicted from the Spreadsheet Model for 2003 and 2002, Respectively.

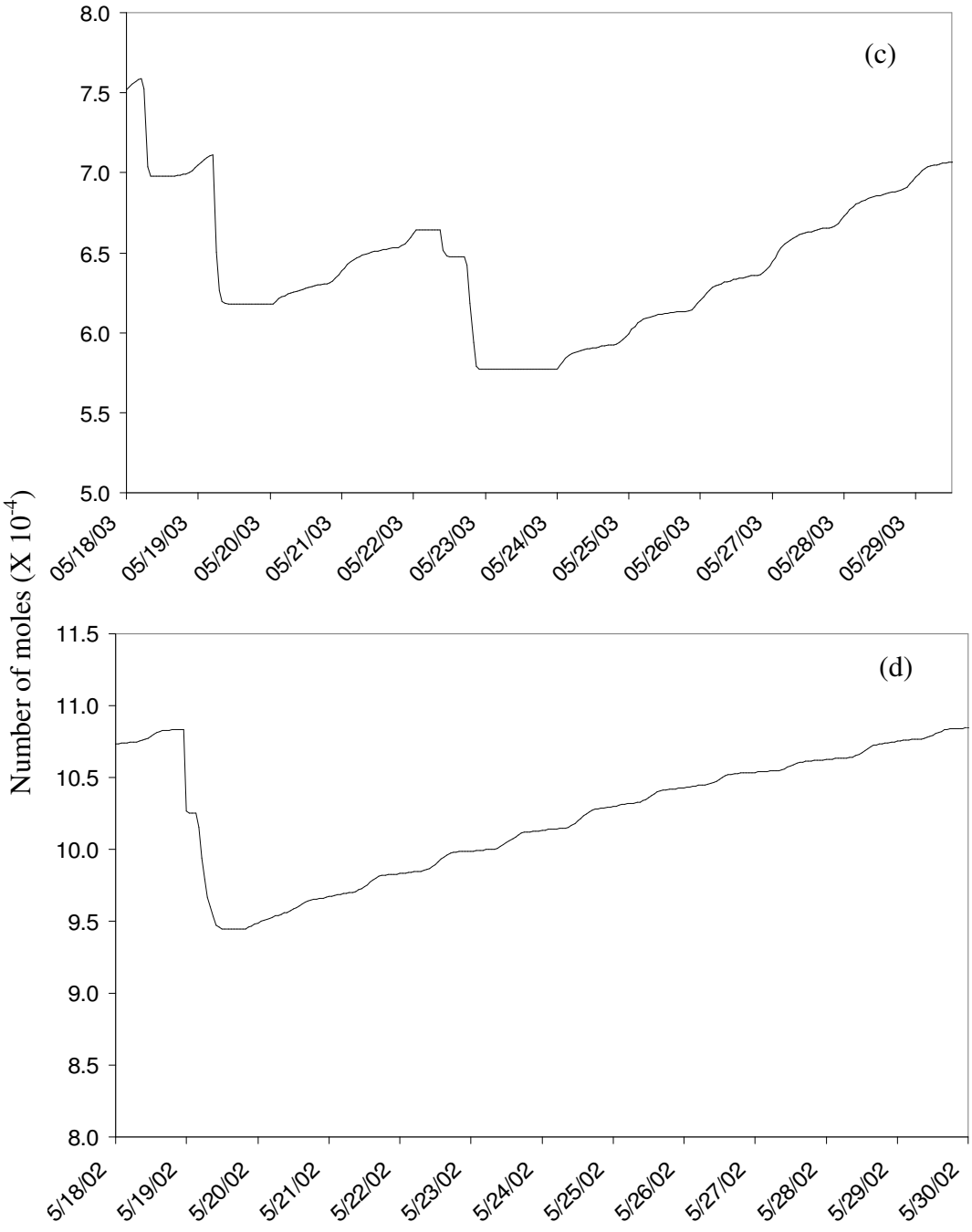

Figure 7.5 (Continued)

Assuming no counter flow (i.e., the number of moles remain constant), a decline of excess pressure from 47 cm (the maximum observed in the HYDRUS analysis) to zero involves a change of 1.15 cm^3 of soil air, using Equation 7.7. This translates to about one percent change in soil water content of the sensors. In other words, even if the soil water content value of the top two sensors changes by a couple of percent the spreadsheet solution will result in major loss of excess pressure.

Figure 7.6 shows the variation of the water content values of top three sensors for portion of May 2003. From the graphs, the occurrence of infiltration events and the propagation of the wetting front can easily be seen. In response to the event on May 18th 2003, the soil moisture sensor at 10 cm shows a sudden spike while the soil moisture sensors at 20 and 30 cm show a much more subdued increase. From the events on May 19th and May 23rd, 2003 it can be easily seen that the wetting front continued to propagate downward as the water content values at 20 cm and 30 cm below land surface keep on increasing. After May 23rd , the 10 and 20 cm sensors show decline and the 30 cm sensor is mostly unchanged indicating that the location of wetting front has progress to at or below 30 cm below the land surface. Thus the soil voids generating excess air pressures will be those entrapped below 30 cm from the land surface.

However due to rapidly declining water content values of the moisture sensors at 10 cm and 20 cm below land surface, the soil air pressure above the wetting front probably recovers to near atmospheric levels. The inherent assumption of uniform pressures in the soil voids in the spreadsheet model thus results in considerable difference in the excess pressure predicted versus the water table departure observed. Figure 7.6, indicates that the water content in the top sensors, especially at 10 cm, can change by a

couple of percent within one or two days after any event without affecting the wetting front, and hence the spreadsheet solution, will cause the excess pressures to dissipate within a day or so after the event, as observed in Figure 7.5(a) and (b). This contrasts the field data which show it takes several days for air pressures to dissipate.

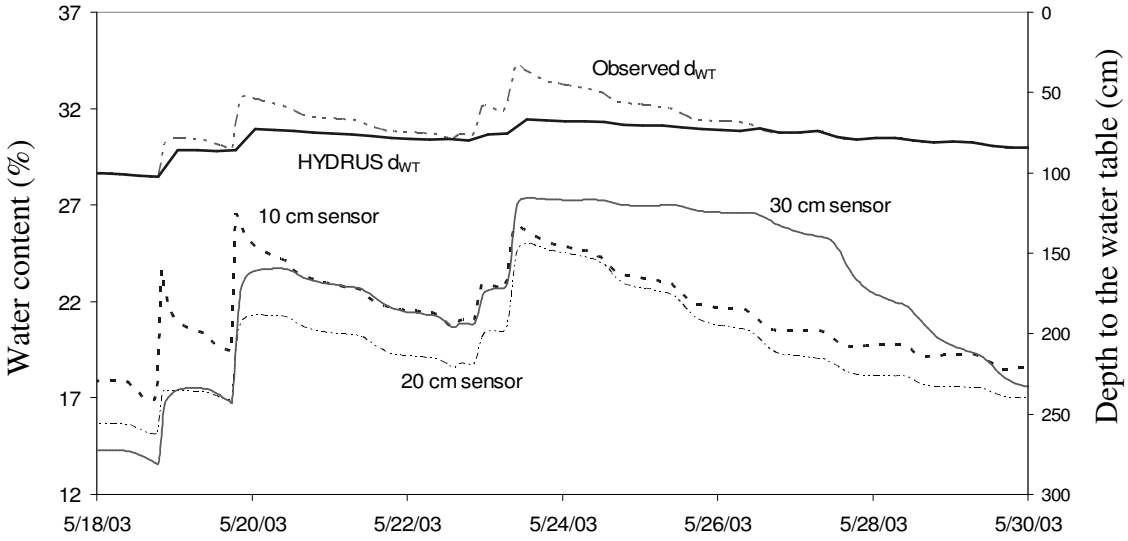

Figure 7.6 Variation of Water Content Values as Obtained from the Sensors Located at 10, 20, and 30 cm Below Land Surface. Also Plotted in the Figure is the Observed and Actual d_{WT}.

The foregoing analysis suggests that the spreadsheet analysis may be overly simplifying the air entrapment behavior in the drying phase. Nevertheless Figure 7.6 presents another indication of air pressurization through observation in the variation in water content values. From the calibrated soil properties (Table 7.2) the thickness of the capillary fringe (zone of tension saturation) is 25 cm. This implies that at any d_{WT}, water content values in a region up to 25 cm above the water table should be at or very near saturated values. Therefore if the observed d_{WT} was correct than on May 23rd, 2003 when

the observed d_{WT} was around 30 cm all soil moisture sensors should have been saturated. However, only the sensor at 30 cm is close to saturation indicating that the observed d_{WT} is higher than the true d_{WT}.

An important feature of the spreadsheet analysis, assuming the HYDRUS solution is a good approximation of the moisture retention physics, is the determination of air eruption and its associated loss of air mass. Figure 7.5(c) and (d) can be used to identify air loss by noting instances when the pressure suddenly decline. Determination of the mass loss during an eruption showed that the loss was consistently about 10-12% of the total mass. Adaptation of Ideal Gas Law has been used in studies (e.g., Sabeh 2004) to quantify air entrapment and have been found to produce good results for single event analysis. However, due to its sensitivity to the soil air volume measurements, multi-event analysis greatly over predicts the loss of excess pressures during drying. This makes the use of perfect gas law, at least assuming uniform void pressure, for long term analysis questionable. Nonetheless, the amount of air loss can be estimated from the thresholds of eruption.

As speculated by Peck (1965) and confirmed by Wang et al. (1997), after air eruption, which takes place at air breaking values (breakthrough threshold), the post air-eruption soil air pressure approaches an excess pressure value called 'air closing value'. In the absence of any data on the location of wetting front, equations for finding air breaking and air closing pressure heads suggested by Wang et al. (1997, 1998) cannot be rigorously applied or validated. However, if a sharp wetting front with its depth equal to infiltration depth is assumed, the air closing values can be estimated to compare these values to the pressure thresholds obtained from HYDRUS. For example, given that on

May 19th, 2003 net infiltration event was about 3 cm, the difference between rainfall and infiltration was observed to be approximately 1 cm. Assuming this to be the ponding depth, the water bubbling pressure for sandy loam type soil was found to be approximately 7 cm (van Genuchten et al. 1991; Carsel and Parrish 1988). Using a relationship for air closing head Hc [L] suggested by Wang et al. (1997)

$$Hc = h_0 + w + h_{wb} \tag{7.9}$$

where, h_0 [L] is the ponding depth, w [L] is the depth of the wetting front, which is the minimum depth in case the wetting front is not sharp, and h_{wb} [L] is the water bubbling pressure of the soil, the value of air closing is approximately 11 cm. This suggests that the value of soil air excess pressure after air eruption should be equal to 11 cm, as opposed to 20 cm as observed from HYDRUS difference. Similarly for the rainfall event on May 23rd, 2003 the value of air closing pressure predicted by Equation 7.9 came out to be 12.5 cm as opposed to a value of 30 cm observed. One possible explanation for the difference can be attributed to the consideration of the isolated event where by the depth of wetting front was defined just on the corresponding infiltration event and no consideration was given for the previous even on May 18th, 2003. Considering the overlapping events it is likely that the wetting front depth would be much longer. The discrepancy again emphasizes the differences that may arise between long term and short term analysis. This is also evident and supported by the prolonged (multiple days) excess air pressures observed in the field data.

7.6 Discussion of Results

The results described above clearly provide field evidence of long term air entrapment and false water table observations as recorded by an observation well cased down through the vadose zone. Analysis showed the importance of antecedent conditions in deciding the amount of excess pressure and the reduction in infiltration, and hence calls for a physically based model to describe the air entrapment process under in situ stresses. Contrasting previous lab experiments, the field conditions are much more variable in space and time and hence the applicability of theoretical relationships obtained from experiments may be questionable. For instance equations given from experiments, (e.g., Wang et al. 1997, 1998), are theoretically and mathematically rigorous, however, the boundary conditions (single continuous event) under which they are derived and validated are seldom observed in the field. The most obvious process that is unaccounted for in laboratory analysis is *ET* recovery of soil air volume. This process was found to play a significant role in the reduction of excess pressure using Ideal Gas Law analysis.

For column experiments generating air confining conditions, the only way soil air can escape is through air eruption from the top, causing a sudden reduction in the excess pressure. The pressure conditions after air eruption were found to be constant and stable, however as can be seen in Figure 7.4, after reaching a peak (at which air eruption may have taken place) the excess pressures in field conditions continue to decline in absence of any rainfall event perhaps responding to *ET*. Root Zone *ET* can bring about changes in the soil column by reducing the length of the wetting front through redistribution of soil water content vertically. Also, near surface root structure includes macro pores which

may cause some air to escape during build up. Another process that is very evident in field but cannot be simulated via soil column is the lateral redistribution of excess pressures due to field scale variability in root zone conditions. Not accounting this condition in practical modeling exercise could over predict excess pressures. The field study by Hammecker et al. (2003) suggested a similar conclusion whereby the authors found that the equations suggested by Wang et al. (1997) greatly over predicted excess pressures. They concluded that a small constant value of excess pressure was found to do a better job. The processes of *ET* and lateral air flow thus significantly reduces instances of air eruption, however, during period of heavy rainfall as in June of 2002, the conditions observed in the field become similar to a soil column experiment with the top layer of the soil being saturated and almost continuous infiltration. This period exhibits sudden rises and drops in air excess pressures suggesting repeated occurrences of air eruption.

The time scale of the air entrapment process is also important especially for multi-event simulation involving a time series of intermittent rainfall and *ET* (e.g., Crosbie et al. 2005). From the current analysis it was found that the time scale of excess pressure or Lisse effect ranged from several days to a week and varied depending on the frequency of infiltration events consistent with what was observed in a previous field study by Meyboom (1967). However the more extensive observation of the present study indicates that d_{WT} also played a big role is determining the occurrence and duration of Lisse effect. For d_{WT} values shallower than a meter below land surface, infiltration events almost always cause some degree of air pressurization. However at d_{WT} around 140 cm an infiltration event of 2.25 cm did not cause any air pressurization. This implies existence

of threshold below which air pressurization does not take place. Heliotis and Dewitt (1987) and Weeks (2002) found this value to be around 1 to 1.3 m below land surface. This analysis further corroborates that the above length scale may be a practical threshold.

A significant departure in the current approach from the previous studies on Lisse effect and air entrapment (e.g., Heliotis and Dewitt 1987 and Sabeh 2004) is the observation and analysis of a time series of events to determine the excess pressures contrary to single events studied by previous researchers. Inherent in this approach is the inclusion of highly variable antecedent soil water and water table conditions in the analysis which significantly affect air pressurization and infiltration. Secondly, multi-event approaches are important when the water table fluctuations are used for estimating ground water recharge and when accurate determination of air pressurization is needed (Healy and Cook 2002; Crosbie et al. 2005). The analysis is also novel from the point of view of marrying the two facets of vadose zone air entrapment, the first one dealing with its effect on reduction in infiltration and the other dealing with its effect on the water table observations.

7.6.1 Implications for Ground Water Modeling

Water table observations are important for ground water modeling aimed at quantifying surface and ground water interactions and for estimating head gradients controlling deeper aquifer recharge. Traditionally ground water models like MODLFOW 2000 (Harbaugh et al. 2000) rely heavily on ground water heads for model calibration and subsequent determination of vertical and horizontal fluxes in the model. Constructed

water table wells are generally cased (no screen) through the vadose zone to prevent short circuiting of percolation, causing erroneous observations. Given this construction practice in shallow water table environments it becomes imperative to carefully screen the water table data for Lisse effect before using it for model calibration. The water table heads, if directly taken from the observation wells and used in the model will significantly overestimate heads and therefore recharge estimates to the water table and deeper aquifer (Weeks 2002; Healy and Cook 2002). Ground water processes like the *ET*, lateral flux, leakage to deep aquifer, etc. as described in the ground water model are directly a function of d_{WT} (e.g., Banta 2000) and hence error in water table observation can bring about large errors in the estimation of these fluxes.

In the literature, methods like the one described by Sophocleous (1991) have been used to estimate natural ground water recharge. These methods were found to give consistent results in deep water table conditions (Sophocleous 1991) as air entrapment would not likely play any role. However, if applied for shallow water table conditions proper care should be taken to apply corrections for excess air pressures. The model proposed by Crosbie et al. (2005) to estimate ground water recharge, provides an innovative method to account for Lisse effect. However, the model parameter accounting for Lisse effect time scale will have to be adjusted depending on the in situ soil conditions, d_{WT} and the time series of meteorological stresses. Air entrapment has also been found to have implication of wetlands used for wastewater treatment. Detailed discussion about the impacts can be found in Heliotis and Dewitt (1987).

7.7 Conclusions

Theoretical one dimensional modeling using field data were utilized to detect and quantify long term air entrapment and Lisse effect. It was found that the air entrapment was dominant only in shallow water table environments ($d_{WT} < 1.4$ m) however, limited observation were available for deeper conditions to rigorously confirm the statement. Also the time scale of observed excess pore pressure ranged from a couple of days to a week. From the analysis it was concluded that antecedent conditions of soil moisture and d_{WT} play a significant role in determining excess pressure and infiltration values. The analysis on continuous multi-event observations found prolonged excess air pressures compounded by successive events, suggesting some useful insights as compared to single event based analysis. It was also concluded that due to restrictive boundaries and the type of stresses applied, the results obtained from soil column experiments may provide adequate prediction of field occurrences of air entrapment. The ratio of water table change to rainfall magnitude resulted in an average value of 45 for both years which was found to be consistent with the range of values reported by Weeks (2002) and Heliotis and Dewitt (1987). The implications of the air entrapment on ground water modeling were also discussed. An attempt was also made to model the excess pressures using Ideal Gas Law and uniform air pressure assumption. However, due to the unpredictable dependency of externally defined air eruption thresholds and sensitivity to soil air volume change, it was not found to provide a satisfactory estimation method at this time. The main limitation is believed to be the scale of vertical variability in air pressurization.

The limitation of this kind of analysis is that it cannot be applied as yet to larger, basin-scale modeling. Further observations of soil moisture profiles, coupled with vertical

measurement of pore pressure variability can provide further understanding of the governing processes. Only following this effect can a simplified predictive model be developed to facilitate regional modeling of the natural system.

Overall, contrary to the conclusion by Weeks (2002), it was found that the Lisse effect is not a rarity but is a common occurrence in shallow water table environments. Furthermore, field data incorporating sufficiently accurate water content measurement can be used to help correct water table observations and provide useful data to reformulate infiltration, percolation and recharge models.

Chapter 8: Summary and Conclusions

The main objective of this dissertation was to talk about the importance of vadose zone soil moisture dynamics in impacting various hydrological processes. First, an innovative way to collect data along a flow transect was discussed. It was shown that water table and soil moisture data when analyzed at a point scale was successful in estimation of spatial and temporal variability of evapotranspiration. The methodology when extended to a flow transect scale resolved not only evapotranspiration variability but was also able to determine the magnitude of other water budget components. The data collection efforts were hence successful in developing a dataset that which compiled time series of all the hydrological processes in a watershed for different land covers. The dataset as used subsequently in Chapter 3, Chapter 6, and Chapter 7 shows its potential to be used as a validating dataset for different modeling concepts for vadose zone processes.

Chapter 3 to Chapter 5 talked about extinction depth, specific yield variability, partitioning of evapotranspiration between vadose zone and ground water, and their effects on the water table fluctuations. Using variable saturation flow theory and field data it was shown that the empirically derived relationships were not adequate to model these concepts. For instance, it was found that an exponential model for decline of ground water component of evapotranspiration was more suitable than using a linear model. Similarly, instead of defining extinction depth arbitrarily, combination of land cover and

soil type can be used to make a more appropriate decision about the extinction depths at a given study site.

In case of usage of specific yield to model water table fluctuation for a given flux rate, it was concluded that for shallow water table environments, neither the assumption of constant specific yield nor the variation of specific yield based on equilibrium conditions in the vadose zone was valid. In addition to this, the commonly used assumption of calculating recharge as a fixed percentage of rainfall was also found to be erroneous. It was shown that the values of specific yield, depending on the antecedent soil moisture conditions and the type of boundary flux vary greatly for different water table elevations. To incorporate vadose zone soil moisture dynamics terms such as free vadose zone storage and non-ground water coupled flux were defined along with the methodology to determine their values. Chapter 4 elucidated details on how the free vadose zone storage and non coupled need to be utilized to correctly model processes such as recharge to the water table, evapotranspiration from ground water or vadose zone etc.

Building upon the concepts discussed in Chapters 2, 3, and 4, Chapter 5 described a simple thresholds based model dependent on soil characteristics and depth to the water table, to determine evapotranspiration. Comparison of theoretical solutions for a given soil type with the results determined from the thresholds based model showed a high degree of match in the values. Such close match between the model and the theoretical solution increases confidence of application of thresholds based models on regional scale modeling where application of Richard's equation to model vadose zone moisture conditions becomes infeasible.

The focus of Chapter 6 in the dissertation shifted to plant roots which are the main cause of moisture variability in vadose zone. Soil moisture and water table data from the study site described in Chapter 2 was used to determine the root water uptake from different sections of the root zone. It was found that the traditionally used models to determine root water uptake were not accurate as they assumed root water uptake to be directly proportional to the relative root fraction. The results clearly indicated that the root water uptake was a function of relative root fraction and ambient soil moisture. Any new model should hence take into account both of these factors. Also, it was found that both grass and trees transpired at potential but taking more water from the bottom wetter layers. Based on the observations from the calculated root water uptake in the first half Chapter 6, a novel concept of using root hydraulic characteristics to develop a framework to model root water uptake was conceptualized. The relationship that was suggested was found to yield results that were similar to the root water uptake calculated from the field data, however additional work to further characterize roots need to be done. The major implication of such analysis for regional scale modeling is the determination of the coefficients that are used to determine actual evapotranspiration from potential value. Unlike using coefficient based on empiricism such analysis can help determine the values which are physically based or measured.

Chapter 7 concluded with description of an interesting concept of air entrapment and a methodology to determine it. Preliminary field observations coupled with numerical and spreadsheet solutions were used to derive the magnitude and duration of air entrapment which cause artificial water table rise in the observation wells. It was found that the air pressurization effect was responsible at time up to 40 cm of water table

rise being recorded by the observation well and the excess pressurization was found to last some where between a day to a week in some cases. The observations are however preliminary and more data need to be collected to confirm about the magnitude and duration of the process and then find out ways to model it.

On the whole the dissertation was successful in showing the importance of the vadose zone in hydrological modeling. It talked about ways to collect data and model different hydrological processes. Moisture variability in the vadose zone was found to be primary factor affecting all the fluxes and hence all modeling efforts need to be concentrated at describing and predicting its behavior. The role of plant roots in impacting the moisture variability in the vadose zone cannot be ignored and hence physically based root water uptake model accounting for roots characteristics, such as distribution and vulnerability, need to be developed and used integrally with any hydrological model. Alternatively, plant coefficients based on roots characteristics and ambient soil moisture conditions need to be developed to facilitate accurate land cover response in regional scale modeling.

This dissertation hence provides a platform on which robust and more comprehensive modeling conceptualizations can be developed. Future work from this point onwards will be to collect similar data from other sites differing in hydro-metrological conditions than the current field site and test the models developed from the current dataset. Having recognized the importance of plant roots, greater efforts needs to be made to sample roots of as many plant types as possible and develop a root distribution as talked about in Chapter 6. Vulnerability characteristics for each vegetation type needs to be determined and then a physically based model as suggested in Chapter 6

needs to be constructed and tested using the root water uptake values calculated from the study site. The process of root characterization though tedious will provide physically based root parameters that can be used with confidence in the future modeling efforts for similar land cover without repeating the whole process.

References

Adrian, D.D. and J.B. Franzini. 1966. Impedance to infiltration by pressure build-up ahead of the wetting front. Journal of Geophysical Research, 71: 5857-5862.

Allen, R.G., I.A. Walter, R.L. Elliot, T.A. Howell, D. Itenfisu, M.E. Jensen, and R.L. Snyder (Eds.). 2005. The ASCE standardized reference evapotranspiration equation. American Society of Civil Engineers, Reston, VA.

Anderson, M.P. and W.W. Woessner. 1992. Applied ground water modeling: simulation of flow and advective transport. Academic Press, New York, NY.

Andersen P.F. and P.A. Weeber. 2000. Use of an integrated ground water/ surface water model to evaluate spatial and temporal variations in aquifer recharge rates *In* Proceeding of hydrology symposium I, modeling aquifer heterogeneity. University of South Carolina, Columbia, SC, January 20-21.

Banta, E.R. 2000. MODFLOW-2000, The U.S. Geological Survey modular ground water model - Documentation of packages for simulating evapotranspiration with a segmented function (ETS1) and drains with return flow (DRT1).U.S. Geological Survey open file report 00-466.

Baird, A.J, and R.L. Wilby (Eds). 1999. Eco-Hydrology: Plants and water in terrestrial and aquatic environments. Routledge, New York, NY.

Barlow,P.M., L.A. DeSimone, A.F. Moench. 2000. Aquifer response to stream-stage and recharge variations- II: Convolution method and applications. Journal of Hydrology, 230: 211-229.

Bicknell, B., Imhoff, J.C., Kittle, J.L., Jr., Jobes, T. H., and Donigian, A.D., Jr. 2001. Hydrological simulation program–FORTRAN (HSPF): User's manual for Version 12. U.S. Environmental Protection Agency, Athens, GA.

Bidlake, W. R., W.M.Woodham, and M.A.Lopez. 1993. Evapotranspiration from areas of native vegetation in west-central Florida: U.S. Geological Survey open file report 93-415.

Blum, V.S., S. Israel, and S.P. Larson. 2001. Adapting MODFLOW to simulate water movement in the unsaturated zone. *In* MODFLOW 2001 and other modeling odysseys proceedings 60-65. International ground water modeling center (IGWMC), Colorado School of Mines, Golden, Colorado, September 11-14.

Brooks, R.H., and A.T. Corey. 1966. Properties of porous media affecting fluid flow. Journal of irrigation and drainage engineering, Division of American Society of Civil Engineering, IR2, 61-88.

Brutsaert, W. 1982. Evaporation into the atmosphere: Theory, history, and applications. Kluwer Academic Publishers, Boston, MA.

Buss, P. 1993. The use of capacitance based measurements of real time soil water profile dynamics for irrigation scheduling. *In* Proceedings of national conference of irrigation association of Australia and national committee of irrigation and drainage association of Australia, Homebush, NSW, Lauceston, Tasmania, May 17-19.

Carlisle, V. W., Sodek, F., Collins, M. E., Hammond, L. C. and Harris, W. G. 1989. Characterization data for selected Florida soils. Soil survey report, U.S. Department of Agriculture 89-1.

Carsel, R.F. and R. S. Parrish. 1988. Developing joint probability distributions of soil water retention characteristics. Water Resources Research, 24: 755-770.

Charbeneau, R. 2000. Groundwater hydraulics and pollutant transport. Prentice-Hall Inc., Upper Saddle River, NJ.

Crosbie, R.S., P.Binning, and J.D.Kalma. 2005. A time series approach to inferring groundwater recharge using the water table fluctuation method. Water Resources Research, 41 w01001, doi:10,1029/2004WR003077.

Das, B.M. 2002.Soil mechanics laboratory manual. Oxford University Press, New York, NY.

De Silva, M., M. H. Nachabe, Jirka Simunek and R. Carnahan. 2007. Modeling evapotranspiration in a heterogeneous vegetative cover. ASCE Journal of Irrigation and Drainage Engineering, (*in press*).

dos Santos, A.G. Jr. and E.G.Youngs .1969. A study of the specific yield in land-drainage situations. Journal of Hydrology, 8:59-81.

Diodato, D.M. 2000. Software spotlight. Ground Water, 38(1):10-11.

Doorenbos, J., and W.O.Pruitt. 1977. Crop Water Requirements. FAO Irrigation and drainage paper 24. Food and agricultural organization of the United Nations, Rome.

Duke, H.R. 1972. Capillary properties of soils- Influence upon specific yield. Transactions of ASAE, 688-699.

Fares, A. and A.K. Alva. 2000. Evaluating the capacitance probes for optimal irrigation of citrus through soil moisture monitoring in an Entisol profile. Irrigation Science, 19:57–64.

Fayer, M.J. and D. Hillel.1986. Air Encapsulation I - Measurement in a field soil. Soil Science Society of America Journal, 50:568-572.

Feddes, R.A., P.J. Kowalik, and H.Zaradny. 1978. Simulation of field water use and crop yield. John Wiley & Sons New York, NY.

Freeze, R. and J. Cherry. 1979. Groundwater. Prentice Hall, Old Tappan, NJ.

Gale, M.R. and D.F. Grigal. 1987. Vertical root distributions of northern tree species in relation to successional status. Canadian Journal of Forest Research, 17:829-834.

Gardner, W.R. 1958. Some steady-state solutions of the unsaturated moisture flow equation with applications to evaporation from a water table. Soil Science, 85**:** 228 - 232.

Gardner, W.R. and M. Fireman. 1958. Laboratory studies of evaporation from soil columns in the presence of a water table. Soil Science, 85:244-249.

Gillham, R.W. 1984. The capillary fringe and its effect on water table response. Journal of Hydrology, 67: 307-324.

Green, W.H. and C.A.Ampt. 1911. Studies on soil physics 1 - Flow of air and water through soils. Journal of Agricultural Science, 4: 1-24.

Hammecker, C, A. C. D. Antonino, J. L. Maeght, and P. Boivin. 2003. Experimental and numerical study of water flow in soil under irrigation in northern Senegal: Evidence of air entrapment. European Journal of Soil Science, 54: 491–503.

Harbaugh, A.W. 2005. MODFLOW-2005, the U.S. Geological Survey modular ground-water model -- the ground-water flow process. U.S. Geological Survey Techniques and Methods 6-A16, Reston, VA.

Harbaugh, A.W., E.R.Banta, M.C. Hill, and M.G. McDonald. 2000. MODFLOW-2000, the U.S. Geological Survey modular ground-water model - User guide to modularization concepts and the ground-water flow process. U.S. Geological Survey Open-File Report 00-92, U.S. Geological Survey, Reston, VA.

Harter, T. and J. W. Hopmans. 2004. Role of vadose zone flow processes in regional scale hydrology: review, opportunities and challenges. *In* Feddes, R.A., G.H. de Rooij and J.C. van Dam (eds.). 2004. Unsaturated zone modeling: Progress, applications, and challenges. Kluwer Academic Publishers, Boston, MA.

HDR and Tampa Bay Water. 1999. Geotechnical Site Characterization Report – Tampa Bay Regional Reservoir Volume I. LAW Project No. 40120-8-0106. December 17.

Healy, R.W. and P.G. Cook. 2002. Using groundwater levels to estimate recharge. Hydrogeology Journal, 10:91-109.

Hernandez, T., M. Nachabe, M. Ross, and J. Obeysekera. 2003. Runoff from variable source areas in humid, shallow water table environments. Journal of the American Water Resource Association, 39(1): 75-85.

Hillel, D. 1980. Applications of soil physics. Academic Press, New York, NY

Hillel, D. 1998. Environmental soil physics. Academic Press, New York, NY

Heliotis, F.D. and C.B. Dewitt. 1987. Rapid water table response to rainfall in a northern peatland ecosystem. Water Resource Bulletin, 23(6):1011- 1016.

Hooghoudt, S.B. 1947. Waaarnemingen van grondwaterstanden voor de landbouw. Commissie voor Hydrologisch TNO, Verlagen TEchnische Bijeenkomsten 1-6: 185-201.

Jackson, R.B., J. Canadell, J.R. Ehleringer, H.A. Mooney, O.E. Sala, and E.D. Schulze. 1996. A global analysis of root distributions for terrestrial biomes. Oecologia, 108:389-411.

Jamison, V.C. and E.M. Kroth. 1958. Available moisture storage capacity in relation to textural composition and organic matter content of several Missouri soils. Soil Science Society of America Proceedings, 22: 189-192.

Jayatilaka, C.J. and R.J. Gillham. 1996. A deterministic-empirical model of the effect of the capillary fringe on near-stream area runoff. Journal of Hydrology, 184:299-315.

Jensen, M.E. and H.R. Haise.1963. Estimation of evapotranspiration from solar radiation. Journal of Irrigation and Drainage Division, Proceedings of the American Society of Civil Engineers, 89: 15-41.

Jury, W.A., W.R. Gardner, and W.H. Gardner. 1991. Soil physics. John Wiley & Sons, New York, NY.

Kite, G.W., and P. Droogers. 2000. Comparing evapotranspiration estimates from satellites, hydrological models and field data. Journal of Hydrology, 229:3–18.

Knowles, L., Jr. 1996. Estimation of evapotranspiration in the Rainbow Springs and Silver Springs basin in north-central Florida. Water Resources Investigation Report. 96-4024. USGS, Reston, VA.

Latifi, H., S. N. Prasad, and O. J. Helweg. 1994. Air entrapment and water infiltration in two-layered soil column. ASCE Journal of Irrigation and Drainage Engineering, 120: 871–891.

Li, K.Y., R.De Jong, and J.B. Boisvert. 2001. An exponential root-water-uptake model with water stress compensation. Journal of hydrology, 252:189-204.

Li,K.Y., R.De Jong, and M.T.Coe. 2006. Root water uptake based upon a new water stress reduction and an asymptotic root distribution function. Earth Interactions, 10(paper 14):1-22.

Linsley, R. K. and J. B. Franzini .1972. Water resources engineering. McGraw-Hill Inc., New York, NY.

Loheide, S. P., II, J. J. Butler Jr., and S. M. Gorelick. 2005. Estimation of ground water consumption by phreatophytes using diurnal water table fluctuations: A saturated-unsaturated flow assessment, Water Resources Research, 41, W07030, doi:10.1029/2005WR003942.

Mahmood, R. and K.G. Hubbard. 2003. Simulating sensitivity of soil moisture and evapotranspiration under heterogeneous soils and land uses. Journal of Hydrology, 280:72–90.

McDonald, M.G. and A.W. Harbaugh. 1988. A modular three-dimensional finite-difference ground-water flow model. U.S. Geological Survey Techniques of Water-Resources Investigations, book 6, chap. A1, Reston, VA.

McWhorter, D.B. 1971. Infiltration affected by the flow of air. Colorado State University Hydrological Paper, 49, Fort Collins, CO.

McWhorter, D.B., and D.K. Sunada. 1977. Ground water hydrology and hydraulics. Water Resources Publications, Fort Collins, CO.

Meyboom, P. 1967. Ground water studies in the Assiniboine river drainage basin: II. Hydrologic characteristics of phreatophytic vegetation in south-central Saskatchewan. Geological Survey of Canada Bulletin 139, no.64.

Mo, X., S. Liu, Z. Lin, and W. Zhao. 2004. Simulating temporal and spatial variation of evapotranspiration over the Lushi basin. Journal of Hydrology, 285:125–142.

Monteith, J. L. 1965. Evaporation and environment. *In* G.E.Fogg (ed). 1965.The state and movement of water in living organisms. Symposium of the Society of Experimental Biology: San Diego, California, Academic Press, New York, p.205-234.

Morel-Seytoux, H.J. and J. Khanji. 1974. Derivation of an equation of infiltration. Water Resources Research, 10:795-800.

Morel-Seytoux, H.J, and J. Khanji. 1975. Equation of infiltration with compression and counterflow effects. Hydrological Science Journal, 20: 505-517.

Morgan,K.T., L.R.Parsona, T.A. Wheaton, D.J.Pitts and T.A.Oberza. 1999. Field calibration of a capacitance water content probe in fine sand soils. Soil Science Society of America Journal, 63: 987-989.

Mualem, Y. 1976. A new model predicting the hydraulic conductivity of unsaturated porous media. Water Resources Research, 12(3):513-522.

Nachabe, M. 2002. Analytical expressions for transient specific yield and shallow water table drainage. Water Resources Research, 38(10): 1193, doi: 10.1029/2001WR001071.

Nachabe, M., N.Shah, M.Ross, and J.Vomacka. 2005. Evapotranspiration of two vegetation covers in a shallow water table environment. Soil Science Society of America Journal, 69:492-499.

Newman, S.P.1987. On methods of determining specific yield. Ground Water, 25(4):679-684.

Niswonger, R.G., D.E.Prudic, and R.S.Regan. 2006. Documentation of the unsaturated-zone flow (UZF1) package for modeling unsaturated flow between the land surface and the water table with modflow-2005. U.S. Geological Survey Techniques and Methods 6-A19, Reston,VA.

Novakowski, K.S., and R.W.Gillham. 1988. Field investigations of the nature of water table response to precipitation in shallow water table environments. Journal of Hydrology, 97: 23-32.

Nwankwor, G.I., J.A. Cherry, and R.W.Gillham.1984. A comparative study of specific yield determinations for a shallow sand aquifer. Ground Water, 22(6):764-772.

Nwankwor, G.I., R.W. Gillham, G.van der Kamp, and F.F. Akindunni.1992. Unsaturated and saturated flow in response to pumping of an unconfined aquifer: Field evidence of delayed drainage. Ground Water, 30(5):690-700.

Parlange, J. Y. and D. E. Hill. 1979. Air and water movement in porous media: Compressibility effects. Soil Science, 127: 257–263.

Peck, A.J. 1965. Moisture Profile Development and air compression during water uptake by bounded porous bodies, 3- Vertical columns. Soil Science, 100:44-51.

Platineanu, I.C., and J.L. Starr. 1997. Real-time soil water dynamics using multi-sensor capacitance probes: Laboratory calibration. Soil Science Society of America Journal, 61:1576-1585.

Penman, H.L. 1948. Natural evaporation from open water, bare soil, and grass. Proceedings of Royal Society of London, Series A, 193: 120-146.

Priestley, C.H.B., and Taylor, R.J. 1972. On the assessment of surface heat flux and evaporation using large-scale parameters. Monthly Weather Review, 100(2): 81-92.

Rahgozar. M. 2006. Estimation of evapotranspiration using continuous soil moisture measurements. PhD Dissertation, Department of Civil and Environmental Engineering, University of South Florida, Tampa, FL.

Rahgozar, M, N. Shah, and M. Ross. 2007. Estimation of evapotranspiration and water budget components using concurrent soil moisture and water table monitoring. Journal of Hydrology, (Accepted pending revisions).

Richard, L.A .1931. Capillary conduction of liquids through porous mediums, Journal of Applied Physics, 1(5), 318-333.

Robock, A., K.Y. Vinnokov, G. Srinivasan, J.K. Entin, S. Hollinger, N.A. Spernskaya, S. Liu, and A. Namkhai. 2000. The global soil moisture data bank. Bulletin of American Meteorological Society, 81:1281–1299.

Rodriguez-Iturbe I. and A. Porporato. 2004. Ecohydrology of water-controlled ecosystems: Soil moisture and plant dynamics. Cambridge University Press, Cambridge, UK.

Ross, M. A., P.D. Tara, J.S. Geurink, and M.T. Stewart. 1997. FIPR hydrologic model, user manual and technical documentation. FIPR-OFR-88-03-085. Florida Institute of Phosphate Research, Bartow, FL.

Ross, M. A., J. Geurink, A. Aly, P. Tara, K. Trout, T. Jobes. 2003. Integrated Hydrologic Model (IHM) Vol. 1: Theory manual. Center for Modeling Hydrologic and Aquatic Systems, Department of Civil and Environmental Engineering, University of South Florida, Tampa, FL.

Ross, M, A. Said, J. Geurink, P. Tara, and A. Aly. 2005. Evapotranspiration hierarchy and allocation for integrated surface and groundwater model in west-central Florida. Hydrological Science and Technology, 21(1-4):157-176.

Ross, M., J. Geurink, A. Said, A. Aly, and P. Tara. 2005. Evapotranspiration conceptualization in the HSPF-MODFLOW integrated models. Journal of the American Water Resources Association, 41(5):1013-1025.

Ross, M., J. Geurink, A. Aly, P. Tara, K. Trout, and T. Jobes. 2004. Integrated Hydrologic Model (IHM) Volume II: Theory manual. University of South Florida. Tampa, FL.

Sabeh, D. 2004. Adapting the Green and Ampt model to account for air compression and counterflow. M.S. Thesis, Department of Civil and Environmental Engineering, University of South Florida, Tampa, FL.

Said, A., M. Nachabe, M. Ross, and J. Vomacka. 2005. Methodology for estimating specific yield in shallow water environment using continuous soil moisture data. ASCE Journal of Irrigation and Drainage Engineering, 131(6):533-538.

Schmid,W., R.T. Hanson,T. Madodock, III, and S.A. Leake. 2006. User Guide for the Farm Process (FMP1) for the U.S.Geological Survey's modular three-dimensional finite-difference ground-water flow model, MODFLOW 2000. U.S. Geological Survey Techniques and Methods 6-A17, Reston,VA.

Schulla, J., Jasper, K. 2000. Model description WaSiM-ETH. IAC, ETH Zurich, Zurich.

Shah, N., and M. Ross. 2007. Variability in Specific Yield for different wetting and drying conditions, ASCE Journal of Hydrologic Engineering (*In Review).*

Shah,N., M. Nachabe, and M.Ross. 2007a. Extinction depth and evapotranspiration from ground water under selected land covers. Ground Water, 45(3):329-338.

Shah, N., M. Ross, and A. Said. 2007b. Vadose zone evapotranspiration distribution using one dimensional analysis and conceptualization for integrated modeling. Proceedings of ASCE EWRI conference, Tampa, FL, May 14-19.

Shah, N., M.Ross, and G.S.Ladde. 2007c. Dynamic modeling of root water uptake using soil moisture data. International Journal of Neural Parallel and Scientific Computations, *In Press*.

Shah, N., J, Zhang, and M. Ross. 2007d. Long term air entrapment affecting runoff and water table observations. Water Resources Research, (Under revision.).

Simunek, J., M.Sejna, and M.Th. van Genuchten. 1998. The HYDRUS 1D software package for simulating the one dimensional movement of water, heat, and multiple solutes in variably-saturated media. Version 2.0. US Salinity Laboratory, ARS/USDA. Riverside, CA.

Simunek, J., M. Th. van Genuchten and M. Sejna. 2005. The HYDRUS-1D software package for simulating the movement of water, heat, and multiple solutes in variably saturated media, version 3.0, HYDRUS software series 1. Department of Environmental Sciences, University of California Riverside, Riverside, CA.

Simunek, J., and M.Th. van Genuchten. 1999. Manual of HYDRUS-2D computer program for simulation water flow, heat and solute transport in variably saturated porous media. USDA, Riverside, CA.

Sophocleous, M.1991. Combining the soil water balance and water-level fluctuation methods to estimate natural groundwater recharge: Practical aspects. Journal of Hydrology, 124:229-241.

Sophocleous, M. 2002. Interactions between ground water and surface water: The state of the science. Hydrogeology Journal, 10:52-67.

Starr, J.L. and I.C. Paltineanu .1998. Soil water dynamics using multi-sensor capacitance probes in non traffic inter-rows of corn. Soil Science Society of America Journal, 62:115-122.

Steudle, E. 2000. Water uptake by plant roots: An integration of views. Plant and Soil, 226:45-46.

Sumner, D.M. 2001. Evapotranspiration from a cypress and pine forest subjected to natural fires, Volusia County, Florida, 1998-99. Water Resources Investigations Report 01-4245. U.S. Geological Survey, Reston, VA.

Sumner, D. 2006. Adequacy of selected evapotranspiration approximations for hydrological simulation. Journal of the American Water Resources Association, 42(3):699- 711.

Sumner, D. 2007. Effects of capillarity and microtopography on wetland specific yield. Wetlands, 27(3): 693-701.

Thornthwaite, C.W. 1948. An approach toward a rational classification of climate. Geographic Review, 38:55-94.

Thompson, D.L. 2003. Specific yield variability and the evolution of ground water evapotranspiration in humid shallow water table environment. MS. Thesis, Department of Civil and Environmental Engineering, University of South Florida Tampa, FL.

Thoms, R.B., R.L.Johnson, and R.W. Healy. 2006. User's guide to the variably saturated flow (VSF) Process for MODFLOW. U.S. Geological Survey Techniques and Methods 6-A18, Reston, VA.

Todd, D.K. 1959. Groundwater hydrology. John Wiley & Sons, New York, NY.

Touma, J., G. Vachaud, and J.Y. Parlange 1984. Air and water flow in a sealed, ponded vertical soil column: Experiment and model. Soil Science, 137:181–187.

Troch,P., .F.De Troch, and W.Brutsaert. 1992. Effective water table depth to describe initial conditions prior to storm rainfall in humid regions. Water Resources Research, 29:427-434.

Trout, K., and M.Ross. 2004. Intensive hydrologic data collection in as small watershed in west-central Florida. Hydrological Science and Technology 21(1-4):187-197.

van Genuchten, M.Th. 1980. A closed-form equation for predicting the hydraulic conductivity of unsaturated soils. Soil Science Society of America Journal, 44:892-898.

van Genuchten, M. Th.1987. A numerical model for water and solute movement in and below the root zone. Research report No 121, U.S. Salinity laboratory, USDA, ARS, Riverside, CA.

van Genuthcen, M.T., F.J.Leji, and S.R.Yates. 1991. The RETC code for quantifying the hydraulic functions of unsaturated soil. U.S. Salinity Laboratory, U.S. Department of Agriculture, Agriculture Research Services Riverside, CA.

Viessman, W Jr. and G. Lewis. 2002. Introduction to hydrology. Pearson Education Inc., Upper Saddle River, NJ.

Wang, Z., J. Feyen, D. R. Nielsen, and M. T. van Genuchten. 1997. Two-phase flow infiltration equations accounting for air entrapment effects. Water Resources Research, 33(12): 2759-2767.

Wang, Z., J. Feyen, D. R. Nielsen, and M. T. van Genuchten. 1998. Air entrapment effects on infiltration rate and flow instability Water Resources Research, 34(2), 213-222.

Weeks, E.P. 2002. The Lisse effect revisited. Ground Water, 40(6): 652-656.

White,W.N. 1932.A method of estimating ground-water supplies based on discharge by plants and evaporation from soil: Results of investigation in Escalante Valley, Utah. Water-Supply Paper 659-A.

Woessner, W. W. 2000. Stream and fluvial plain ground-water interactions: Re-scaling hydrogeologic thought. Ground Water, 38(3):423-429.

Yang, J., B. Li, and S. Liu. 2000. A large weighing lysimeter for evapotranspiration and soil water-groundwater exchange studies. Hydrological Processes, 14:1887–1897.

Youngs, E.G., and A.J. Peck. 1964. Moisture profile development and air compression during water uptake by bounded porous bodies, 1- Theoretical introduction. Soil Science, 98:290-294.

Zalewski, M., G.A. Januer, and G.Jolankaj. 1997. Ecohydrology : A new paradigm for the sustainable use of aquatic resources. *In* Conceptual background, working hypothesis, rationale and scientific guidelines for the implementation of the IHP-V projects 2.3/2.4 technical documents in hydrology No. 7. UNESCO, Paris.

Zhang, J. and M. A Ross. 2007. A 2-layer vadose zone model for surface-groundwater interactions. ASCE Journal of Hydrologic Engineering, *In Press*.

About the Author

Nirjhar Shah received his Bachelor's Degree in Civil Engineering from the Indian Institute of Technology, Roorkee, India in 2003. Right after getting Bachelor's Nirjhar joined the direct PhD program at the Department of Civil and Environmental Engineering, in the University of South Florida (USF), Tampa. Working with Dr.Mahmood Nachabe and Dr.Mark Ross, Nirjhar has specialized in the field of hydrological modeling specially modeling of vadose zone soil moisture dynamics. His research interests include Eco-Hydrology, integrated surface and ground water modeling and application of GIS in water resources. During last four years during his stint at USF, Nirjhar has co-authored more than eight journal articles and presented more than ten papers in various conferences.

Apart from academics, Nirjhar has been also involved in dramatics, and has been a part of more than fifteen professional level plays. He likes to play badminton, squash, racquetball, and of course cricket (one game which every Indian likes).